Tore Skjellnes

Digital Control
of
Grid Connected Converters
for
Distributed Power Generation

Doctoral thesis
for the degree of doktor ingeniør

Trondheim, March 2008

Norwegian University of Science and Technology
Faculty of Information Technology, Mathematics
and Electrical Engineering
Department of Electric Power Engineering

NTNU

Norwegian University of Science and Technology

Doctoral thesis
for the degree of doktor ingeniør

Faculty of Information Technology, Mathematics
and Electrical Engineering
Department of Electric Power Engineering

ISBN 978-82-471-7653-5 (printed version)
ISBN 978-82-471-7636-8 (electronic version)
ISSN 1503-8181

Doctoral theses at NTNU, 2008:82

Printed by NTNU-trykk

Abstract

Pulse width modulated converters are becoming increasingly popular as their cost decreases and power rating increases. The new trend of small-scale power producers, often using renewable energy sources, has created new demands for delivery of energy to the grid.

A major advantage of the pulse width modulated converter is the ability to control the output voltage at any point in the voltage period. This enables rapid response to load changes and non-linear loads. In addition it can shape the voltage in response to the output current to create an outward appearance of a source impedance. This is called a virtual impedance.

This thesis presents a controller for a voltage controlled three phase pulse width modulated converter. This controller enables operation in standalone mode, in parallel with other converters in a microgrid, and in parallel with a strong main grid.

A time varying virtual impedance is presented which mainly attenuates reactive currents. A method of investigating the overall impedance including the virtual impedance is presented.

New net standards have been introduced, requiring the converter to operate even during severe dips in the grid voltage. Experiments are presented verifying the operation of the controller during voltage dips.

Acknowledgements

First of all, I would like to thank my father Asle Skjellnes for his help and support which have been invaluable to my work. I would also like to thank my main supervisor Professor Lars Norum for his helpful support.

NFR, Siemens Teknologiutvikling, and Powec are all acknowledged for sponsoring my work.

I would like to thank my current employer, SmartMotor AS, for the use of laboratory facilities and personell for my experiments. This laboratory was sponsored by the participants of the research program "Weight reduced windgenerator systems." A special thanks to Sigurd Øvrebø, CTO at SmartMotor, for his encouragement and comments.

I would also like to thank my fellow students William Gullvik and Erik Hoff for discussions and support, and the rest of the people at the Energy Conversion Group at NTNU for their help and encouragement.

Finally, I would like to thank my friends, family and colleges for making life fun, interesting and meaningful.

Contents

List of Figures

List of Tables

Nomenclature

$\dot{(\cdot)}$ Time derivate of element, vector or matrix

$(\cdot)_\alpha$ α-axis parameter or variable

$(\cdot)^{\alpha\beta}$ Vector in the $\alpha\beta$-coordinate system, without null vector

$(\cdot)^{\alpha\beta 0}$ Vector in the $\alpha\beta$-coordinate system, with null vector

$(\cdot)_\beta$ β-axis parameter or variable

$(\cdot)_\theta$ θ-axis parameter or variable

$(\cdot)_0$ The null-component (average) of a three phase signal

$\|\cdot\|_2$ The regular 2-norm, i.e. the length, of the vector. Also called the Euclidean norm. Calculated as

$$\|\boldsymbol{x}\|_2 = \left(|x_1|^2 + \cdots + |x_n|^2\right)^{\frac{1}{2}} = \left(\boldsymbol{x}^{\mathrm{T}}\boldsymbol{x}\right)^{\frac{1}{2}}.$$

$(\cdot)_a$ a-phase parameter or variable

$(\cdot)_{ab}$ Difference between a-phase and b-phase parameter or variable

$(\cdot)^{abc}$ Vector in the abc-coordinate system

$(\cdot)_b$ b-phase parameter or variable

$(\cdot)_{bc}$ Difference between b-phase and c-phase parameter or variable

$(\cdot)_c$ c-phase parameter or variable

$(\cdot)_{ca}$ Difference between c-phase and a-phase parameter or variable

$(\cdot)_{\mathrm{d}}$ d-axis parameter or variable

$(\cdot)^{\mathrm{dq}}$ Vector in the dq-coordinate system, without null vector

$(\cdot)^{\mathrm{dq0}}$	Vector in the dq-coordinate system, with null vector
$(\cdot)_m$	m-axis parameter or variable
$(\cdot)^{m\theta}$	Vector in the $m\theta$-coordinate system
$(\cdot)_{\mathrm{q}}$	q-axis parameter or variable
α_0	Nominal phase for the dq-current controller [rad]
α_{ref}	Reference phase for the voltage generator [rad]
δ_ω	Relative deviation of frequency from nominal value
δ_m	Relative deviation of magnitude from nominal value
ϵ	Angular error estimate
ζ	Filter voltage angular observer damping constant
θ	Angle of the dq-coordinate system [rad]
θ_{meas}	Measured phase angle [rad]
$\hat{\theta}$	Estimated voltage observer phase angle [rad]
ϑ	Voltage phase of a general three phase voltage [rad]
ω	General voltage angular frequency [rad s^{-1}]
ω_0	Nominal angular frequency for the dq-current controller [rad s^{-1}]
ω_f	Voltage observer filter gain
ω_n	Base angular frequency [rad s^{-1}]
ω_p	Resonance frequency of the undamped LCL-filter with the grid short circuited.
ω_{ref}	Reference angular frequency for the voltage generator [rad s^{-1}]
$\hat{\omega}$	Estimated voltage observer frequency [rad s^{-1}]
$\boldsymbol{A}$	The state-to-state matrix of a general state space model
$\boldsymbol{B}$	The input-to-state matrix of a general state space model
$\boldsymbol{C}$	The state-to-output matrix of a general state space model

C_f Filter capacitance of a LCL-filter [F]

C_n Base capacitance [F]

e Euler's number, defined as

$$\mathrm{e} = \lim_{n\to\infty}\left(1+\frac{1}{n}\right)^n$$

f_h Bandwidth for the highpass filter of the active damping controller [Hz]

f_n Nominal frequency [Hz]

$\boldsymbol{H}_i$ Shaping transfer function matrix for the active damping controller

$\boldsymbol{H}_v$ Shaping transfer function matrix for the voltage shape controller

$i_{0,q}$ Nominal reactive current component for steady state in the power controller

$\boldsymbol{i}_e$ Output current vector from the PWM-unit [p.u.]

$\boldsymbol{i}_f$ Capacitor current vector PWM-unit [p.u.]

$\boldsymbol{i}_{f,\mathrm{ref}}$ Reference current for the capacitor in the LCL-filter [p.u.]

$\boldsymbol{i}_g$ Output current vector to the grid [p.u.]

$\hat{I}_n$ Base current [A]

$I_{n,\mathrm{RMS}}$ Rated current [A-rms]

j The imaginary unit, $\mathrm{j} = \sqrt{-1}$.

k_θ Feedback gain for the phase component in the dq-current controller

k_a Gain constant for the active damping controller

k_d Constant for the phase lifting filter of the active damping controller

k_h Constant for the highpass filter of the active damping controller

$\boldsymbol{K}_i$ Gain matrix for the active damping controller

k_m Feedback gain for the magnitude component in the dq-current controller

k_n Filter gain for voltage magnitude observer

$k_{p\omega}$ Active power droop gain for deviations of frequency

k_P Feedback gain for the active power component in the power controller

k_{pm} Active power droop gain for deviations of magnitude

$k_{q\omega}$ Reactive power droop gain for deviations of frequency

k_Q Feedback gain for the reactive power component in the power controller

k_{qm} Reactive power droop gain for deviations of magnitude

$\boldsymbol{K}_v$ Gain matrix for the voltage shape controller

k_v Gain constant for the voltage shape controller

$\boldsymbol{K}_z$ Gain matrix for the virtual impedance controller

k_z Constant giving the gain of the constant virtual impedance of the impedance controller

$\tilde{k}_z$ Constant giving the gain of the time varying virtual impedance of the impedance controller

L_f Converter side filter inductance of a LCL-filter [H]

L_g Grid side filter inductance of a LCL-filter [H]

L_n Base inductace [H]

P_e Active power delivered to the LCL-filter capacitor from the converter [p.u.]

P_g Active power delivered from the LCL-filter capacitor to the grid [p.u.]

$P_{g,0}$ Nominal active power for the droop control [p.u.]

$P_{g,\mathrm{ref}}$ Reference for the active power of the power controller [p.u.]

$\boldsymbol{q}^{abc}$ Three phase vector of ones, i.e. $\boldsymbol{q}^{abc} = \begin{bmatrix} 1 & 1 & 1 \end{bmatrix}^{\mathrm{T}}$

Q_e Reactive power delivered to the LCL-filter capacitor from the converter [p.u.]

Q_g Reactive power delivered from the LCL-filter capacitor to the grid [p.u.]

$Q_{g,0}$ Nominal reactive power for the droop control [p.u.]

$\mathbf{R}_{\mathrm{dq0}}^{\alpha\beta0}$ Rotation matrix to convert a vector from the dq0 coordinate system to the $\alpha\beta0$ system

$\mathbf{R}_{\alpha\beta0}^{\mathrm{dq0}}$ Rotation matrix to convert a vector from the $\alpha\beta0$ coordinate system to the dq0 system

R_f Converter side filter resistance of a LCL-filter [Ω]

r_f Converter side filter resistance of a LCL-filter [p.u.]

R_g Grid side filter resistance of a LCL-filter [Ω]

r_g Grid side filter resistance of a LCL-filter [p.u.]

s The Laplace transform variable [rad s^{-1}]

S_n Rated apparent power [VA]

T The switching period [s]

$\mathbf{T}_{abc}^{\Delta}$ Transformation matrix to convert a vector from the phase-to-neutral coordinate system to the phase-to-phase (Δ) system

$\mathbf{T}_{\Delta}^{abc}$ Transformation matrix to convert a vector from the phase-to-phase (Δ) coordinate system to the phase-to-neutral system

$\mathbf{T}_{\mathrm{dq0}}^{abc}$ Transformation matrix to convert a vector from the dq0 coordinate system to the phase-to-neutral system

$\mathbf{T}_{\alpha\beta0}^{abc}$ Transformation matrix to convert a vector from the $\alpha\beta0$ coordinate system to the phase-to-neutral system

$\mathbf{T}_{abc}^{\alpha\beta0}$ Transformation matrix to convert a vector from the phase-to-neutral coordinate system to the $\alpha\beta0$ system

$\mathbf{T}_{abc}^{\mathrm{dq0}}$ Transformation matrix to convert a vector from the phase-to-neutral coordinate system to the dq0 system

$\boldsymbol{u}(t)$ The inputs of a general state space model

u_k The input signal at time-step k of a difference equation

v_0	Nominal voltage magnitude for the dq-current controller [p.u.]
v_{DC}	DC link/bus voltage [p.u.]
$\boldsymbol{v}_e$	Output voltage vector of the PWM-unit [p.u.]
$\boldsymbol{v}_f$	Capacitor voltage vector of the LCL-filter [p.u.]
$v_{f,n}$	The voltage at the star point of the capacitors in the LCL-filter [p.u.]
$\boldsymbol{v}_{f,\text{ref}}$	Reference voltage for the capacitor in the LCL-filter [p.u.]
$\boldsymbol{v}_g$	Grid voltage vector [p.u.]
v_m	Voltage magnitude of a general symmetric three phase voltage [p.u.]
$\hat{V}_n$	Base voltage (peak phase voltage) [V]
$V_{n,\text{RMS}}$	Rated line voltage [V-rms]
$\boldsymbol{v}_{\text{PWM}}$	Reference voltage for the PWM-unit [p.u.]
v_{ref}	Reference voltage magnitude for the voltage generator [p.u.]
$\boldsymbol{v}_z$	Reference voltage for the capacitor in the LCL-filter after modification by the virtual impedance controller [p.u.]
$\boldsymbol{x}(t)$	The states of a general state space model
x_f	Converter side filter inductance of a LCL-filter [p.u.]
x_g	Grid side filter inductance of a LCL-filter [p.u.]
x_p	The resulting inductance of the two inductances of the LCL-filter connected in parallel [p.u.]
$\boldsymbol{y}(t)$	The outputs of a general state space model
y_f	Filter capacitance of a LCL-filter [p.u.]
y_k	The output signal at time-step k of a difference equation
z	The z-transform variable
Z_n	Base impedance [Ω]

List of Abbreviations

ABB	Asea Brown Boveri Ltd
AC	Alternating Current
ARMAX	Autoregressive moving average model with exogenous inputs
CAN	Controller Area Network
DC	Direct Current
DSP	Digital Signal Processor
EBL	Energibedriftenes Landsforening (Norwegian Electricity Industry Association)
EEPROM	Electrically Erasable Programmable Read-Only Memory
IEEE	Institute of Electrical and Electronics Engineers
IEC	International Electrotechnical Commission
IGBT	Insulated Gate Bipolar Transistor
LEM	Liaisons Electroniques-Mécaniques
MMACS	Million Multiply Accumulate Cycles per Second
NFR	Norges Forskningråd (The Research Council of Norway)
NORPIE	Nordic Workshop on Power and Industrial Electronics
NVE	Norges vassdrags- og energidirektorat (The Norwegian Water Resources and Energy Directorate)
NTNU	Norges Teknisk-Naturvitenskapelige Universitet (Norwegian University of Science and Technology)

PSS/E	Power System Simulator for Engineering
p.u.	Per Unit
PWM	Pulse Width Modulation
RMS	Root Mean Square
RPM	Rotations Per Minute
RS-232	Recommended Standard 232
SINTEF	Stiftelsen for industriell og teknisk forskning ved Norges tekniske høgskole (The foundation for industrial and technical research at Norwegian Institute of Technology)
TSO	Transmission System Operator
UPS	Uninterruptable Power Supply

Introduction

Distributed power generation

Distributed power generation with small scale producers is an emerging trend in the power grid. These producers often utilizes renewable power sources such as windmills and solar panels.

Other small scale producers of power are industrial processes that can generate power for a very small cost as a side effect of the process. Steam turbine generators powered by the waste heat from furnaces are well known.

These producers need to deliver energy to the main grid. A flexible way of delivering power is connecting to the grid using pulse width modulated (PWM) converters.

Grid connected pulse width modulated converters; possibilities and limitations.

A PWM converter with intelligent control can be controlled to give any current waveform to the grid. They enable optimization of the control of both the local power source and of the connection to the grid.

If the connection to the main grid is broken, the grid connected PWM converters can be operated in island mode. The load is shared using droop control for voltage and frequency. No further communication is strictly neccessary. Weak grids can also be boosted.

The power flow of the converter is bidirectional. This means that it can draw power from the grid as well. This can be useful to provide the DC-link with power if the generator is off-line. The DC-link can have local consumers attached which need more power than the generator provides, or the link can provide startup power for the power generation process. If the DC-link has local storage capabilities, the power draw can also be used to reduce temporary overvoltages on the grid.

The LCL-filter used between the power switches (IGBTs) and the grid

can be minimized by introducing active filter damping in the control algoritm. A grid connected converter can also be operated as an active power conditioner. It works as an active filter by reducing the voltage harmonics, and as a phase compensator by stabilizing the voltage magnitude. Voltage symmetry can be improved.

The converter can even continue to run during a voltage dip of the grid, caused by for example a short circuit. Note that due to the sudden reduction of delivered power to the grid, the power source can make the DC-link voltage rise to an unacceptable level. This extra energy must either be stored or burned away locally.

The main limitation of the PWM-converter is the switching frequency. The switching frequency is limited by the switching losses of the IGBTs. It causes a time delay from the measurement of signals to the output voltage is updated. This time delay will limit the bandwidth of any controller.

A related limitation of the converter is the requirement for a low-pass filter to smoothen the voltage output. The ripple current induced by the switching output voltage and the bandwidth of the controller dictate the minimum size of the these filter components.

Using cybernetic theory and tools to influence the output impedance of a PWM-converter has been known in the UPS marked since the 1980's. Varying this impedance according to operational situations has been known the last ten years. This thesis implements a virtual impedance and shows its effect on the converters' current response. By varying the impedance in the voltage period, the current response can be shaped to give different responses for active and reactive currents.

New netstandards

The trend of distributed small scale power producers has created new demands for connecting to the grid. A specification has been made targetting these small-scale plants, giving guidelines for wind farms greater than 10 MVA [1]. This specification include toleration limits of faults in the grid.

Contrary to the old regulations, where a distributed power producer must disconnect when the grid voltage dropped below 70 - 80 % of nominal value, the new netstandard states that all producers shall remain connected and produce reactive current even if the voltage drops to 15 % for 0.5 s. Different countries have different numbers, but the principle is the same. These demands can be met by using grid side pulse width modulated converters.

Industrial context

The work in this thesis are included as a part of a large research program called "Weight reduced windgenerator systems." This research program is sponsored by EBL, Statkraft, NVE, Lyse, Shell, Wärtsilä, SmartGenerator and NFR.

The research program focus on wind power systems where all aspects from the turbineshaft to the grid connection are evaluated. The program includes development of PSS/E models of the wind power system. The focus for the work in this thesis was to develop and test novel control methods for a wind power system in a small scale laboratory test.

A paper describing wireless load sharing optimized for non-linear loads for single phase converters was released at the NORPIE conference in 2002 [2].

Contributions

The main contributions in this thesis are:

- Implementation of an interperiodic time varying virtual impedance. This impedance enables better individual control over the response to active and reactive currents.
- Empirically creating a map of the active and reactive current response to show the effect of the virtual impedance for the current response of the converter.
- Using said map to find a good decoupling for the current into a magnitude part and a phase part, and also to find a good feed forward signal for a current regulator.
- Experiments indicating that the grid side converter controller similar to the one developed in this thesis can be used to meet the guidelines given by a new net standard.

Outline of this thesis

Chapter 1 presents an overview of the grid side converter system. A three phase pulse width modulation unit including different switching patterns is introduced, and a per unit model of a three phase LCL-filter is derived. Some important implementation details for the converter system are also given.

Chapter 2 describes the laboratory setup for the test system used in this thesis. The different parts of the setup is described in detail, and the per unit system and the state space model for the test system is presented.

Chapter 3 introduces a voltage observer which is used to find the phase and amplitude of a three phase voltage measurement.

Chapter 4 presents a voltage controller which regulates the filter capacitor voltage. It includes active dampening, voltage shape control and virtual impedance. Of particular interest is the implementation of an interperiodic time varying virtual impedance.

Chapter 5 uses the voltage controller presented in chapter 4 together with current feedback signals to control the active and reactive power delivered by the converter. This is done by using the measured converter current to create an amplitude and frequency reference for a three phase voltage generator which feed its generated signal to the voltage controller.

Chapter 6 uses the active and reactive power controller presented in chapter 5 to implement droop control. This droop control enables a converter to run in parallel with other converters or synchronous machine generators.

Chapter 7 gives evidence that the grid converter presented in this thesis can be used to implement the grid codes given by the transmission system operator of Norway, Statnett.

Chapter 8 gives a summary and proposes future work.

Some general mathematical tools used in this thesis is presented in the appendices.

CHAPTER 1

System description

This chapter presents an overview of the grid converter system. An introduction to a general three phase pulse width modulator unit is given. A per unit model is developed for a LCL-filter, and implementation details of a grid side converter unit are discussed.

1.1 Overview

The grid side converter used in this thesis is comprised of a three phase PWM converter connected to a LCL-filter. Figure 1.1 shows an overview of the controller and the physical system. v_0 and ω_0 are the nominal voltage magnitude and frequency. $P_{g,0}$ and $Q_{g,0}$ are the active and reactive power output reference for nominal operation. $\boldsymbol{v}_f^{abc}$ and $\boldsymbol{i}_f^{abc}$ are the measured capacitor voltage and capacitor current of the LCL-filter. $\boldsymbol{i}_e^{abc}$ is the measured converter output current. v_{DC} is the measured DC-link voltage. $\boldsymbol{v}_{\text{PWM}}^{\alpha\beta}$ is the output from the controller to the PWM-unit.

The controller can be split further into parts. Figure 1.2 shows an overview of the different parts of the controller. The parts of the controller are presented in the coming chapters.

1.2 The pulse width modulator

The pulse width modulator (PWM) unit has become a very common component in power electronics. An introduction with emphasis of the peculiarities of a three phase PWM unit is given here. A much more thorough investigation can be found in e.g. Holmes [3].

The basic idea behind the PWM unit is to use transistors to periodically switch a voltage between the two levels of the DC bus such that the average

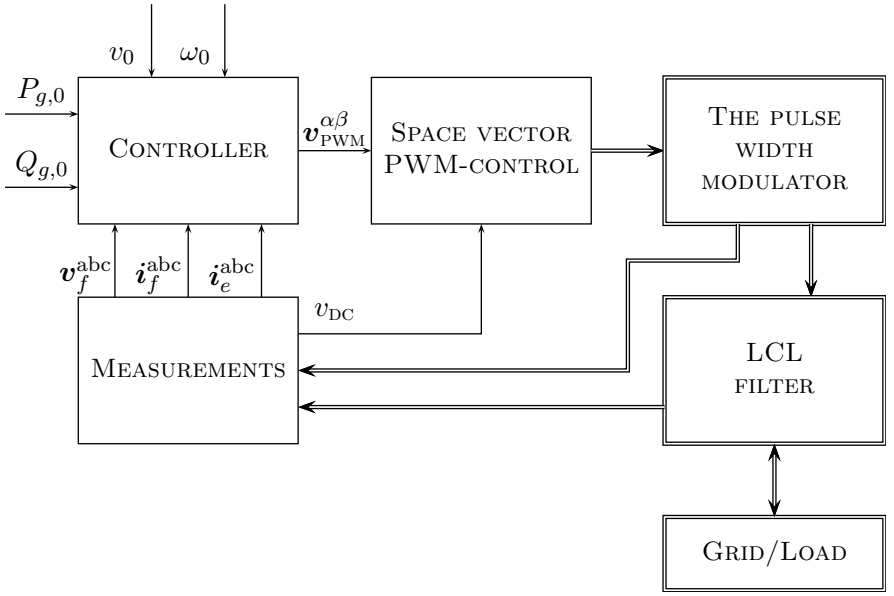

Figure 1.1 – Overview of the converter system. Physical parts of the system are marked using double lines.

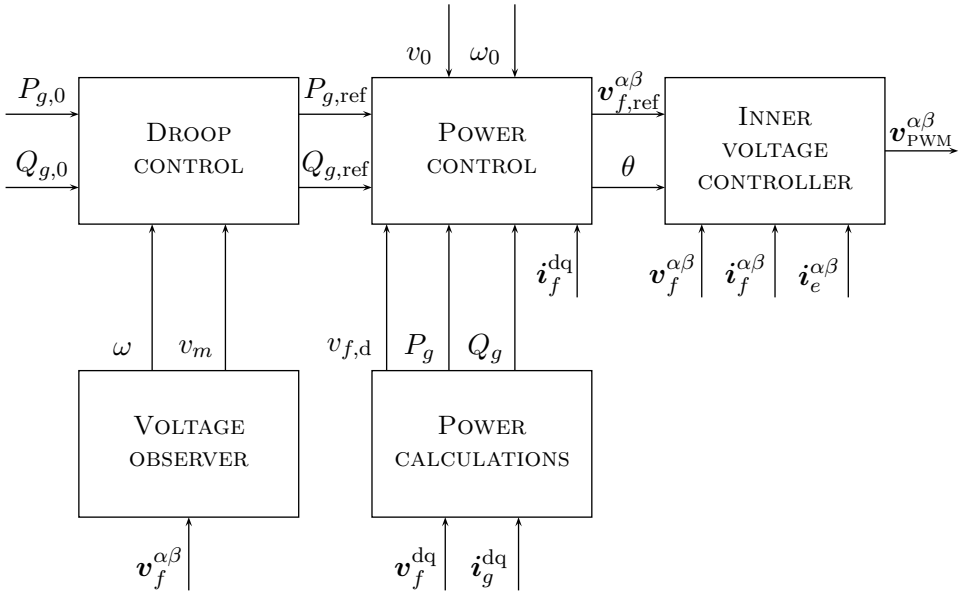

Figure 1.2 – Overview of the controller of the converter. The coordinate transformations are not included in the figure.

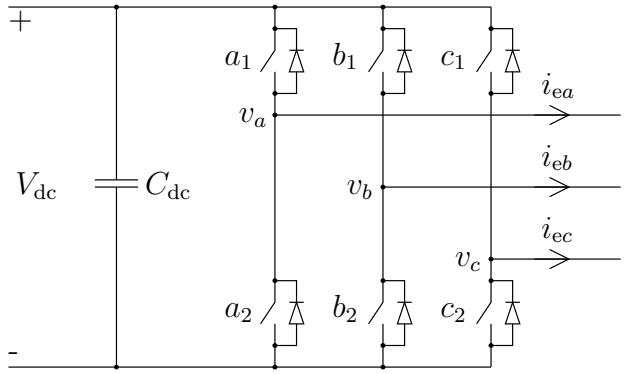

Figure 1.3 – A three phase pulse width modulator unit.

of the signal becomes the required output voltage. The word output has been chosen here to indicate the positive sign of the current flow which is out from the DC bus. The use of transistors enables current and thus power to flow in as well as out from the DC bus, unlike e.g. a thyristor rectifier.

Figure 1.3 shows an idealized model of the unit. One or more capacitors are normally connected to the DC link to provide a relatively stable voltage, and has been included in the figure.

The negative DC link voltage is defined in this thesis as the reference voltage (i.e. zero voltage). Another practice sometimes encountered in the litterature is the use of the "middle" voltage potential of the capacitor as the reference voltage. That would have given a positive link voltage of $\frac{1}{2}v_{\mathrm{DC}}$ and negative link voltage of $-\frac{1}{2}v_{\mathrm{DC}}$.

The two transistors and their corresponding diodes connecting the DC link to a output of the converter are called a leg of the converter. It can be in one of four states depending on the states of its transistors. In particular, consider leg a:

1. If a_1 is on and a_2 is off, the voltage v_a will be v_{DC}.

2. If a_1 is off and a_2 is on, the voltage v_a will be 0.

3. If both are off, the voltage will still be clamped by the diodes to be between 0 and v_{DC} depending on the load current.

4. If both are on, this will cause a short of the DC link through the transistor, possibly burning them out. This is called shoot-through and must be avoided.

Table 1.1 – Transistor configurations for a three-phase PWM converter.

l_a	l_b	l_c	v_a	v_b	v_c	v_α	v_β	v_0
0	0	0	0	0	0	0	0	0
0	0	1	0	0	v_{DC}	$-\frac{1}{3}v_{\mathrm{DC}}$	$-\frac{\sqrt{3}}{3}v_{\mathrm{DC}}$	$\frac{1}{3}v_{\mathrm{DC}}$
0	1	0	0	v_{DC}	0	$-\frac{1}{3}v_{\mathrm{DC}}$	$\frac{\sqrt{3}}{3}v_{\mathrm{DC}}$	$\frac{1}{3}v_{\mathrm{DC}}$
0	1	1	0	v_{DC}	v_{DC}	$-\frac{2}{3}v_{\mathrm{DC}}$	0	$\frac{2}{3}v_{\mathrm{DC}}$
1	0	0	v_{DC}	0	0	$\frac{2}{3}v_{\mathrm{DC}}$	0	$\frac{1}{3}v_{\mathrm{DC}}$
1	0	1	v_{DC}	0	v_{DC}	$\frac{1}{3}v_{\mathrm{DC}}$	$-\frac{\sqrt{3}}{3}v_{\mathrm{DC}}$	$\frac{2}{3}v_{\mathrm{DC}}$
1	1	0	v_{DC}	v_{DC}	0	$\frac{1}{3}v_{\mathrm{DC}}$	$\frac{\sqrt{3}}{3}v_{\mathrm{DC}}$	$\frac{2}{3}v_{\mathrm{DC}}$
1	1	1	v_{DC}	v_{DC}	v_{DC}	0	0	v_{DC}

Leg b and leg c are of course identical to leg a.

Each leg is normally in one of the first two states for most of the switching period. Only considering these two normal states per leg gives a total of 8 states for the converter. Table 1.1 shows the output voltages for different transistor configurations. l_a, l_b, and l_c are logic variables giving the state of the individual leg. I.e. when l_a is 1, transistor a_1 is closed, and when l_a is 0, a_2 is closed.

By periodically alternating between the two normal states of a leg, the average of the output voltage can be controlled. Deciding when to switch between the upper and lower transistor can be done by using a triangle signal and a comparator. Figure 1.4 shows the principle of the symmetrical switching pattern. A counter counts from 0 up to $r_{\max}$ and down again using a fixed timer base. The counter is compared to a value r_a. When the value is greater the lower transistor a_2 is switched on, and when lesser the higher transistor a_1 is switched on*. Similarly, values r_b and r_c are compared against the same counter for the b and c leg. The comparison and the corresponding transistor control signal generation is a supported feature for all microcontrollers used for converter control.

Normally the period of the triangle signal, T, is held constant. However, there exists switching schemes that involves changing the period. One example is lowering the frequency to lessen the switching losses and thus the temperature of the transistors when the system is running in overload conditions. Another example is adding a randomized factor to the period to spread the acoustic noise and to spread electromagnetic noise caused by the switching over a wider area of the frequency spectrum.

*Sometimes the control signals of the upper and lower transistor are swapped. If this is the case, the comparison values can be changed to $r_{\max} - r_{(\cdot)}$.

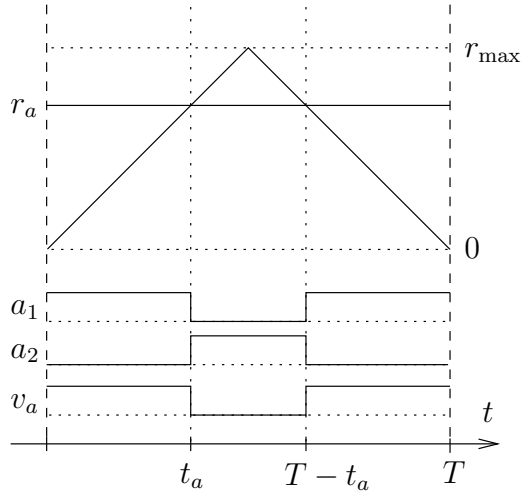

Figure 1.4 – The symmetric switching pattern.

The average output voltages are given as

$$\begin{aligned} \bar{v}_a &= \frac{r_a}{r_{\max}} v_{\mathrm{DC}} = \frac{2t_a}{T} v_{\mathrm{DC}} = d_a v_{\mathrm{DC}}, \\ \bar{v}_b &= \frac{r_b}{r_{\max}} v_{\mathrm{DC}} = \frac{2t_b}{T} v_{\mathrm{DC}} = d_b v_{\mathrm{DC}}, \\ \bar{v}_c &= \frac{r_c}{r_{\max}} v_{\mathrm{DC}} = \frac{2t_c}{T} v_{\mathrm{DC}} = d_c v_{\mathrm{DC}}, \end{aligned} \tag{1.1}$$

where the ratios d_a, d_b, and d_c are the PWM duty cycle ratios.

Thus, to get a particular output voltage from the converter, the duty cycles should be set to

$$d_a = \frac{\bar{v}_a}{v_{\mathrm{DC}}}, \qquad d_b = \frac{\bar{v}_b}{v_{\mathrm{DC}}}, \qquad d_c = \frac{\bar{v}_c}{v_{\mathrm{DC}}}. \tag{1.2}$$

A very straight forward switching pattern can be implemented by setting the (average) null system to $\frac{v_{\mathrm{DC}}}{2}$. For a three phase signal, this gives a maximum amplitude of $\frac{v_{\mathrm{DC}}}{2}$.

1.2.1 The space vector switching pattern

Normally the null system of the output voltages is of no interest. Recognizing this hints at the possibility to increase the maximum amplitude.

Figure 1.5 shows the relationship of the different transistor configurations of table 1.1 and the $\alpha\beta$-coordinate system. Here, $\boldsymbol{v}_{0^\circ}^{\alpha\beta}$ is the $\alpha\beta$-vector

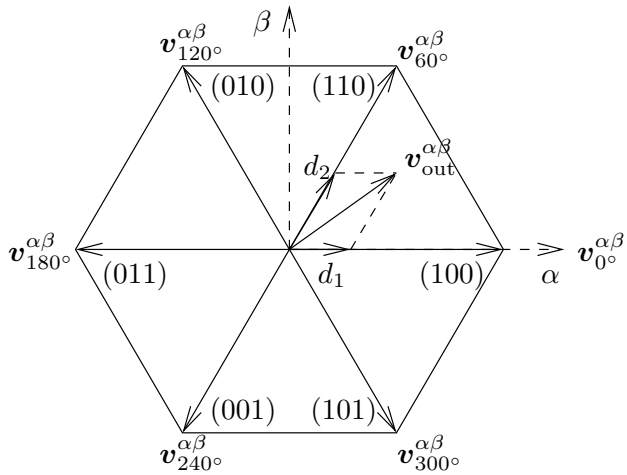

Figure 1.5 – The basic space vectors in the $\alpha\beta$-coordinate system.

given by the table entry for the 100 configuration, i.e. $l_a = 1$, $l_b = 0$, and $l_c = 0$. $\boldsymbol{v}^{\alpha\beta}_{60^\circ}$ is the $\alpha\beta$-vector for the 110 configuration and so on. The two configurations 000 and 111 is not shown in the figure, as they only contributes to the null system.

The output voltage can be calculated from the time spent in each configuration. If it e.g. stays in the 001 configuration for the whole switching period, the output voltage would be

$$\boldsymbol{v}^{\alpha\beta 0}_{\text{out}} = \boldsymbol{v}^{\alpha\beta 0}_{240^\circ} = \begin{bmatrix} -\frac{1}{3} \\ -\frac{\sqrt{3}}{3} \\ \frac{1}{3} \end{bmatrix} v_{\text{DC}}. \tag{1.3}$$

The wanted output $\alpha\beta$-vector can be decomposed into the two nearest neighbouring transistor configuration vectors. E.g. for the output vector in figure 1.5

$$\boldsymbol{v}^{\alpha\beta}_{\text{out}} = d_1 \boldsymbol{v}^{\alpha\beta}_{0^\circ} + d_2 \boldsymbol{v}^{\alpha\beta}_{60^\circ} = \begin{bmatrix} \frac{2d_1 + d_2}{3} \\ -\frac{\sqrt{3} d_2}{3} \end{bmatrix} v_{\text{DC}}. \tag{1.4}$$

When not in either of these configurations, the transistors are either in the 000 or 111 configuration, which just contributes to the null-component. The time in each of these configurations are often split evenly.

Figure 1.5 shows that the maximum magnitude of the $\alpha\beta$-vector, and thus the maximum output voltage amplitude, is limited by the inner radius of the hexagon. The height of one of the equilateral triangle sectors gives

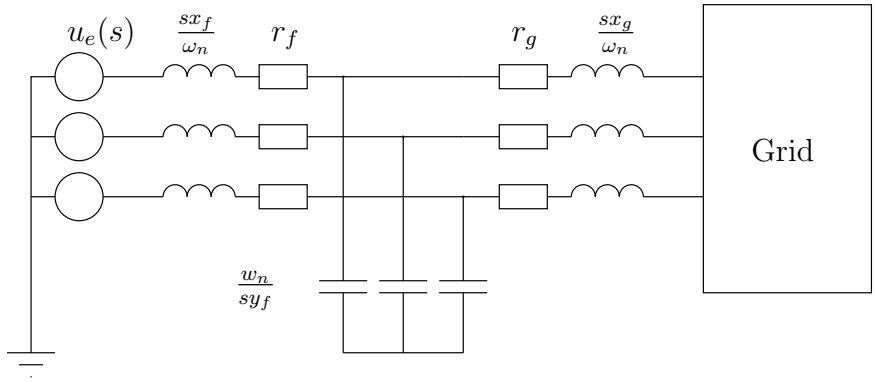

Figure 1.6 – A three phase LCL-filter.

the maximum output voltage amplitude for a sinusoidal signal as

$$v_{\max} = \frac{1}{\sqrt{3}} v_{\mathrm{DC}} \approx 0.57735 v_{\mathrm{DC}}. \tag{1.5}$$

Note that this is not the peak-to-peak value, but the maximum amplitude of a single phase. The maximum output phase-to-phase value is v_{DC}.

This switching pattern are called the space vector switching pattern, and increases the maximum amplitude of the output voltage amplitude by approximately 28.9 % compared to the "naïve" symmetrical switching pattern.

The null system for a three phase sinusoidal output voltage using this space vector switching pattern is a triangle signal. The higher harmonics of this triangle signal could create unwanted parasitic effects due to e.g. capacitive couplings towards ground. To avoid these effects another switching pattern is sometimes used which injects only the third harmonic component of the space vector triangle signal. This switching pattern has a maximum amplitude which is the same as the space vector switching pattern for a purely sinusoidal output signal.

1.3 The LCL-filter

Figure 1.6 shows the topology of the three phase LCL-filter. The grid is drawn as a box in the figure as its configuration is unknown.

There are two main concerns when choosing the component sizes for the LCL-filter. The ripple current through the inductor between the converter and the capacitor must be kept reasonable. A reasonable choice is for this current to be between 20 % and 50 % of the fundamental harmonic current at nominal operation.

Table 1.2 – Grid side unit ratings.

Parameter	Symbol
Rated line voltage	$V_{n,\text{RMS}}$
Rated apparent power	$S_n = \sqrt{3} V_{n,\text{RMS}} I_{n,\text{RMS}}$
Nominal frequency	f_n
Rated current	$I_{n,\text{RMS}} = \frac{S_n}{\sqrt{3} V_{n,\text{RMS}}}$

Another dimensioning factor is the resonance frequency of the filter when the grid is very strong or short circuited. The resulting resonance frequency must be below the bandwidth of the active damping of the PWM-controller.

Typical values are around 0.05 p.u.[†] for both inductors, and 0.15 p.u. for the capacitor of the LCL-filter.

For more information about filter design there are many sources. For grid connected converters, IEEE has released a standard IEEE 519-1992 [4] entitled "IEEE Recommended Practices and Requirements for Harmonic Control in Electric Power systems." See e.g. Pradeep [5] for optimized filter design in the context of IEEE 519 compliant grid connected converters.

1.4 The three-phase converter model

A model is needed to be able to analyse the converter. By using a per unit system, the model variables are scaled as fractions of defined base units. This makes the model independent of scale, and will also facilitate any software implementation of the control by avoiding numerical problems.

As the configuration of the grid is unknown, it is modelled as voltage inputs. These inputs can then be made dependent of e.g. the grid current to model different load conditions.

1.4.1 The per unit system

A per unit system of a three phase power electronic device can be created from its rated line voltage and rated apparent power as well as the nominal grid frequency. Typical rating parameters are listed in table 1.2. These are used to create the per unit system summarized in table 1.3. The base inductance and base capacitance are often not explicitly expressed, but are included here for completeness.

[†]The per unit system is presented below in section 1.4.1.

Table 1.3 – Grid side unit per unit system.

Parameter	Symbol
Base voltage (peak phase voltage)	$\hat{V}_n = \sqrt{\frac{2}{3}} V_{n,\mathrm{RMS}}$
Base current	$\hat{I}_n = \sqrt{2} I_{n,\mathrm{RMS}}$
Base angular frequency	$\omega_n = 2\pi f_n$
Base impedance	$Z_n = \frac{\hat{V}_n}{\hat{I}_n} = \frac{V_{n,\mathrm{RMS}}}{\sqrt{3} I_{n,\mathrm{RMS}}}$
Base inductance	$L_n = \frac{Z_n}{\omega_n} = \frac{V_{n,\mathrm{RMS}}}{\sqrt{3} I_{n,\mathrm{RMS}} 2\pi f_n}$
Base capacitance	$C_n = \frac{1}{Z_n \omega_n} = \frac{\sqrt{3} I_{n,\mathrm{RMS}}}{V_{n,\mathrm{RMS}} 2\pi f_n}$

Table 1.4 – Grid side unit parameters.

Parameter	Physical size symbol	Per unit symbol
Converter side filter inductance	L_f	x_f
Converter side filter resistance	R_f	r_f
Filter capacitance	C_f	y_f
Grid side filter inductance	L_g	x_g
Grid side filter resistance	R_g	r_g

1.4.2 The PWM-unit model

As the LCL-filter smoothens out the output voltage of the PWM unit, it can simply be modelled as three voltage sources giving an output voltage equal to the reference voltage.

Be aware that pulse width modulation introduces a time delay from the reference is set until the output is updated. This time delay must be included in a model when investigating higher frequencies.

The output voltages are limited by the DC-link voltage, which means that the voltage sources should also be limited when simulating the system.

1.4.3 The LCL-filter model

The parameters of the grid side unit are the inductances and capacitance of its LCL-filter. The physical parameters and their per unit counterparts are listed in table 1.4.

The relation between currents and voltages in the filter can be found

using Ohm's law:

$$\boldsymbol{v}_e^{abc} - \boldsymbol{v}_f^{abc} = \left(\frac{s}{\omega_n}\boldsymbol{x}_f^{abc} + \boldsymbol{r}_f^{abc}\right)\boldsymbol{i}_e^{abc}, \tag{1.6}$$

$$\boldsymbol{v}_f^{abc} - v_{f,n}\boldsymbol{q}^{abc} = \frac{\omega_n}{s}\left(\boldsymbol{y}_f^{abc}\right)^{-1}\boldsymbol{i}_f^{abc}, \tag{1.7}$$

$$\boldsymbol{v}_f^{abc} - \boldsymbol{v}_g^{abc} = \left(\frac{s}{\omega_n}\boldsymbol{x}_g^{abc} + \boldsymbol{r}_g^{abc}\right)\boldsymbol{i}_g^{abc}, \tag{1.8}$$

where $v_{f,n}$ is the voltage of the star point of the capacitors, and

$$\boldsymbol{x}_f^{abc} = \begin{bmatrix} x_{f,a} & 0 & 0 \\ 0 & x_{f,b} & 0 \\ 0 & 0 & x_{f,c} \end{bmatrix}, \qquad \boldsymbol{x}_g^{abc} = \begin{bmatrix} x_{g,a} & 0 & 0 \\ 0 & x_{g,b} & 0 \\ 0 & 0 & x_{g,c} \end{bmatrix}, \tag{1.9}$$

$$\boldsymbol{y}_f^{abc} = \begin{bmatrix} y_{f,a} & 0 & 0 \\ 0 & y_{f,b} & 0 \\ 0 & 0 & y_{f,c} \end{bmatrix}, \qquad \boldsymbol{q}^{abc} = \begin{bmatrix} 1 \\ 1 \\ 1 \end{bmatrix}. \tag{1.10}$$

Kirchoffs current law gives the relations between the currents as

$$\boldsymbol{i}_g^{abc} = \boldsymbol{i}_e^{abc} - \boldsymbol{i}_f^{abc}, \tag{1.11}$$

$$0 = \left(\boldsymbol{q}^{abc}\right)^{\mathrm{T}}\boldsymbol{i}_f^{abc}, \tag{1.12}$$

$$0 = \left(\boldsymbol{q}^{abc}\right)^{\mathrm{T}}\boldsymbol{i}_e^{abc}. \tag{1.13}$$

If the parameters of the corresponding components in the filter are different in each phase, the system is said to be unsymmetric. Solving these equations to make them linearly independent in this case gives rather complex equations. However, converting the equations to the $\alpha\beta$-coordinate system and assuming that the system is symmetric greatly simplifies them.

A linear state space equation of a multivariable system can be written in the time plane as

$$\begin{aligned} \dot{\boldsymbol{x}}(t) &= \boldsymbol{A}\boldsymbol{x}(t) + \boldsymbol{B}\boldsymbol{u}(t), \\ \boldsymbol{y}(t) &= \boldsymbol{C}\boldsymbol{x}(t), \end{aligned} \tag{1.14}$$

where $\boldsymbol{x}(t)$ is the system state vector, $\boldsymbol{u}(t)$ the system input vector, and $\boldsymbol{y}(t)$ the system output vector. $\boldsymbol{A}$, $\boldsymbol{B}$, and $\boldsymbol{C}$ are real, normally time independent matrices.

Let the states, inputs and outputs of the LCL-filter in the $\alpha\beta$-coordinate system be

$$\boldsymbol{x}^{\alpha\beta} = \begin{bmatrix} \boldsymbol{i}_e^{\alpha\beta} \\ \boldsymbol{i}_f^{\alpha\beta} \\ \boldsymbol{v}_f^{\alpha\beta} \end{bmatrix}, \qquad \boldsymbol{u}^{\alpha\beta} = \begin{bmatrix} \boldsymbol{v}_e^{\alpha\beta} \\ \boldsymbol{v}_g^{\alpha\beta} \end{bmatrix}, \qquad \boldsymbol{y}^{\alpha\beta} = \begin{bmatrix} \boldsymbol{v}_f^{\alpha\beta} \\ \boldsymbol{i}_e^{\alpha\beta} \\ \boldsymbol{i}_f^{\alpha\beta} \\ \boldsymbol{i}_g^{\alpha\beta} \end{bmatrix}, \tag{1.15}$$

where the time dependence (t) has been dropped.

Assume the filter parameters to be symmetrical, i.e. $\boldsymbol{x}_f^{abc} = \boldsymbol{I}x_f$ etc. Then a state space model of the filter is

$$\begin{aligned} \dot{\boldsymbol{x}}^{\alpha\beta} &= \boldsymbol{A}^{\alpha\beta}\boldsymbol{x}^{\alpha\beta} + \boldsymbol{B}^{\alpha\beta}\boldsymbol{u}^{\alpha\beta}, \\ \boldsymbol{y}^{\alpha\beta} &= \boldsymbol{C}^{\alpha\beta}\boldsymbol{x}^{\alpha\beta}, \end{aligned} \tag{1.16}$$

where $\boldsymbol{A}^{\alpha\beta}$, $\boldsymbol{B}^{\alpha\beta}$, and $\boldsymbol{C}^{\alpha\beta}$ are

$$\boldsymbol{A}^{\alpha\beta} = \omega_n \begin{bmatrix} -\frac{r_f}{x_f} & 0 & 0 & 0 & -\frac{1}{x_f} & 0 \\ 0 & -\frac{r_f}{x_f} & 0 & 0 & 0 & -\frac{1}{x_f} \\ -\frac{r_f}{x_f} + \frac{r_g}{x_g} & 0 & -\frac{r_g}{x_g} & 0 & -\frac{1}{x_f} - \frac{1}{x_g} & 0 \\ 0 & -\frac{r_f}{x_f} + \frac{r_g}{x_g} & 0 & -\frac{r_g}{x_g} & 0 & -\frac{1}{x_f} - \frac{1}{x_g} \\ 0 & 0 & \frac{1}{y_f} & 0 & 0 & 0 \\ 0 & 0 & 0 & \frac{1}{y_f} & 0 & 0 \end{bmatrix}, \tag{1.17}$$

$$\boldsymbol{B}^{\alpha\beta} = \omega_n \begin{bmatrix} \frac{1}{x_f} & 0 & 0 & 0 \\ 0 & \frac{1}{x_f} & 0 & 0 \\ \frac{1}{x_f} & 0 & \frac{1}{x_g} & 0 \\ 0 & \frac{1}{x_f} & 0 & \frac{1}{x_g} \\ 0 & 0 & 0 & 0 \\ 0 & 0 & 0 & 0 \end{bmatrix}, \quad \boldsymbol{C}^{\alpha\beta} = \begin{bmatrix} 1 & 0 & 0 & 0 & 0 & 0 \\ 0 & 1 & 0 & 0 & 0 & 0 \\ 0 & 0 & 1 & 0 & 0 & 0 \\ 0 & 0 & 0 & 1 & 0 & 0 \\ 0 & 0 & 0 & 0 & 1 & 0 \\ 0 & 0 & 0 & 0 & 0 & 1 \\ 1 & 0 & -1 & 0 & 0 & 0 \\ 0 & 1 & 0 & -1 & 0 & 0 \end{bmatrix}. \tag{1.18}$$

Note that the α and β system are completely decoupled. This means that analysis of the combined $\alpha\beta$ system can be simplified to an analysis of a single phase system. Any coupling between the two systems comes as a result of the inputs, i.e. the converter or the grid voltage. In particular, an unsymmetric load will cause the systems to become coupled.

A state space model of the filter in the dq-coordinate system can be found by using equation A.29:

$$\begin{aligned} \dot{\boldsymbol{x}}^{\mathrm{dq}} &= \boldsymbol{A}^{\mathrm{dq}}\boldsymbol{x}^{\mathrm{dq}} + \boldsymbol{B}^{\mathrm{dq}}\boldsymbol{u}^{\mathrm{dq}}, \\ \boldsymbol{y}^{\mathrm{dq}} &= \boldsymbol{C}^{\mathrm{dq}}\boldsymbol{x}^{\mathrm{dq}}, \end{aligned} \tag{1.19}$$

where $\boldsymbol{A}^{\mathrm{dq}}$, $\boldsymbol{B}^{\mathrm{dq}}$, and $\boldsymbol{C}^{\mathrm{dq}}$ are:

$$\boldsymbol{A}^{\mathrm{dq}} = \omega_n \begin{bmatrix} -\frac{r_f}{x_f} & \Omega_r & 0 & 0 & -\frac{1}{x_f} & 0 \\ -\Omega_r & -\frac{r_f}{x_f} & 0 & 0 & 0 & -\frac{1}{x_f} \\ -\frac{r_f}{x_f} + \frac{r_g}{x_g} & 0 & -\frac{r_g}{x_g} & \Omega_r & -\frac{1}{x_f} - \frac{1}{x_g} & 0 \\ 0 & -\frac{r_f}{x_f} + \frac{r_g}{x_g} & -\Omega_r & -\frac{r_g}{x_g} & 0 & -\frac{1}{x_f} - \frac{1}{x_g} \\ 0 & 0 & \frac{1}{y_f} & 0 & 0 & \Omega_r \\ 0 & 0 & 0 & \frac{1}{y_f} & -\Omega_r & 0 \end{bmatrix}, \tag{1.20}$$

$$\boldsymbol{B}^{\mathrm{dq}} = \boldsymbol{B}^{\alpha\beta}, \quad \boldsymbol{C}^{\mathrm{dq}} = \boldsymbol{C}^{\alpha\beta}, \tag{1.21}$$

$$\Omega_r = \frac{\dot{\theta}}{\omega_n}. \tag{1.22}$$

As can be seen from equation 1.20, the d and q system states are coupled by a factor proportional to the frequency of the reference system.

The model of the ignored null system are simply

$$v_{f,0} = v_{g,0} = v_{e,0}, \qquad i_{f,0} = i_{g,0} = i_{e,0} = 0. \tag{1.23}$$

1.5 Grid side converter implementation details

This section gives general implementation details for a grid side converter.

1.5.1 Measurements of filter states

A grid side converter needs extra measurements compared to e.g. a motor drive. The capacitor or output voltages must be measured to know the state of the grid, and the capacitor currents must be measured to provide effective active damping.

The sensors add hardware complexity and lessens the system reliability against sensor failure. There exists methods to estimate both the capacitor currents and capacitor voltages using only the PWM output currents (see e.g. [6]), but these are not used in this thesis as they add implementation complexity and might introduce issues of their own.

For regulation purposes the phase shift for a measurement signal is very important. It is important that the bandwidth of the filter measurement channels are sufficient for the bandwidth of the regulator. The bandwidth of the regulator is typically quite close to the sampling frequency and thus the Nyquist frequency. A certain amount of aliasing of the measured signals is usually preferrable to a loss of phase. Using higher order filters are often tempting for anti-aliasing filters, but care must be taken as these higher order filters rapidly add a significant phase shift to the measured signal. A first order filter with the bandwidth set to around the Nyquist frequency is often sufficient.

1.5.2 The DC link

The task of the DC link is to be a short term energy storage. It should be of sufficient size to handle the induced ripple current from the PWM module, and also be able to handle any transients in the power regulation.

The internal diodes of the IGBTs will work as a diode rectifier against an active grid. This will cause a large inrush current when the converter is connected to the grid if the DC link is not precharged. The LCL-filter will limit this inrush current, but can cause the DC link voltage to significantly overshoot. To avoid this a precharger mechanism can be used, for example a resistor in series with the inrush current which can be short circuited by a contactor when the DC link has been charged.

A brake chopper can be used to avoid overvoltages, particularly if the grid side is disconnected or short circuited when a generator providing power to the DC bus is running at full power. The brake chopper burns off the excess power produced by the generator while the generator regulator ramps down the power generation. A properly designed brake chopper circuit can potentially also limit any overvoltage given by the inrush current discussed in the previous paragraph.

1.5.3 Protection functions

A robust grid side converter needs protection functions both for protection of the converter and loads on the grid.

Overcurrent protection

A large difference between the output voltage of the converter and the grid will cause a substantial current to flow. This can for example be caused by a short circuit of the grid, or if the converter is running out of phase with

the grid. Being often only of a transient nature, such currents should not immediately disable the converter.

To avoid damage to the converter the currents must nevertheless be limited. This can be done by temporary turning off both transistors connected to the phase output which have the overcurrent until the current is below the disable limit again.

As a worst case example, assume the grid is ideally shorted out. If the positive DC bus voltage be connected to phase a, and the negative DC bus voltage be connected to phase b and phase c, this gives an output voltage of

$$\boldsymbol{v}^{\alpha\beta} = \mathbf{T}_{abc}^{\alpha\beta}\boldsymbol{v}^{abc} = \frac{1}{3}\begin{bmatrix} 2 & -1 & -1 \\ 0 & \sqrt{3} & -\sqrt{3} \end{bmatrix}\begin{bmatrix} v_{\mathrm{DC}} \\ 0 \\ 0 \end{bmatrix} = \begin{bmatrix} \frac{2}{3}v_{\mathrm{DC}} \\ 0 \end{bmatrix}. \tag{1.24}$$

If the resistance of the inductances is ignored, this gives an output current of

$$\boldsymbol{i}_e^{\alpha\beta}(t) = \frac{\omega_n}{x_f}\int_0^t \boldsymbol{v}^{\alpha\beta}dt + \boldsymbol{i}_e^{\alpha\beta}(0). \tag{1.25}$$

Here, the β-current is unchanged, as can be expected. The α-current, however, is

$$i_{e,\alpha}(t) = \frac{2\omega_n v_{\mathrm{DC}}}{3x_f}t + i_{e,\alpha}(0). \tag{1.26}$$

To cut the current after it has risen beyond a given threshold, the comparator must detect it in

$$t_{\mathrm{detect}} = (i_{\text{absolute-max}} - i_{\mathrm{threshold}})\frac{3x_f}{2\omega_n v_{\mathrm{DC}}}. \tag{1.27}$$

Given some typical values: $x_f = 5\%$, $\omega_n = 314.15$ rad s^{-1}, $v_{\mathrm{DC}} = 2$, and a difference in current of 10%, this gives a detection time limit of 11.9 µs. In other words, a monitoring frequency of at least 83.8 kHz.

A monitoring frequency of 83.8 kHz is quite taxing, but can still be considered within the limits of a modern microcontroller. This is a very conservative limit as it does not take the resistances and grid inductance into account, so the requirements can be lowered some.

Note that some microcontrollers taylored for the power electronics market have a built-in capability to disable individual transistor pairs dependent on external signals. This capability in combination with e.g. external comparators enables a much simpler solution at the cost of some hardware.

Even with a good software solution of this protection, it is also good practice to include a hardware detection circuit in addition to the software

solution for protection of the converter against software failures or even faster current transients. Such a detection circuit will typically shut off all three phases of the converter as a last effort to protect it.

DC-overvoltage protection

The power flow of a converter is bidirectional. This means that it is possible to feed power to the DC link, making its voltage level rise.

Software protection can be used to reduce or reverse the power flow to the DC link from the grid if the link voltage rises above a certain level. However, in case of both hardware and software faults a hardware high DC voltage detection circuit should be included. This will normally shut off the transistors of all three phases of the converter, but keep any braking chopper running to help limit the overvoltage.

Overtemperature protection

If the cooling of the converter is insufficient, the temperature of some of the components of the converter will rise above their maximum recommended operating temperature. This can be caused by running the converter in an overload situation. When the temperature rises above a certain level, an operator can be notified so corrective action can be taken. Depending upon the application, it can be desirable to automatically reduce the power. At an even higher temperature level, the system is normally tripped to avoid damage.

The timeconstants for the temperature monitoring is large, typically seconds or even minutes.

CHAPTER 2

Laboratory setup

An example system was set up to illustate the concepts and validate the different theories in this thesis. This chapter introduces this setup.

2.1 Overview

The laboratory equipment consists of two converters, a synchronous generator, various test loads and diode bridges. Transformators are used for galvanic separation and transformation of voltages. A typical setup for an experiment showing the various laboratory equipment is shown in figure 2.1. The source voltages for the diode bridges and the asynchronous drive voltages are only indicated using dashed lines with a double arrow.

2.2 The grid converter system

The grid side converters are the most important part of the setup, as they are the focal point of this thesis. The system consists of two converters which can be connected together or to a grid through a LCL filter. It is also possible to run one of the converters as a generator drive to create a full generator to grid drive train.

The two converters with their LCL filters are put into a cabinet for ease of use and mobility. Figure 2.2 shows a picture of the cabinet.

2.2.1 The pulse width modulated converters

The two main components of the setup is two 2-level PWM converters developed and built by NTNU in cooperation with SINTEF Energy AS. They have six IGBTs for the three outputs, with an additional IGBT for a brake

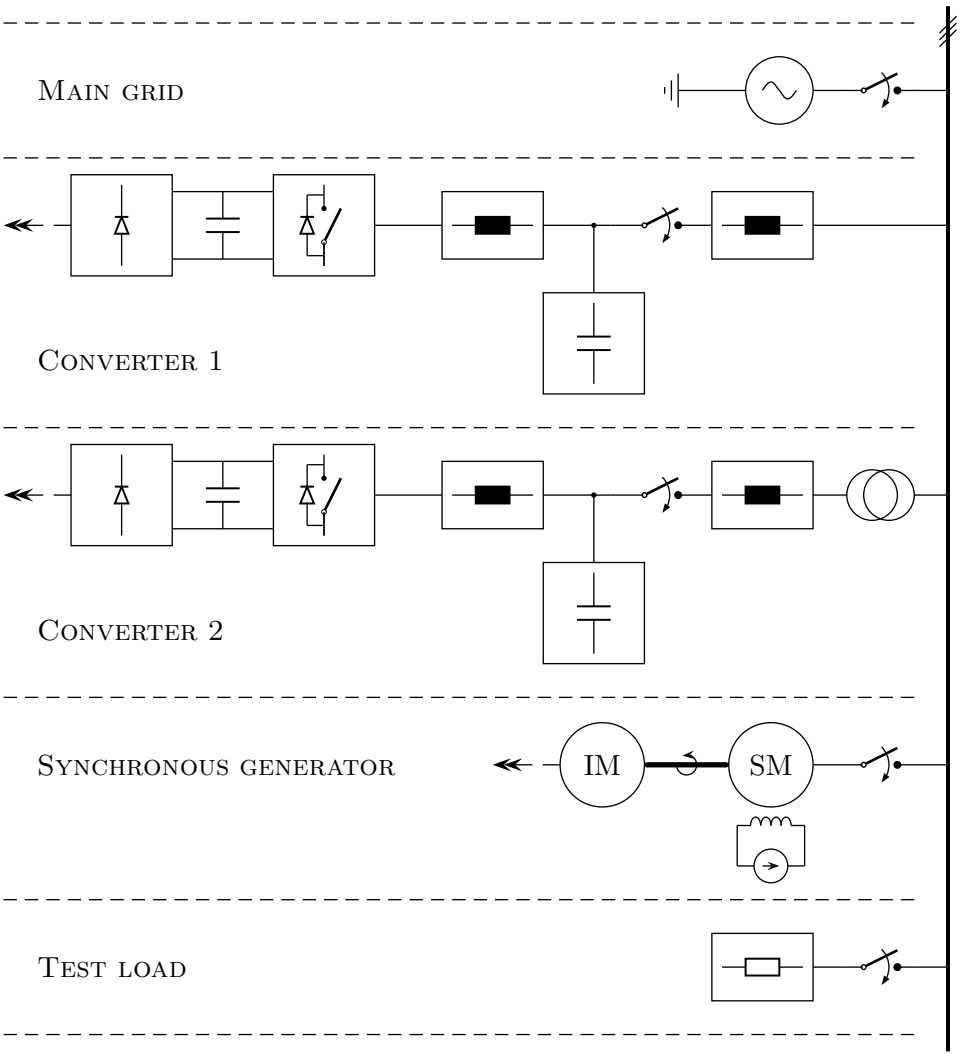

Figure 2.1 – Overview of typical laboratory setup for running two converters with LCL-filters in parallel with a synchronous generator or the main grid.

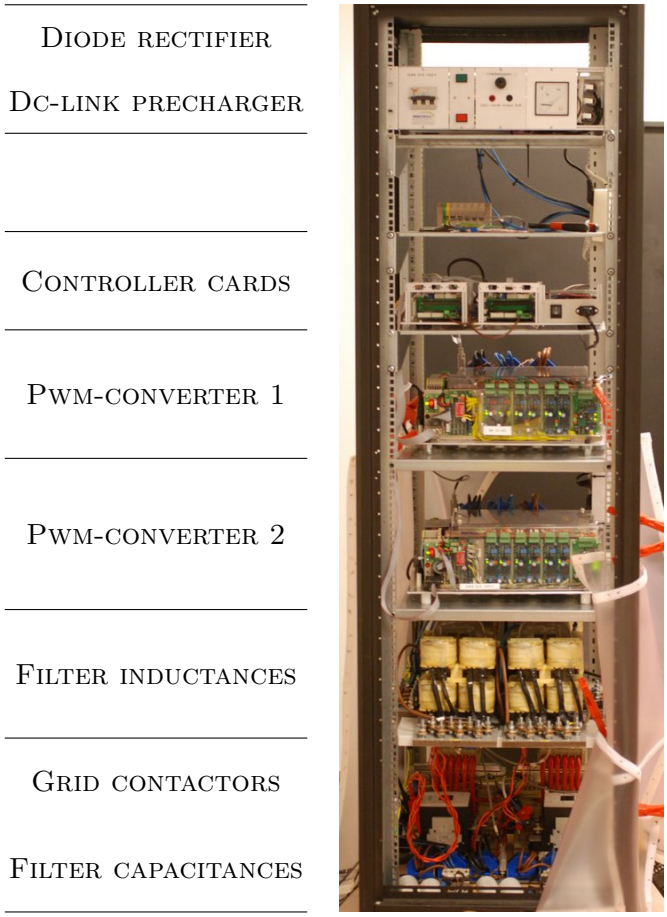

Figure 2.2 – Picture of the grid converter cabinet. The contents of each of the cabinet shelves are described to the left.

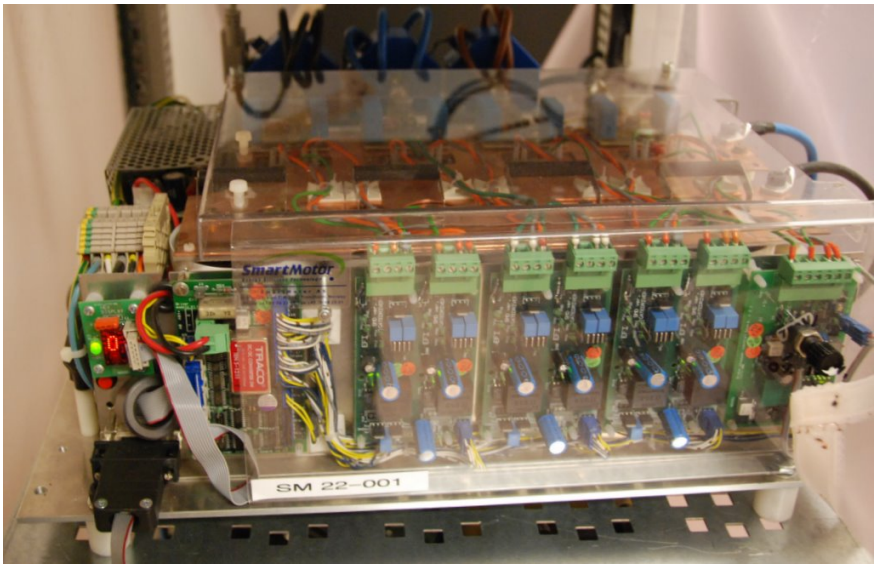

Figure 2.3 – Closeup picture of a PWM converter. The current measurement sensors can be seen in the background.

chopper output. The converter is rated for up to 760 V DC, with a DC bus capacitance of 3300 µF. The IGBTs used for the chopper outputs are rated for 1200 V and 400 A. Figure 2.3 shows a picture of one of the converters.

The converters have gate drivers with built-in hardware blanking time generation, in addition to protection for overcurrents, overvoltages and overtemperature. They interface individually with an external DSP/microcontroller board through an external cable containing the pulse width modulation signals and controller signals for the supervision circuits.

The controller card is built around a DSP from Texas Instrument named TMS320F2812. It is a 32-bit, fixed point, 150 MHz, 1.9 V low power DSP capable of up to 150 MMACS*. In addition to the DSPs internal 36 KiB of ram and 256 KiB of flash memory, the board is fitted with an additional 256 KiB of external memory and a 8 KiB EEPROM.

The DSP has a built-in 12 bit analog to digital converter with a minimum conversion time of 80 ns. However, internal noise in the DSP lowers the actual analog to digital converter resolution to about 10 bits. The board has four inputs for connecting current signals from current or voltage sensors, but more signals are possible by using an extra measurement expansion card. This card has four extra current signal inputs. Figure 2.4 shows a

*Million Multiply Accumulate Cycles per Second

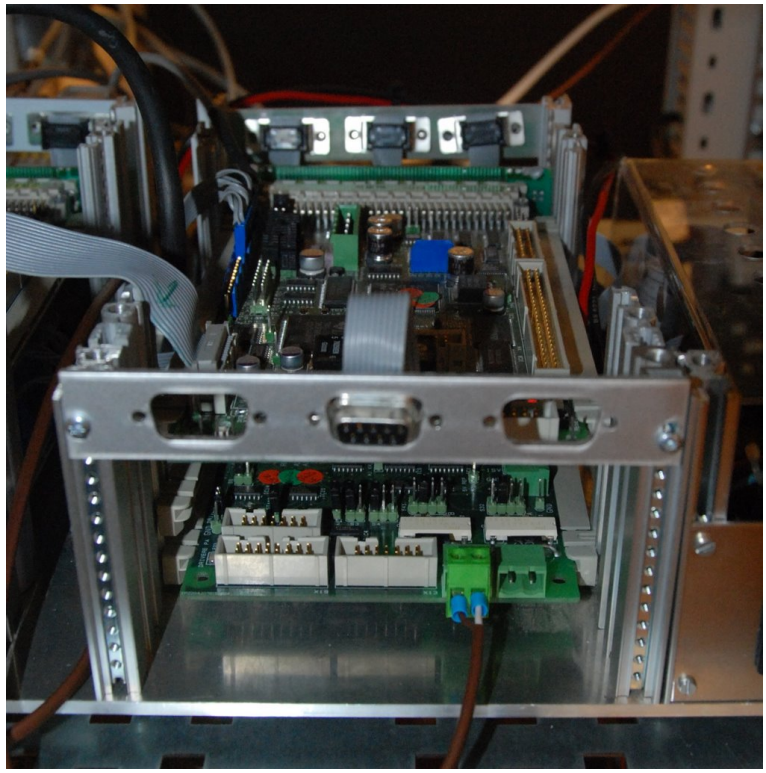

Figure 2.4 – Picture of a controller circuit board and its measurement circuit board. The controller circuit board is the one on top and the measurement circuit board is the one below.

picture of a controller circuit board and its measurement circuit board.

The currents out from the converter are measured using the current transducer LA 205-S from LEM. These are bidirectional sensors with a primary nominal measurement current up to 200 A. As the rated output current from the system is lower, the output cables are looped through the sensors four times. This quadruples the signal strength.

The DC bus voltage is measured using a voltage transducer LV 25-800 also from LEM. It has a primary nominal voltage of 800 V. It is a bidirectional sensor, but the ad input channel has been configured as a unidirectional sensor to increase the ad resolution.

The controller board is equipped with a RS-232 serial communication port used for control and debugging of the software. It has also a CAN-bus connector capable of speeds up to 1 Mbps, which can be used to communicate with other controller boards.

2.2.2 The LCL filter

The LCL filter consists of six individual inductors and three star connected capacitors. A contactor switch can connect and disconnect the filter from the grid. The contactor is controlled by the DSP from a relay output on the controller board.

There are three voltage sensors and three current sensor in the LCL filter to measure the voltages and currents of the capacitors. However, only two of each is used by the converter, as the third is redundant. The current sensors are the same type as the ones used in the converter. The voltage sensors are also of the same type as the DC bus measurement in the converter, but the ad input channels have been configured for bidirectional measurement.

The six inductors which makes up the Ls in the LCL filter are separated into individual units. These are in turn split into four coils for one iron core. These coils can be configured in series or parallel to give miscellaneous inductances in the range 250 μH to 2 mH.

The three capacitances of the filter have a capacitance of approximately 50 μF. Three small RC-filters have been added in parallel with the capacitors to reduce noise, as the large capacitors lose their capacitance characteristics for high frequencies.

2.3 The synchronous generator

To simulate different grid conditions, a synchronous machine is used as a generator to generate the grid voltage. This generator is linked with an asynchronous machine which provides the power for the generator.

The synchronous machine is a seasoned generator built by Siemens-Schuckert Werke[†], and is a 3-phase, 220 V, 10 kVA machine with a $\cos\phi$ of 0.8. The nominal speed is 1500 RPM which give an output voltage of 50 Hz. A pulse width modulated current source has been built from the power electronic parts of an electrical actuator from Smart Actuator AS. The current source provides an adjustable magnetizing current of the generator, up to the rated maximum of 2.8 A at a DC voltage of 300 V. This enables changing the amplitude of the generated grid voltage.

The asynchronous machine is a brand new motor built by ABB. It is a 3-phase, 400 V, 15 kW machine with a $\cos\phi$ of 0.82. The nominal speed is 1460 RPM. It is driven by a commercial motor drive from Vacon, which is speed regulated. This enables changing the frequency of the grid voltage.

[†]Siemens-Schuckert Werke AG, Siemens & Halske AG, and Siemens Reiniger-Werke AG merged into Siemens AG in 1966.

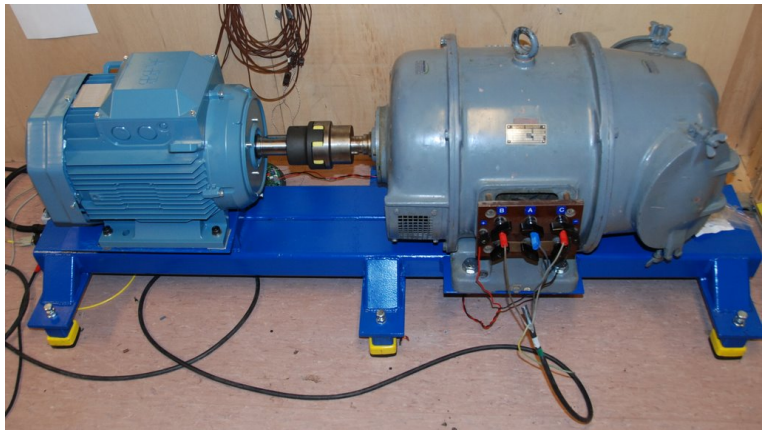

Figure 2.5 – Picture of the grid generating synchronous machine generator linked to an asynchronous machine motor.

Figure 2.5 shows a picture of the synchronous machine generator linked to the asynchronous machine motor.

2.4 Software

The software is written in a mixture of C++ and optimized assembly, using the Code Composer Studio compiler suite from Texas Instruments. It is supported by a limited operating system to help development and debugging. This operating system provides services to download a program, and control and inspect it from a personal computer over the RS-232 serial communication link.

For a switching period of 8 kHz the time from the first analog to digial convertion is started to the PWM output registers must have been updated is 62.5 µs. This short time period is all that is available for all the different grid converter controllers to be updated with the new measurements. In addition, the high speed software detection of overcurrent makes the time available even less. This short time period made it necessary to focus on speed when developing the software. A good optimizing C++-compiler made the task easier, but many of the commonly used library functions and certain other speed bottlenecks were hand-optimized further using assembly language.

The software is built around interrupts based on the triangle signal used for the generation of the pulse width modulation signals. The analog converter is started at the top of the triangle, and generates an interrupt when

done. These measurements are then used to update the PWM compare registers, which will then be loaded at the next triangle bottom. In addition, measurements are done with a corresponding interrupt five extra times during a triangle signal period to implement software overcurrent protection. At 8 kHz switching frequency this gives a monitoring frequency of 48 kHz.

The Texas Instrument TMS320F2812 DSP supports very fast multiplication and addition of 32-bit fixed point values. Floating points however, is not very well supported for this generation of DSPs[‡], and was avoided in the software altogether.

The fixed point representation used for most of the variables in the software is 32-bit integers scaled by 2^{20}. This scaling is often called Q20. The maximum values supported is approximately ± 2000, and the resolution is 2^{-20} which is approximately 9.5×10^{-7}. This means that care must be taken to avoid numerical problems arising from too small or large values. The per unit system introduced in the system chapter will avoid most of these problems, as the variables of the system is scaled to around 1. However, for digital filters the fixed point representation can still give trouble. The difference equations presented in this thesis have taken this into account.

2.5 The per unit system of the grid side system

The system was dimensioned for a 230 V phase to phase RMS voltage with a nominal apparent output power of 5 kVA. Even though the converters are capable of more, this power was chosen to fit with other components in the system.

Table 2.1 summarizes the ratings of the system, including the PWM switching frequency[§] This creates the per unit system in table 2.2. The physical quantities of the LCL filter and their per unit counterparts are summarized in table 2.3.

The small resistances of the inductors are dependent upon both frequency and temperature, and are therefore very unaccurate. In particular, the resistance is much higher than the stated resistance for frequencies at and above the resonance frequency. However, by setting them this low but non zero they represent a "worst case" resistance, yet makes the model stable and thus easier to e.g. simulate.

[‡]The new generation of this family of DSPs starting with the TMS320F28335 adds support for fast floating point operations.

[§]8009 Hz was selected instead of the more "intuitive" frequency 8000 Hz because 8009 is a prime number. A prime number runs less chance of being a multiple of another external frequency, reducing aliasing problems.

Table 2.1 – Grid side unit system ratings. See table 1.2 for the relationships between the ratings.

Parameter	Symbol	Physical value
Rated line voltage	$V_{n,\mathrm{RMS}}$	230 $\mathrm{V_{RMS}}$
Rated apparent power	S_n	5 kVA
Nominal frequency	f_n	50 Hz
Rated current	$I_{n,\mathrm{RMS}}$	12.551 $\mathrm{A_{RMS}}$
PWMswitching frequency	f_{sw}	8009 Hz

Table 2.2 – Grid side unit per unit system. See table 1.3 for the relationships between the parameters.

Parameter	Symbol	Physical value
Base voltage (peak phase voltage)	$\hat{V}_n$	187.79 V
Base current	$\hat{I}_n$	17.75 A
Base angular frequency	ω_n	314.159 rad s^{-1}
Base impedance	Z_n	10.58 Ω
Base inductance	L_n	33.677 mH
Base capacitance	C_n	300.86 µF

Table 2.3 – Grid side unit parameters.

Parameter	Symbol	Quantity	p.u.	Quantity
Converter side filter inductance	L_f	1.95 mH	x_f	0.05642
Converter side filter resistance	R_f	0.5 mΩ	r_f	47.2610^{-6}
Filter capacitance	C_f	50 µF	y_f	0.1662
Grid side filter inductance	L_g	1.35 mH	x_g	0.04009
Grid side filter resistance	R_g	0.35 mΩ	r_g	32.7210^{-6}

The $\alpha\beta$-state space model of the LCL filter is given by equation 1.16, and the dq-state space model is given by equation 1.19. Assuming $\dot{\theta} = \omega_n$ for the dq-system and inserting the values of the example system gives the matrices

$$\boldsymbol{A}^{\alpha\beta} = \begin{bmatrix} -0.256410 & 0 & 0 & 0 & -5425.64 & 0 \\ 0 & -0.256410 & 0 & 0 & 0 & -5425.64 \\ 0 & 0 & -0.256410 & 0 & -13262.7 & 0 \\ 0 & 0 & 0 & -0.256410 & 0 & -13262.7 \\ 0 & 0 & 1890.36 & 0 & 0 & 0 \\ 0 & 0 & 0 & 1890.36 & 0 & 0 \end{bmatrix}, \tag{2.1}$$

$$\boldsymbol{A}^{\mathrm{dq}} = \begin{bmatrix} -0.256410 & 314.159 & 0 & 0 & -5425.64 & 0 \\ -314.159 & -0.256410 & 0 & 0 & 0 & -5425.64 \\ 0 & 0 & -0.256410 & 314.159 & -13262.7 & 0 \\ 0 & 0 & -314.159 & -0.256410 & 0 & -13262.7 \\ 0 & 0 & 1890.36 & 0 & 0 & 314.159 \\ 0 & 0 & 0 & 1890.36 & -314.159 & 0 \end{bmatrix}, \tag{2.2}$$

$$\boldsymbol{B}^{\alpha\beta} = \boldsymbol{B}^{\mathrm{dq}} = \begin{bmatrix} 5425.64 & 0 & 0 & 0 \\ 0 & 5425.64 & 0 & 0 \\ 5425.64 & 0 & 7837.04 & 0 \\ 0 & 5425.64 & 0 & 7837.04 \\ 0 & 0 & 0 & 0 \\ 0 & 0 & 0 & 0 \end{bmatrix}. \tag{2.3}$$

CHAPTER 3

A voltage observer

The voltage observer is used to find the phase and amplitude of a three phase voltage signal. This information can be used by the voltage regulator to synchronize to an external grid before connecting the converter. It can also be used to monitor the output voltage while the converter is running. If the grid is "strong" it can be used to run the converter at a fixed phase shift or fixed difference in amplitude.

3.1 Ideal symmetrical three phase voltage

An ideal symmetrical three phase voltage signal can be given as

$$\boldsymbol{v}^{abc} = v_m \begin{bmatrix} \cos(\vartheta) \\ \cos(\vartheta - 120°) \\ \cos(\vartheta - 240°) \end{bmatrix}, \tag{3.1}$$

where v_m is the voltage amplitude and ϑ the time varying phase angle of the grid. The phase angle can also be written as

$$\vartheta = \omega t + \vartheta_0 \tag{3.2}$$

to underline its dependence of time. Here, ω is the angular phase speed of the grid and ϑ_0 the phase offset of the grid at time $t = 0$.

Using the $\alpha\beta$-transform, the three phase voltage signal can be transformed into

$$\boldsymbol{v}^{\alpha\beta} = \mathbf{T}^{\alpha\beta}_{abc}\boldsymbol{v}^{abc} = v_m \begin{bmatrix} \cos(\vartheta) \\ \sin(\vartheta) \end{bmatrix}. \tag{3.3}$$

Solving equation 3.3 with respect of v_m and ϑ gives the magnitude and phase of the voltage signal. The grid voltage can be found using the mag-

nitude of the $\alpha\beta$-vector

$$\begin{aligned}\|\boldsymbol{v}^{\alpha\beta}\|_2 &= \sqrt{v_\alpha^2 + v_\beta^2} \\ &= \sqrt{(v_m\cos(\vartheta))^2 + (v_m\sin(\vartheta))^2} \\ &= v_m\sqrt{\sin(\vartheta)^2 + \cos(\vartheta)^2} = v_m\end{aligned} \tag{3.4}$$

The phase can be found dividing the two components

$$\frac{v_\beta}{v_\alpha} = \frac{v_m\sin\vartheta}{v_m\cos\vartheta} = \tan\vartheta \implies \vartheta = \arctan\frac{v_\beta}{v_\alpha} \tag{3.5}$$

Equation 3.5 is however only valid for angles $\vartheta \in \left\langle -\frac{\pi}{2}, \frac{\pi}{2}\right\rangle$. To find the phase for all four quadrants, another related function called arctan2 found in most computer libraries can be used instead*.

To summarize, the magnitude and the phase of a three phase signal is given by

$$v_m = \sqrt{v_\alpha^2 + v_\beta^2} \tag{3.7}$$

$$\vartheta = \arctan2\left(v_\beta, v_\alpha\right) \tag{3.8}$$

3.2 The magnitude observer

A very simple voltage magnitude observer can be made by low pass filtering equation 3.7, e.g.:

$$\overline{v}(s)_m = \frac{1}{\frac{s}{\omega_{\text{bw}}} + 1} v_m(s) \tag{3.9}$$

The filter bandwidth, ω_{bw}, should be made low enough to attenuate any transient disturbances.

*The relationship between the regular arctan function and the four quadrant version arctan2 can be defined as

$$\arctan2\left(y, x\right) = \begin{cases} \arctan\left(\frac{y}{x}\right) & x > 0 \\ \pi + \arctan\left(\frac{y}{x}\right) & y \geq 0,\ x < 0 \\ -\pi + \arctan\left(\frac{y}{x}\right) & y < 0,\ x < 0 \\ \frac{\pi}{2} & y > 0,\ x = 0 \\ -\frac{\pi}{2} & y < 0,\ x = 0 \\ \text{undefined} & y = 0,\ x = 0 \end{cases} \tag{3.6}$$

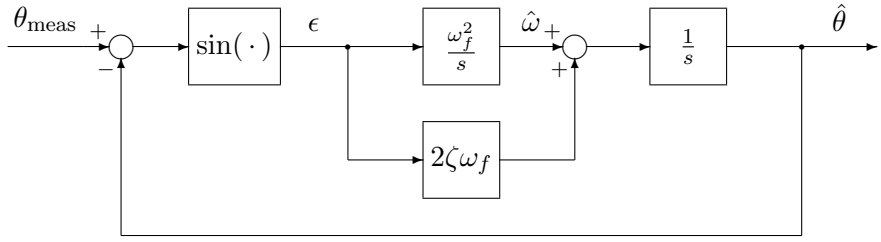

Figure 3.1 – Block diagram of an analog frequency observer

This filter can be discretized using e.g. Euler's method described in section A.2.1. This gives the difference equation:

$$\overline{v}_{m,k+1} = \overline{v}_{m,k} + k_n \left(v_{m,k} - \overline{v}_{m,k}\right) \tag{3.10}$$

where:

$$k_n = \frac{1}{1 + \frac{1}{T\omega_{\text{bw}}}} \tag{3.11}$$

Additional notch filters can be added for any unwanted frequencies if necessary.

3.3 The angular observer

The grid voltage is often distorted by e.g. transient disturbances and non linear loads, as well as measurement errors. An observer is used to suppress these disturbances.

An angular observer is presented in [7] as

$$\dot{\hat{\omega}} = \omega_f^2 \epsilon, \tag{3.12}$$

$$\dot{\hat{\theta}} = \hat{\omega} + 2\zeta\omega_f \epsilon, \tag{3.13}$$

where $\hat{\omega}$ is the estimated frequency, $\hat{\theta}$ the estimated phase, and ϵ is an angular error estimation. ω_f and ζ are filter constants. The angular error estimation is given by:

$$\epsilon = \sin(\theta_{\text{meas}} - \hat{\theta}) \tag{3.14}$$

Proof of global stability towards points where $\epsilon = 0$ for a constant frequency of this non-linear system is also presented.

Figure 3.1 shows a block diagram of the frequency observer in the s-plane.

For small perturbations the error estimation can be simplified to:

$$\epsilon \approx \theta_{\text{meas}} - \hat{\theta} \tag{3.15}$$

Inserting this into equation 3.12 and equation 3.13 and converting to the s-plane gives the transfer functions:

$$\hat{\omega}(s) = \frac{1}{\frac{s^2}{\omega_f^2} + 2\zeta\frac{s}{\omega_f} + 1}\omega_{\text{meas}}(s), \tag{3.16}$$

$$\hat{\theta}(s) = \frac{2\zeta\frac{s}{\omega_f} + 1}{\frac{s^2}{\omega_f^2} + 2\zeta\frac{s}{\omega_f} + 1}\theta_{\text{meas}}(s), \tag{3.17}$$

where $\omega_{\text{meas}}(s) = s\theta_{\text{meas}}(s)$.

The speed of convergence and robustness against disturbances of the estimator can be tuned by the filter bandwidth constant ω_f. The damping constant of the filter, ζ, is set to 1 to have a critically damped filter. For a constant frequency, the steady state error is zero for both the phase and the frequency.

For digital control, the estimator is converted into a discrete model using e.g. the Euler's method described in section A.2.1. This gives the following difference equations:

$$\hat{\omega}_{k+1} = \hat{\omega}_k + T\omega_f^2\epsilon_k, \tag{3.18}$$

$$\hat{\theta}_{k+1} = \hat{\theta}_k + T\hat{\omega}_k + 2h\zeta\omega_f\epsilon_k, \tag{3.19}$$

where T is the sampling interval.

3.3.1 Phase synchronization using discrete events

Sometimes the voltage phase information is only known at discrete points in time. The discrete estimator in the previous section can accommodate this by setting ϵ to 0 whenever the phase information is unavailable. One example of this is when only the sign bit of a voltage is available.

Another more involved example is if the system is required to synchronize over a communication bus. Synchronization over the widely available CAN bus is an example. It is not known in advance when a package having phase information is successfully transmitted. This is because there may be other traffic on the bus when first trying to transmit, or a communication error caused the package to be retransmitted. However, it is known when the package was sent after the fact. Another package can then be sent telling the other controller how old the phase information in the previous package

was. The error can then be found using the difference between that phase and the estimated phase at that period in time, i.e.:

$$\epsilon = \sin\left(\hat{\theta} - \hat{\omega}\Delta t - \theta_{\text{meas}}\right) \tag{3.20}$$

As this CAN bus synchronization can be made very accurate[†], especially for fixed frequencies, it can also be used for other purposes than grid synchronization. In particular it is possible to reduce the DC-link voltage ripple when several converters share the same DC-link by synchronizing the pwm-triangle signal.

[†]Experiments have been done using a Texas Instruments TMS320F2809 DSP with a CAN bus bit rate of 1 MHz. These show that the time of a package transmission/reception can be determined with an accuracy of less than 100 ns, only a tenth of the bit width of the communication medium.

CHAPTER 4

Inner voltage controller

There are many ways to control a grid side converter. In this thesis, a voltage controller is used for the innermost control loop. This voltage controller enables operation of the converter for both when the converter is connected to a strong grid and when the converter is operating in islanding mode.

This controller regulates the capacitor filter voltage based on a voltage reference vector and measurements of currents and voltages in the LCL-filter. It creates a voltage vector which is then output by the PWM unit. Generation of the voltage reference vector is discussed in the next chapter.

4.1 Overview

Figure 4.1 shows a block diagram of the controller. Here, $\boldsymbol{v}_{\text{PWM}}^{\alpha\beta}$ is the output voltage vector from the inner voltage controller to the PWM module. $\boldsymbol{v}_{f,\text{ref}}^{\alpha\beta}$ is the voltage reference vector, and $\boldsymbol{v}_{z}^{\alpha\beta}$ is the voltage reference modified by the impedance feedback loop. $\boldsymbol{i}_{e}^{\alpha\beta}$ is the measured PWM module output current vector, $\boldsymbol{i}_{f}^{\alpha\beta}$ is the measured capacitor current vector and $\boldsymbol{v}_{f}^{\alpha\beta}$ is the measured capacitor voltage vector. $\boldsymbol{i}_{f,\text{ref}}^{\alpha\beta}$ is the capacitor current vector reference, possibly calculated from the voltage reference $\boldsymbol{v}_{f,\text{ref}}^{\alpha\beta}$. $\boldsymbol{i}_{g}^{\alpha\beta} = \boldsymbol{i}_{e}^{\alpha\beta} - \boldsymbol{i}_{f}^{\alpha\beta}$ is the grid current vector.

$\boldsymbol{K}_v$, $\boldsymbol{K}_i$ are constant, diagonal matrices that gives the gain of the voltage feedback signal and active damping controller loops respectively. $\boldsymbol{H}_v(z)$ and $\boldsymbol{H}_i(z)$ are diagonal filter matrices that filters out the "uninteresting" part of the loopback signals. $\boldsymbol{K}_z(\theta)$ is a possibly phase dependent matrix that gives the gain of the impedance loop.

All the variables of the inner voltage controller are given in the $\alpha\beta$-coordinate system, not the dq-coordinate system. This means that the

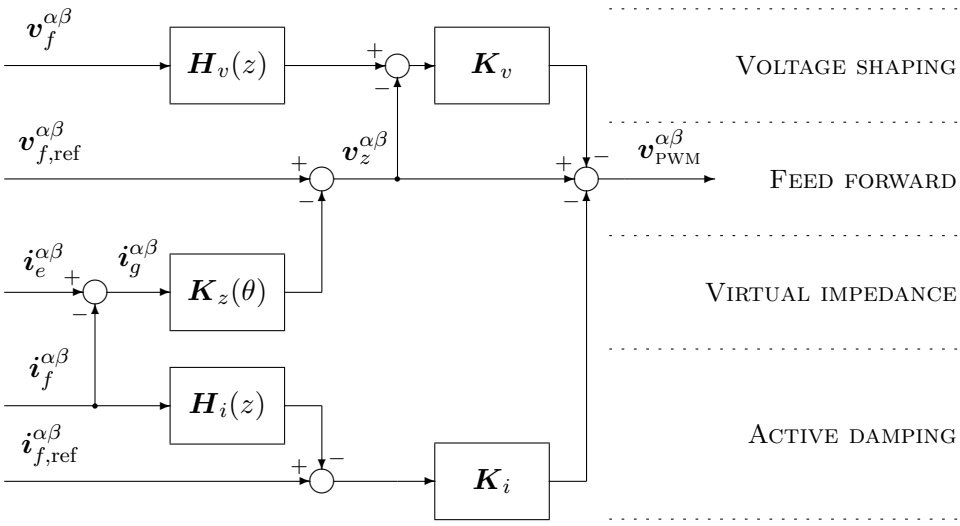

Figure 4.1 – Block diagram of the inner voltage controller. The individual parts of the controller is indicated using dotted lines at the right of the diagram.

reference vector is a sinusoidal, and that the regulation of the voltage is a servo problem. Accurate tracking is however not necessary, and any integral action in the feedback loop could create problems as the converters interact with each other.

The system chapter shows that a symmetric three phase LCL filter can be decoupled into two separate single phase systems using the $\alpha\beta$-transform. To simplify the discussion and design in this chapter a single phase system is introduced and often used instead of the full three phase system.

The controller is split into four parts. The first part is the feed forward signal. This is a simple feed forward from the reference, modified by the virtual impedance part discussed below.

The second part is the active damping. To avoid overvoltages in the LCL filter, the resonance tendencies of the filter must be damped out.

The third part is the voltage shape controller. To have good performance, specifically for non-linear loads, a voltage feedback loop is introduced to reduce deviations from the sinusoidal voltage shape.

The fourth and last part is the programmable virtual impedance. This impedance can be used to avoid excessive currents if the converter is out of phase with the grid. It can also be used to "burn off" any oscillatory tendencies between converters connected to the same grid without any real energy loss.

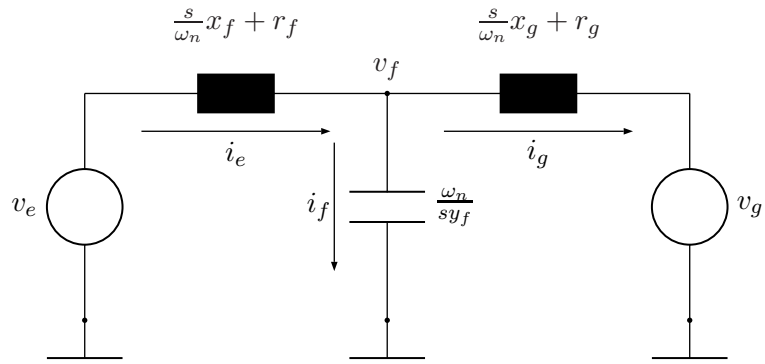

Figure 4.2 – A single phase LCL filter connected to a strong grid.

4.2 A single phase LCL filter

Figure 4.2 shows a circuit diagram of a single phase LCL filter connected directly to a strong grid. Here, v_e is the converter voltage, and v_g the grid voltage. x_f is the inductance and r_f the resistance of the converter side inductor, and x_g is the inductance and r_g the resistance of the grid side inductor. y_f is the capacitance of the filter.

The two inductors and the capacitor of the LCL filter will cause certain resonance frequencies to be amplified. These resonance frequencies can be excited by both the converter and maybe more importantly by the grid. If they are not damped, they can cause overvoltages by excessive amplification of any voltage harmonics.

The filter is studied when it connected directly to a voltage source, i.e. a strong grid, as this is a worst case situation. This case conveniently also includes a short circuit situation, which can be seen as a special case with the grid voltage set to zero.

The Laplace transformation of the voltage over the capacitor of this single phase system, $v_f(s)$, is

$$v_f(s) = \frac{(\frac{s}{\omega_n}x_g + r_g)v_e(s) + (\frac{s}{\omega_n}x_f + r_f)v_g(s)}{y_f x_g x_f \frac{s^3}{\omega_n^3} + y_f(r_g x_f + x_g r_f)\frac{s^2}{\omega_n^2} + (r_f r_g y_f + x_f + x_g)\frac{s}{\omega_n} + r_f + r_g}, \tag{4.1}$$

and the current through the capacitor, $i_f(s)$, can simply be written as

$$i_f(s) = s\frac{y_f}{\omega_n}v_f(s). \tag{4.2}$$

The resistances are normally so small that ignoring them can still give a good approximation of the real filter if the system is not required to be asymptically stable. This simplifies the function of the voltage to

$$v_f(s) = \frac{\frac{x_p}{x_f} v_e(s) + \frac{x_p}{x_g} v_g(s)}{y_f x_p \frac{s^2}{\omega_n^2} + 1}, \tag{4.3}$$

$$x_p = \frac{x_f x_g}{x_f + x_g}, \tag{4.4}$$

where x_p is the inductance of the two inductances connected in parallel. This is an undamped resonance system with a resonance frequency of

$$\omega_p = \frac{\omega_n}{\sqrt{y_f x_p}}. \tag{4.5}$$

For the experimental system the parameters in table 2.3 gives the gains, poles, and zeros as

$$\begin{aligned} K_e &= 1.02564 \cdot 10^7, & K_g &= 1.48148 \cdot 10^7, \\ p_1 &= -0.256410, & p_{2,3} &= -0.128205 \pm 5007.12\text{j}, \\ z_{1,e} &= -0.256410 & z_{1,g}, &= -0.256410, \end{aligned}$$

where the function has been written in the canonical zero-poles format

$$v_f(s) = \frac{K_e(s + z_{1,e})v_e(s) + K_g(s + z_{1,g})v_g(s)}{(s + p_1)(s + p_2)(s + p_3)}. \tag{4.6}$$

The resonance frequency is thus 5007.12 rad $\text{s}^{-1} \approx 800$ Hz. Figure 4.3 shows the bode diagrams of the system.

4.3 Damping of the LCL filter

Methods to damp out the resonances can be split into two main groups, passive damping methods and active damping methods.

4.3.1 Passive damping

Passive damping methods introduces new passive components to the filter. A very simple method connects a resistor in series with the capacitor. More complex methods uses e.g. RLC circuits in parallel with the capacitor. See for example [6] which in turn bases its presentation on [5] and [8]. More exotic possibilities may include custom made resistors created specifically

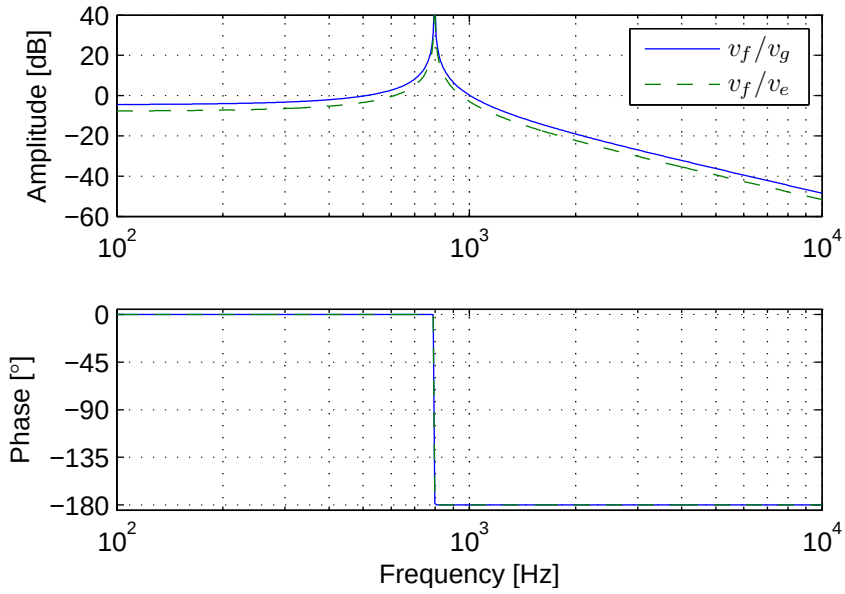

(a) Bode diagram of $\frac{v_f}{v_g}(\mathrm{j}\omega)$ and $\frac{v_f}{v_e}(\mathrm{j}\omega)$

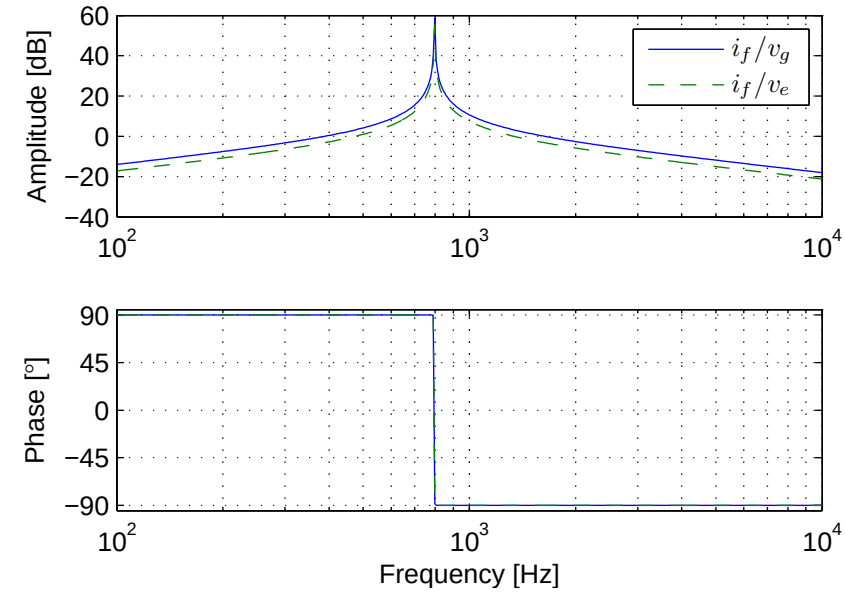

(b) Bode diagram of $\frac{i_f}{v_g}(\mathrm{j}\omega)$ and $\frac{i_f}{v_e}(\mathrm{j}\omega)$

Figure 4.3 – Bode diagrams of the transfer functions of the LCL-filter without any active damping.

to have low resistance for low frequencies but high resistance for frequencies around and above the resonance frequency.

However, all passive damping methods introduces extra components to the filter. This increases the cost and lowers the reliability, especially for the more complex schemes. Any resistors in the filter will dissipate energy as well, which reduces the efficiency of the system and increases cooling requirements.

4.3.2 Active damping

A more energy efficient and less costly solution than passiv damping is to actively control the converter voltage v_e to dampen out oscillations in the filter. Numerous methods for active damping have been presented in the literature, see [9–13] for active damping in various situations.

Recently methods have been introduced for active damping inspired by sensorless control for motor drives, see e.g. [6, 14, 15]. Sensorless control avoids measuring the voltages and currents of the LCL-filter and only estimates them using the converter current measurements.

The method chosen in this thesis uses a classical proportional feedback from the capacitor current measurement. This is a reasonably simple and tried method and can be thought of as introducing a "virtual" resistance in the filter.

A very simple active damping algorithm can be implemented by subtracting a proportional feedback of the capacitor current from the voltage reference

$$v_e(s) = -k_a i_f(s) + \tilde{v}_e(s), \tag{4.7}$$

where k_a is the feedback gain constant. Ideally, the new Laplace transformed function of the filter voltage, ignoring the resistances of the inductances, becomes

$$v_f(s) = \frac{\frac{x_p}{x_f}\tilde{v}_e(s) + \frac{x_p}{x_g}v_g(s)}{y_f x_p \frac{s^2}{\omega_n^2} + k_a \frac{y_f x_p}{x_f}\frac{s}{\omega_n} + 1}. \tag{4.8}$$

This is a second order, damped oscillator. It can be made critically damped by selecting the feedback constant k_a as

$$k_a = 2\sqrt{\frac{x_f}{y_f}\left(\frac{x_f}{x_g} + 1\right)}. \tag{4.9}$$

Note however that the discrete control and PWM nature of the converter introduces a time delay from the measurement of the current is done to the output voltage has changed.

The filter is normally designed with a resonance frequency so high that this time delay must be included in an analysis. Equation 4.3 shows that the resonance frequency is particularly high if the filter is connected to a strong grid or is in a short circuit situation. A high as possible resonance frequency of the filter is favored as it decreases the cost and size requirements of the filter. Also, a higher frequency enables a higher bandwidth for use in active filtering of the grid and improved response for non-linear loads.

Several approximations for this time delay and the pulse width modulation nature of the converter voltage can be used. Section A.2.3 shows that the pulse width modulation can be split into a time delay part and a gain attenuation part.

Measurements are done in the top of the triangle illustrated by figure 1.4, and the centre of the next pulse output of the converter is at the next top. Equation A.59 gives the transfer function of the pulse width modulator. For frequencies below the Nyquist frequency, $\frac{f_{\mathrm{sw}}}{2}$, the gain loss from the pulse width modulation is always less than 4 dB

$$\frac{\sin(\frac{\pi}{2})}{\frac{\pi}{2}} = \frac{2}{\pi} \approx 0.6366 \tag{4.10}$$

Ignoring this attenuation of the amplitude leaves the time delay

$$v_e(s) = -k_a \mathrm{e}^{-sT} i_f(s) + \tilde{v}_e(s) \tag{4.11}$$

where $T = \frac{1}{f_{\mathrm{sw}}}$ is one switching period.

The open loop transfer function for the feedback control including the time delay, $L_d(s)$, can be written as

$$L_d(s) = \mathrm{e}^{-sT} \frac{i_f}{v_e}(s) \tag{4.12}$$

The time delay can be approximated using a Padé approximation introduced in section A.2.4. This creates rational transfer functions that can be analysed using normal, analytical feedback tools. The open loop transfer functions using a first order approximation, a first order approximation with frequency shift, and a second order approximation are:

$$L_{d,1}(s) = \frac{1 - \frac{sT}{2}}{1 + \frac{sT}{2}} \frac{i_f}{v_e}(s) \qquad \text{1. order Padé,} \tag{4.13}$$

$$L_{d,\gamma}(s) = \frac{1 - \frac{s\gamma T}{2}}{1 + \frac{s\gamma T}{2}} \frac{i_f}{v_e}(s) \qquad \text{1. order Padé with frequency shift,} \tag{4.14}$$

$$L_{d,2}(s) = \frac{1 - \frac{sT}{2} + \frac{(sT)^2}{12}}{1 + \frac{sT}{2} + \frac{(sT)^2}{12}} \frac{i_f}{v_e}(s) \qquad \text{2. order Padé.} \tag{4.15}$$

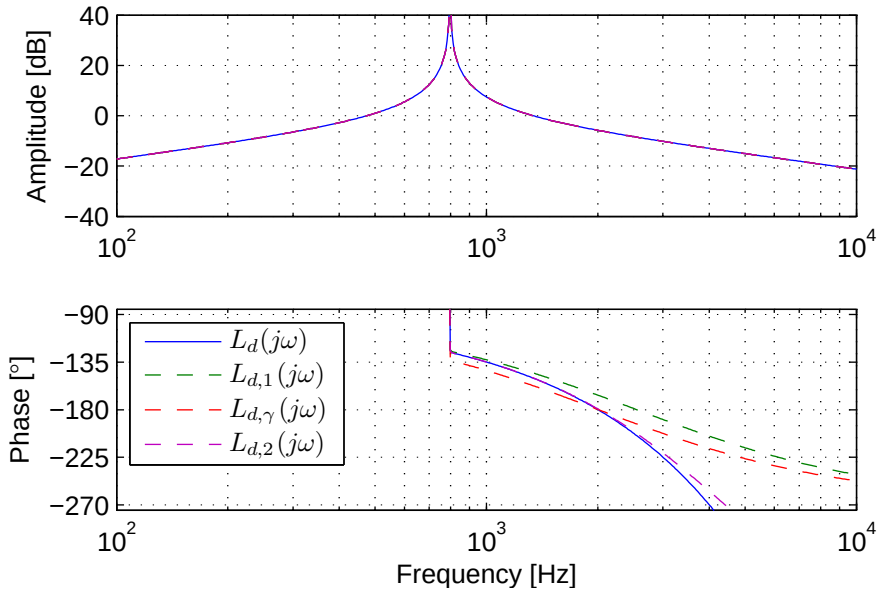

Figure 4.4 – Open loop function of the active damping feedback with time delay. The real open loop response is plotted together with three responses where the time delay has been approximated using different types of Padé approximations. Note that the magnitude for all four responses are the same.

The transfer function $\frac{i_f}{v_e}(s)$ shifts rapidly from $+90°$ to $-90°$ at the resonance frequency. This suggest that the phase of $L_d(\mathrm{j}\omega)$ is around $-180°$ when the phase of $\mathrm{e}^{-\mathrm{j}T\omega}$ is $-90°$. Solving for ω at this approximate crossing of the $-180°$ phase of the open loop function gives

$$\omega_{-180°} = \frac{\pi}{2h}. \tag{4.16}$$

Using this and equation A.66 to find the frequency shift factor for the first order Padé approximation gives

$$\gamma = \frac{\tan\left(\frac{\pi}{4}\right)}{\frac{\pi}{4}} = \frac{4}{\pi} \approx 1.27 \tag{4.17}$$

A plot of the open loop transfer function and their approximations is shown in figure 4.4. The frequency shift factor, γ, is set to 1.27. The figure shows that the first order approximation without the frequency shift factor is not satisfactory for an analysis of the example system. The frequency shift factor, however, corrects the phase to the phase crossing at $-180°$.

For systems where the first order approximation is still valid, an analytical estimation of the limit of the gain of the feedback loop can be found. Let the time delay in equation 4.11 be approximated with a first order frequency shifted Padé approximation

$$v_e(s) \approx -k_a \frac{1-\alpha\frac{s}{\omega_n}}{1+\alpha\frac{s}{\omega_n}} i_f(s) + \tilde{v}_e(s), \quad \alpha = \frac{\omega_n \gamma T}{2}. \tag{4.18}$$

This feedback gives the filter voltage transfer function

$$v_f(s) = \frac{\frac{x_p}{x_f}(\frac{s}{\omega_n}\alpha + 1)\tilde{v}_e(s) + \frac{x_p}{x_g}(\frac{s}{\omega_n}\alpha + 1)v_g(s)}{y_f x_p \alpha \frac{s^3}{\omega_n^3} + y_f x_p (1 - \frac{k_a \alpha}{x_f})\frac{s^2}{\omega_n^2} + x_p(\alpha + \frac{y_f k_a}{x_f})\frac{s}{\omega_n} + 1}. \tag{4.19}$$

It can be shown (see e.g. [16] or [17]) that a third order polynom equation

$$x^3 + ax^2 + bx + c = 0 \tag{4.20}$$

will have all its roots in the left half plane if and only if

$$a > 0, \quad b > 0, \quad 0 < c < ab \tag{4.21}$$

Normalizing the denominator of equation 4.19 and using the terms in equation 4.21 gives the condition

$$k_a < x_f \left(\frac{2}{T\gamma\omega_n} - \frac{T\gamma\omega_n}{2 y_f x_p} \right) \tag{4.22}$$

for a stable transfer function. This shows analytically that a time delay will make the system unstable if the feedback gain is too large. For the example system and $\gamma = 1.27$, the estimated gain limit is $k_a < 1.95$. This is a gain of 5.8 dB, which can be verified as the approximate gain margin in figure 4.4.

A closer study of the bode plot of $L_d(s)$ in figure 4.4 shows that a simple proportional feedback will give a poor phase margin for any significant feedback gain. A derivative action in the current feedback loop can be used to lift the phase around the wanted crossing frequency.

The phase can be lifted by the controller with a derivative action. This can be done by using a discrete derivate action for higher frequencies. A simple phase lifting filter has the transfer function*

$$H_{i,d}(z) = \frac{1 + k_d}{1 + k_d z^{-1}}, \tag{4.23}$$

* This can be extended to a slightly more complex filter, $H_{i,d}(z) = \frac{1+k_d+k_2 z^{-1}}{1+(k_d+k_2)z^{-1}}$ if more control over the phase is required.

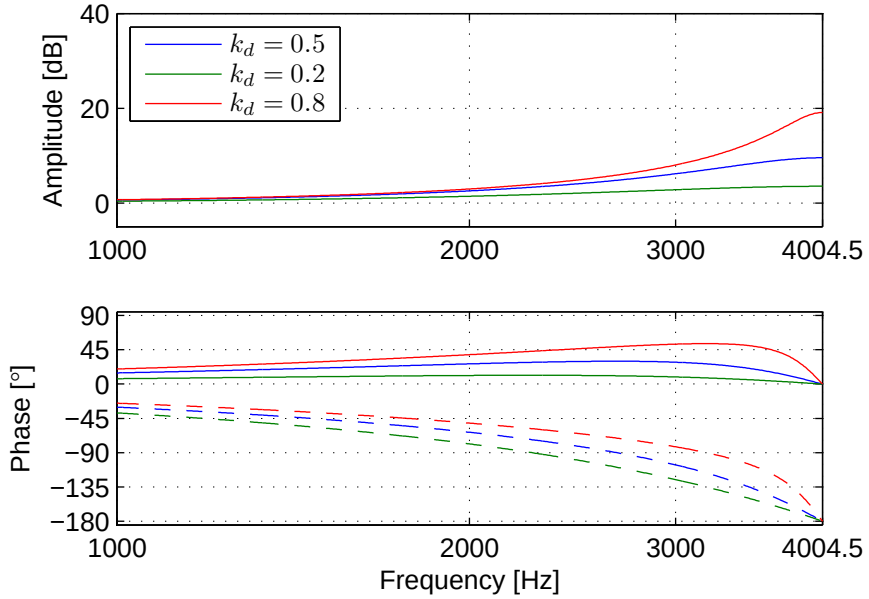

Figure 4.5 – Bode diagrams of $H_{i,d}(z) = \frac{1+k_d}{1+k_d z^{-1}}$ for different values of k_d. The dashed lines in the phase plot includes a one sample period delay.

which have the difference equation

$$y_k = u_k + k_d(u_k - y_{k-1}) \tag{4.24}$$

Figure 4.5 shows the bode diagrams for this filter for different values of k_d. The figure also shows the impact on the phase of a one sample time delay.

The new loop gain transfer function including this derivative action can be approximated as

$$L_{d,d}(s) = \frac{(1+k_d)\mathrm{e}^{-sT}}{1+k_d\mathrm{e}^{-sT}} \frac{i_f}{u_e}(s) \tag{4.25}$$

Figure 4.6 shows a comparison of the new function and the old. The amplitude peak at the Nyquist frequency hints at problems with the gain margin and noise from the measurement. However, experiments on the real system show that antialiasing filters and the pulse width modulation attenuation helps with the response of the system.

This current loop will also be active for the nominal frequency used for the voltage reference. If the current reference is set to zero, it will in particular impact the phase of the reference voltage. Figure 4.7 shows the

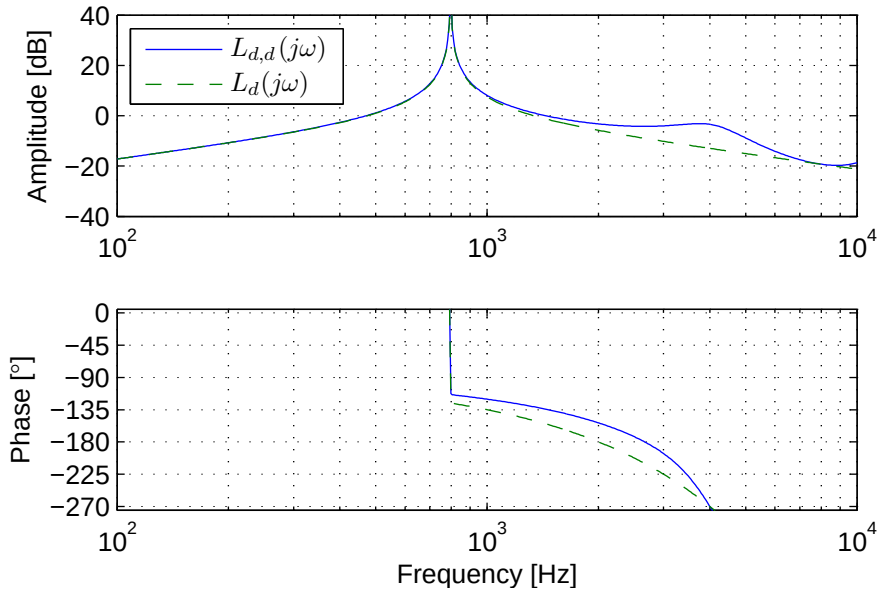

Figure 4.6 – Bode diagram of the open loop transfer function with derivative action.

impact on the voltage reference of a zero current reference for an actively damped converter with no load, i.e. $i_g = 0$.

To avoid the impact of the current loop on any voltage regulation, the current shaping filter can be augmented with a highpass filter. This will lessen the impact of the current loop on the voltage regulaton of the lower harmonics. As an added bonus this filter will remove any DC-offset in the current sensors. In fact, as the DC-component is not needed for the active damping, the capacitor current sensor can be of a simpler AC-only type if this is convenient.

Equation A.50 gives a simple high pass filter with bandwidth f_h as

$$H_{i,h}(z) = \frac{k_h + 1}{2} \frac{1 - z^{-1}}{1 - k_h z^{-1}}, \quad k_h = \frac{1}{1 + 2\pi f_h T} \tag{4.26}$$

The full current shaping function $H_i(z)$ is then given by equation 4.23 and equation 4.26 as

$$H_i(z) = H_{i,d}(z) H_{i,h}(z) \tag{4.27}$$

A bode diagram is shown in figure 4.8 for this combined function with the phase lifting filter constant set to $k_d = 0.5$ and different bandwidths of the highpass filter.

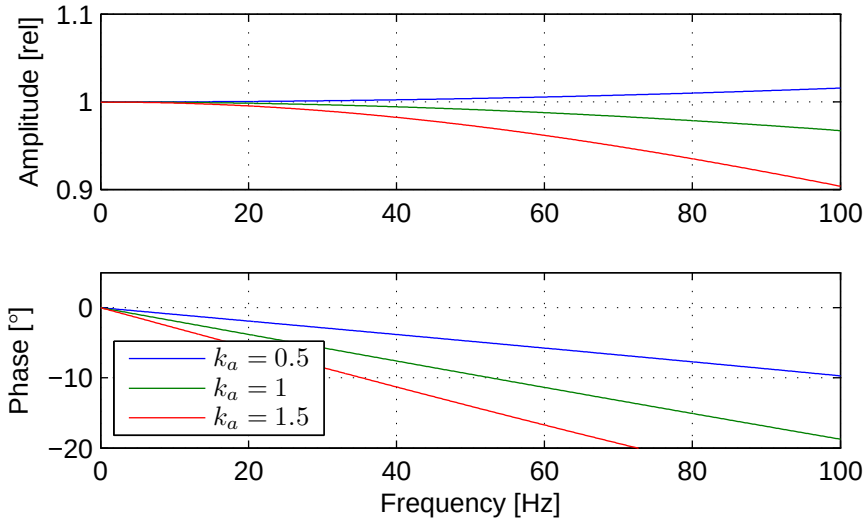

Figure 4.7 – Impact on the voltage reference from the active damping around the nominal frequency. The plot shows the relative magnitude and phase shift of $\frac{v_f}{v_{\text{ref}}}(\text{j}\omega)$. The converter is not connected to a load, and the filter current reference is set to zero.

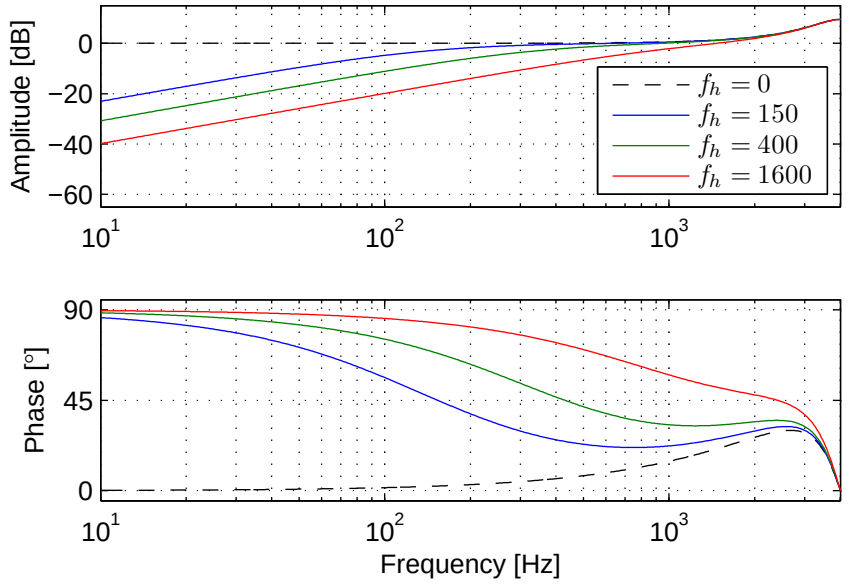

Figure 4.8 – Bode diagram of the current shaping function $H_i(z)$ for different highpass bandwidth constants.

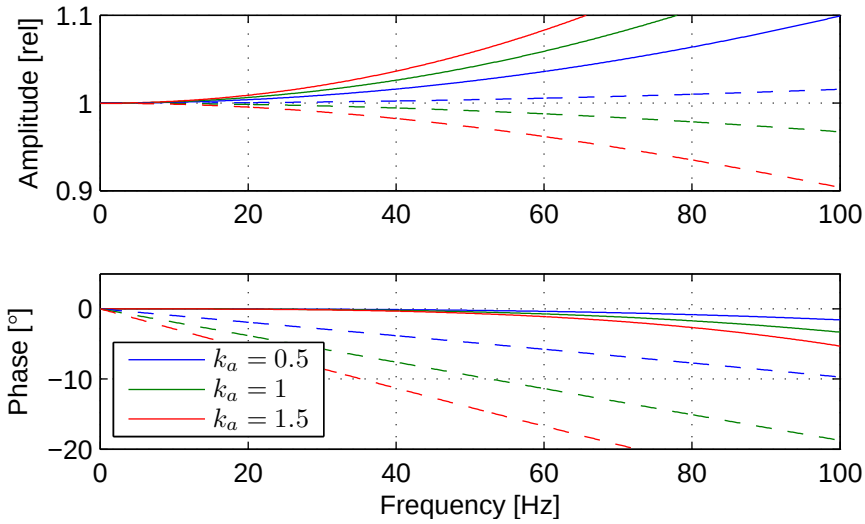

Figure 4.9 – Impact on the filter voltage from the active damping with highpass filter around the nominal frequency. The plot shows the relative magnitude and phase shift of $\frac{v_f}{v_{\text{ref}}}(\mathrm{j}\omega)$. The converter is not connected to a load, and the filter current reference is set to zero. The dashed lines are the responses for the corresponding active damping without the highpass filter.

The bandwidth of the highpass filter is chosen as $f_h = 400$. The new impact on the filter voltage from the active damping when the highpass filter is included is shown in figure 4.9. The old impact from figure 4.7 is included as dashed lines for comparison.

To summarize, the active damping function and gain in figure 4.1 is given by

$$\boldsymbol{H}_i(z) = \begin{bmatrix} H_i(z) & 0 \\ 0 & H_i(z) \end{bmatrix}, \tag{4.28}$$

$$\boldsymbol{K}_i = \begin{bmatrix} k_a & 0 \\ 0 & k_a \end{bmatrix}, \tag{4.29}$$

with $H_i(z)$ given in equation 4.27.

4.4 Voltage shape controller

The voltage shape controller is used to correct deviations from the sinusoidal voltage shape. It reduces any lower harmonics in the capacitor voltage filter, which improves the performance for non-linear loads.

It is implemented as a feedback loop using a pure proportional controller. An integrating controller is avoided as it might interact unfavorably with other converters with integrating controllers.

The voltage feedback shaping function $\boldsymbol{H}_v(z)$ in figure 4.1 is simply set to the identity matrix $\boldsymbol{I}$ in this thesis. If better performance for certain frequencies are wanted, one or several peak filters can be used to boost these frequencies. A low pass filter could also be included to avoid noise amplification and interactions with the active damping.

Thus:

$$\boldsymbol{H}_v(z) = \begin{bmatrix} 1 & 0 \\ 0 & 1 \end{bmatrix}, \tag{4.30}$$

$$\boldsymbol{K}_v = \begin{bmatrix} k_v & 0 \\ 0 & k_v \end{bmatrix}. \tag{4.31}$$

4.5 The virtual impedance feedback

The programmable virtual impedance feedback reduces the output voltage depending on the output current to give the apperance of an impedance between the converter and the grid.

Consider first the constant diagonal matrix

$$\boldsymbol{K}_z = \begin{bmatrix} k_z & 0 \\ 0 & k_z \end{bmatrix} \tag{4.32}$$

The equation of the load current, i_g, of the equivalent single phase system is

$$v_f - v_g = \frac{sx_g}{\omega_n} i_g \tag{4.33}$$

Ignoring the time delay and assuming perfect control of v_f, the impedance feedback changes the output voltage to

$$v_{\text{ref}} - k_z i_g - v_g = \frac{sx_g}{\omega_n} i_g \implies v_{\text{ref}} - v_g = \left(\frac{sx_g}{\omega_n} + k_z \right) i_g. \tag{4.34}$$

This shows that the virtual impedance introduced by this feedback will have the same effect as an ohmic resistor connected in series with the output inductor. The virtual resistor will, unlike a real resistor, not use any energy. The time delay which was ignored here will limit the maximum obtainable impedance and create non-ohmic response for frequencies where the above assumptions does not hold.

An ohmic resistor is useful in series with the inductance in a number of situations. It reduces the output current from the converter in case

the converter voltage and grid voltage are out of phase, and dampens the phase locking mechanism. The resistor will also dampen and stabilize any subharmonic oscillations between the converter and other generators in the grid.

As the impedance is programmable, it can be changed during operation. This can be used to help synchronize it after e.g. a short circuit where the phase information of the net has been lost, or to connect or disconnect "softly" to and from a grid.

A non-ohmic response can also be considered using the derivative of the output current. Using a negative virtual inductance can for instance reduce the effect of the inductance connecting the converter to the grid. This derivative will typically have a significant noise component and phase shift for higher harmonics which will limit the shaping of the impedance to the lower harmonics. It is also possible to tune the virtual impedance for individual harmonics by shaping the feedback signal using peak and notch filters.

4.5.1 Interperiodic virtual impedance control

A side effect of the virtual resistor is a drop in the output voltage as the load increases. For linear loads, a slower outer controller can adjust the reference amplitude to compensate. But for non-linear loads like e.g. diode rectifiers the response will be deteriorated by the impedance. However, it is possible to mitigate this.

The phase related and non-linear load related effects take mostly place in different places in the voltage period. Consider first a single phase system. Figure 4.10 shows two unit voltages, one phase delayed by 5°, and their difference. This difference creates currents which can be reduced by using a virtual impedance to allow for a larger phase shift between the voltages. It is maximum at the zero crossing, and close to zero at the top. On the other hand, a diode rectifier only pulls current at the voltage peaks, where there is no effect of the phase shift.

By updating the impedance within the voltage period to be large at the voltage zero crossing and small at the voltage peaks, both the positive effects of the virtual impedance and a good response to non-linear loads can be obtained. For a single phase system this virtual impedance can be shaped as

$$f_z(\theta) = \tilde{k}_z(\sin\theta)^2 \tag{4.35}$$

This signal is smooth and avoids introducing higher harmonics into the voltage. Figure 4.11 shows a plot of this impedance function together with

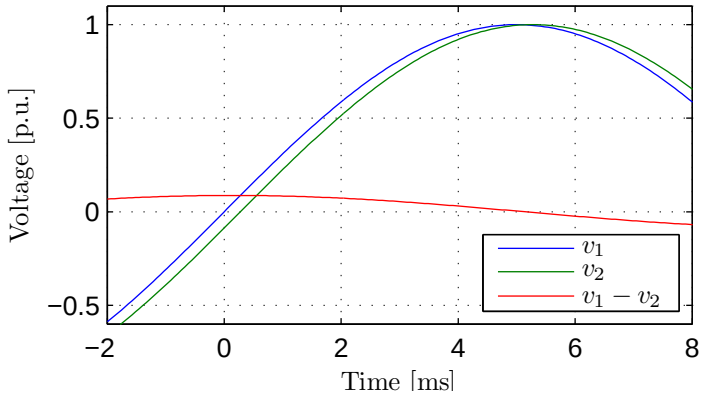

Figure 4.10 – Two sinusoidal voltages separated by 5° and their difference.

its corresponding single phase voltage. This virtual impedance for single phase systems was proposed in a paper released at Norpie 2002 [2].

For a three phase system, the situation is a bit more complicated. A three phase system has three linearly dependent output voltages, which can be reduced to two decoupled systems by ignoring the null system. Similarly, one virtual output impedance for each of the three phases can be reduced to two virtual impedances for the decoupled systems.

Let there be three individual virtual impedances instead of a symmetric one. The feedback signal in the *abc*-frame is then

$$\boldsymbol{v}_z^{abc} = \boldsymbol{K}_z^{abc}\boldsymbol{i}_g^{abc} = \begin{bmatrix} k_{z,a} & 0 & 0 \\ 0 & k_{z,b} & 0 \\ 0 & 0 & k_{z,c} \end{bmatrix} \boldsymbol{i}_g^{abc}. \tag{4.36}$$

This can be converted to the $\alpha\beta$-frame using the $\alpha\beta$-transform:

$$\begin{aligned} \boldsymbol{v}_z^{\alpha\beta} &= \mathbf{T}_{abc}^{\alpha\beta}\boldsymbol{K}_z^{abc}\mathbf{T}_{\alpha\beta}^{abc}\boldsymbol{i}_g^{\alpha\beta} \\ &= \frac{1}{6}\begin{bmatrix} 4k_{z,a} + k_{z,b} + k_{z,c} & -\sqrt{3}(k_{z,b} - k_{z,c}) \\ -\sqrt{3}(k_{z,b} - k_{z,c}) & 3k_{z,b} + 3kz, c \end{bmatrix} \boldsymbol{i}_g^{\alpha\beta} \\ &= \boldsymbol{K}_z^{\alpha\beta}\boldsymbol{i}_g^{\alpha\beta}. \end{aligned} \tag{4.37}$$

Equation 4.37 and equation 4.35 can be used to find an interperiodic virtual impedance similarly to the interperiodic impedance for the single

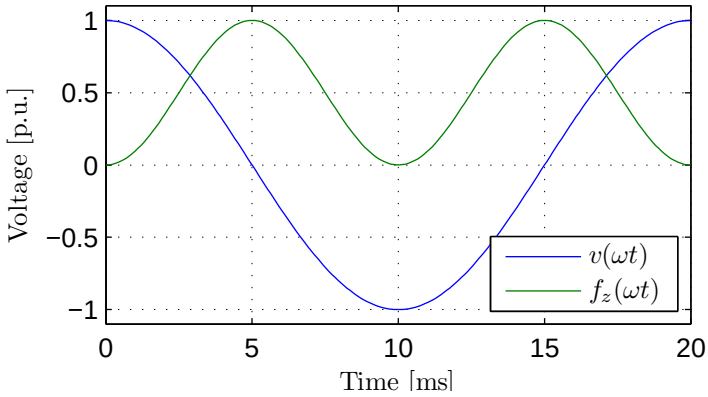

Figure 4.11 – Plot of the time varying virtual impedance function.

Table 4.1 – Response for non linear load for different virtual impedances.

Description	$V_{\text{DC,load}}$ [V]
No virtual impedance	302.8 V
Time varying virtual impedance of $\tilde{k}_z = 0.1$	299.0 V
Fixed virtual impedance of $k_z = 0.05$	295.5 V

phase system. Let the individual virtual impedances be

$$\begin{aligned} k_{z,a} &= k_z + \tilde{k}_z \left(\sin\theta\right)^2, \\ k_{z,b} &= k_z + \tilde{k}_z \left(\sin(\theta - 120°)\right)^2, \\ k_{z,c} &= k_z + \tilde{k}_z \left(\sin(\theta - 240°)\right)^2. \end{aligned} \tag{4.38}$$

Inserting this into equation 4.37 gives the feedback matrix

$$\boldsymbol{K}_z(\theta) = k_z + \frac{\tilde{k}_z}{2} \begin{bmatrix} 1 - \frac{1}{2}\cos(2\theta) & -\frac{1}{2}\sin(2\theta) \\ -\frac{1}{2}\sin(2\theta) & 1 + \frac{1}{2}\cos(2\theta) \end{bmatrix}. \tag{4.39}$$

Here, k_z tunes the static impedance and $\tilde{k}_z$ the time varying impedance.

An experiment was done to confirm the improved response to non-linear loads. A three phase diode rectifier with a capacitor bank of 3300 µF and resistance of 36 Ω was placed as the load of the converter. The output of the converter was set to 1 p.u., i.e. a phase-to-phase voltage of 230 V_{RMS}.

The DC-voltage of the capacitor bank was then measured using a multimeter. The results are summarized in table 4.1. Later, in section 5.5.2, the

current response for a phase shift is shown to be much lower for the time varying impedance as well.

One difference between the single phase system and the three phase system for the interperiodic time-variant virtual impedance, is that the resulting three phase system impedance never goes to zero impedance. Let $\theta = 0$ and $k_z = 0$, then

$$\begin{aligned} k_{z,a} &= 0, \\ k_{z,b} &= \tilde{k}_z \left(\sin(-120^\circ)\right)^2 = \frac{3}{4}\tilde{k}_z, \\ k_{z,c} &= \tilde{k}_z \left(\sin(-240^\circ)\right)^2 = \frac{3}{4}\tilde{k}_z. \end{aligned} \tag{4.40}$$

The resulting virtual impedance for the phase a current will be the parallel of the phase b and phase c impedance, i.e. $\frac{3}{8}\tilde{k}_z = 0.375\tilde{k}_z$. An alternative if a smaller impedance is wanted is to use

$$f_z(\theta) = \tilde{k}_z(\sin\theta)^{2n} \tag{4.41}$$

with n an integer > 1. As an example, for $n = 4$ the resulting minimum impedance is

$$\left(\frac{3}{4}\right)^4 \tilde{k}_z \approx 0.1582\tilde{k}_z. \tag{4.42}$$

Other, less smooth interperiodic impedances can also be considered.

4.6 Experimental tuning of parameters

The active damping can be tested by short circuiting the grid voltage, i.e. $v_g = 0$, and sending a short pulse from the converter. The pulse will set the resonance of the filter ringing. The active damping is then released to dampen out the ringing. Figure 4.12 compares the short circuited filter response without any feedback, with only active damping, and with full damping and voltage feedback.

The active damping must also work when the grid is not connected. In this case the resonance frequency of the filter is much lower. The damping can be tested in the same way as for the short circuited case. Figure 4.13 compares the responses for a filter not connected to the grid without and with the active damping.

A synchron machine generator was used to illustrate the active damping. The machine generates slot harmonics at 17 times its fundamental harmonic frequency. The generator was run at different speeds with the

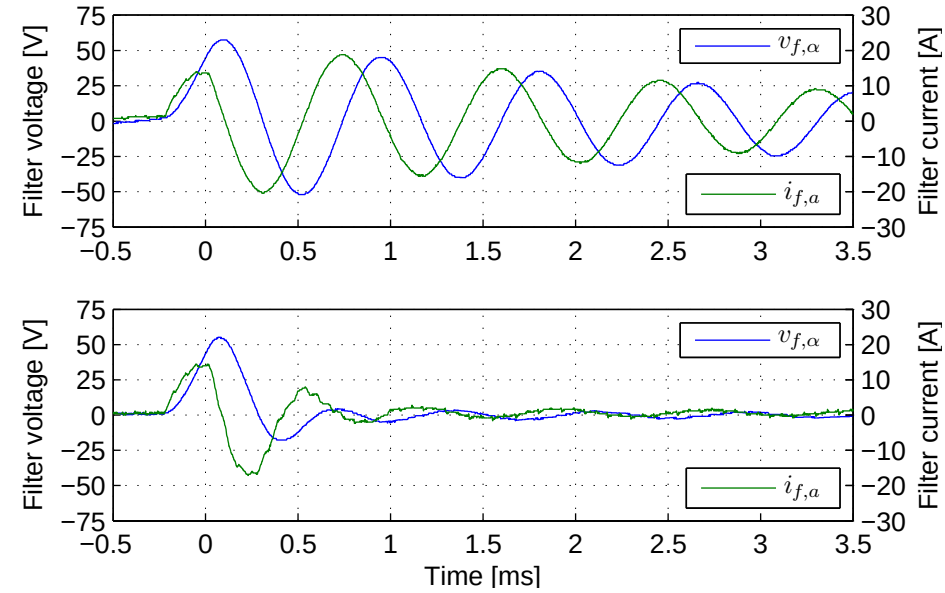

Figure 4.12 – Plot of measurements for filter response without and with active damping for short circuited grid.

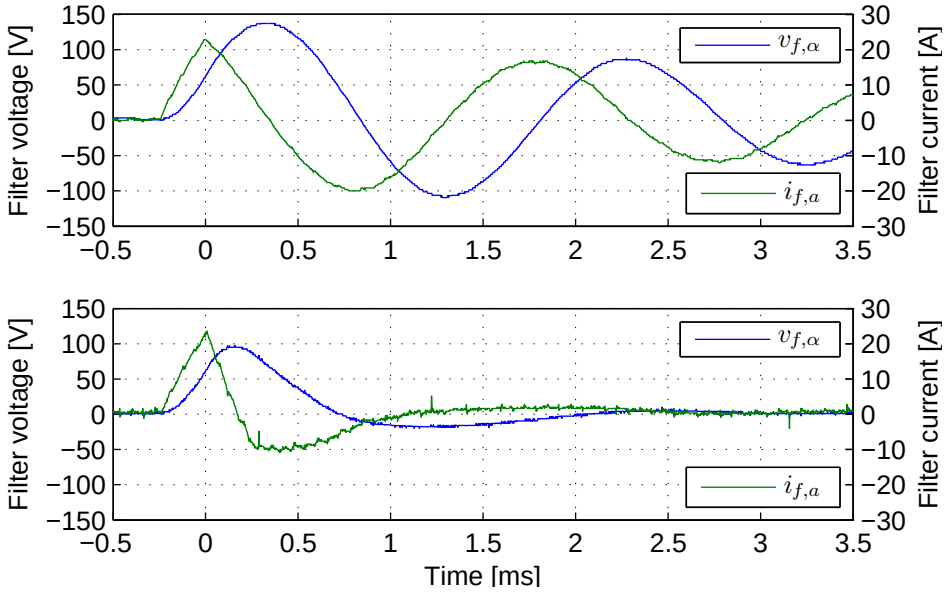

Figure 4.13 – Plot of measurements for filter response without and with active damping for disconnected grid.

filter connected to locate the resonance frequency. It was found at approximately 500 Hz. The converter was then enabled with its active damping. Figure 4.14 shows measurement plots and net topologies of this case.

If the synchronous generator is run at its nominal speed giving a 50 Hz voltage, its slot harmonics induces a 850 Hz capacitor current. This is above the bandwidth of the filter and its controller. Being above the bandwidth, the signal is not damped. Figure 4.15 shows measurement plots of this case.

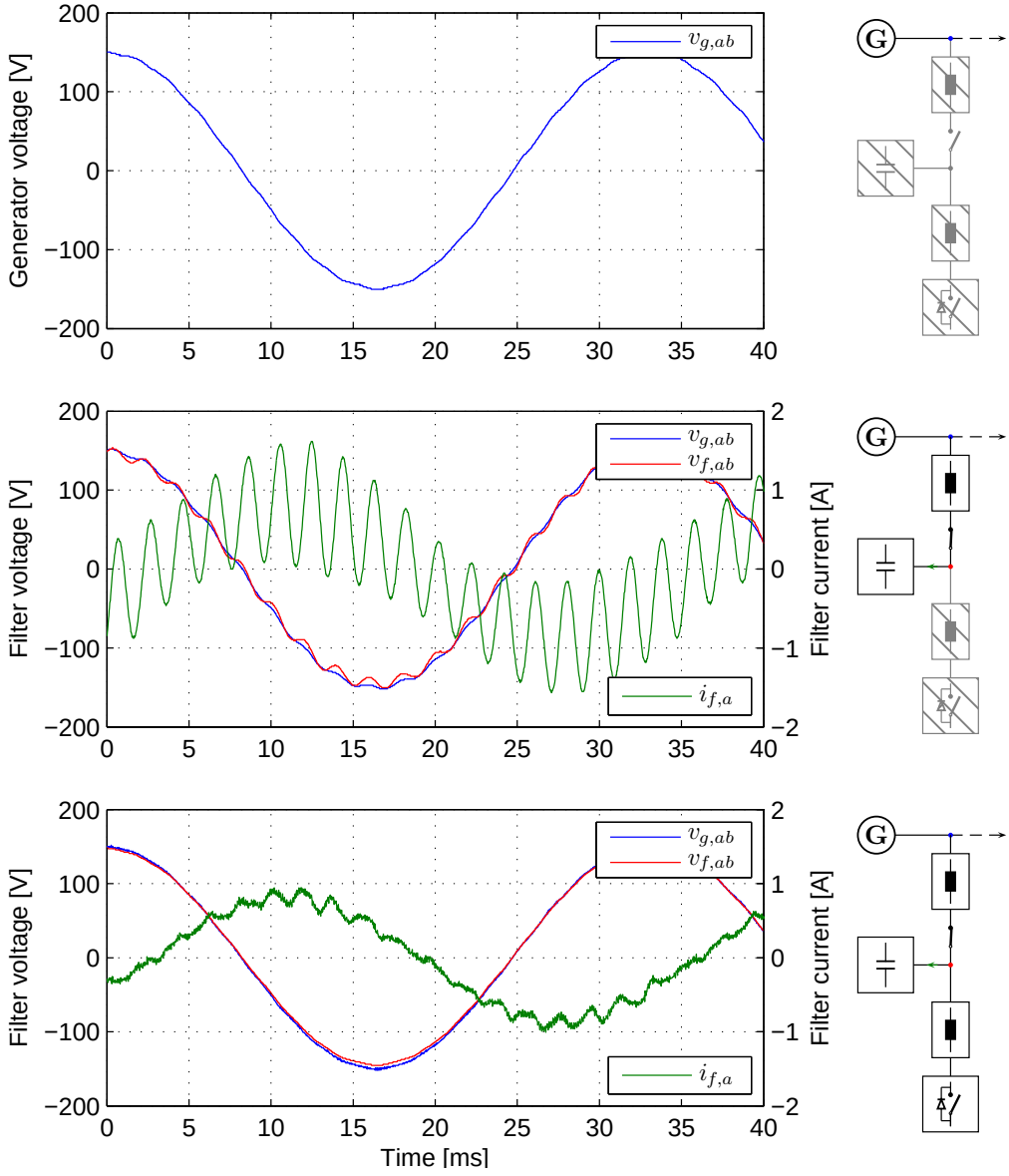

Figure 4.14 – Measurements of voltage and current with actively damped LCL filter. A generator is run at approximately 30 Hz which induces slot harmonics of 510 Hz. This excites the resonance frequency of the filter. The top figure shows the generator running without the filter connected. The middle figure shows the generator running with the filter connected but the converter disabled. The bottom figure shows the generator running with the filter connected and the converter enabled. The net topologies of the experiments are shown to the right of the plots.

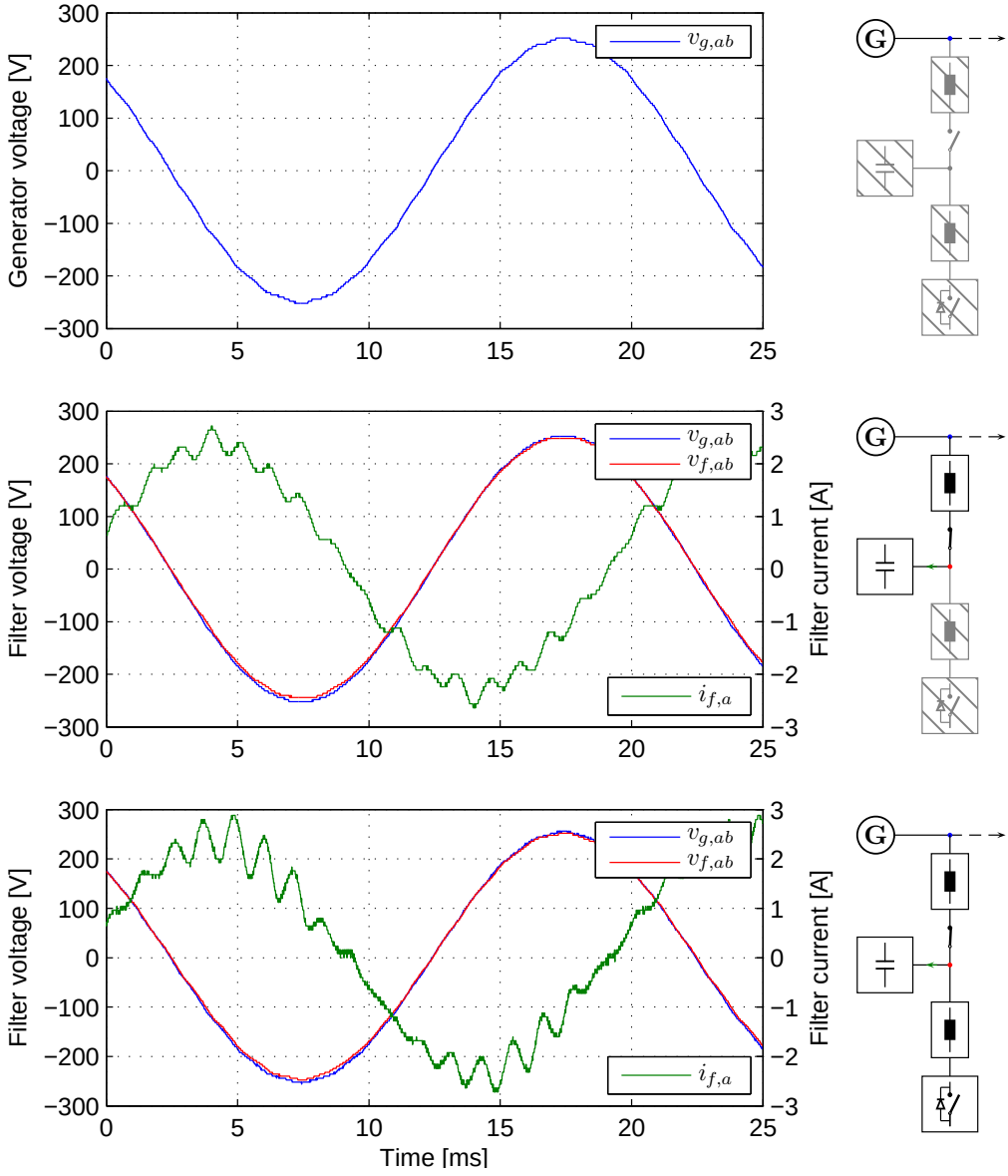

Figure 4.15 – Measurements of voltage and current with actively damped LCL filter without sufficient bandwidth. A generator is run at 50 Hz which induces slot harmonics of 850 Hz. The top figure shows the generator running without the filter connected. The middle figure shows the generator running with the filter connected but the converter disabled. The bottom figure shows the generator running with the filter connected and the converter enabled. This does not dampen out the harmoics as the bandwidth of the filter is to low. The net topologies of the experiments are shown to the right of the plots.

CHAPTER 5

Active and reactive power control

The active and reactive power control uses the capacitor voltage generated by the inner voltage controller to control the flow of active and reactive power from the converter.

5.1 Overview

Figure 5.1 shows an overview of the power controller. The inputs are the active power reference $P_{g,\mathrm{ref}}$, and the reactive power reference $Q_{g,\mathrm{ref}}$.

The parameters are the nominal voltage, v_0, and the nominal frequency ω_0. A nominal phase, α_0, can also be included here as a tuning parameter.

The measurements are the active power P_g, the reactive power Q_g, and the converter current $\boldsymbol{i}_e^{\mathrm{dq}}$. The d-component of the capacitor voltage, $v_{f,\mathrm{d}}$, is also used by the active and reactive power controller to calculate the feed

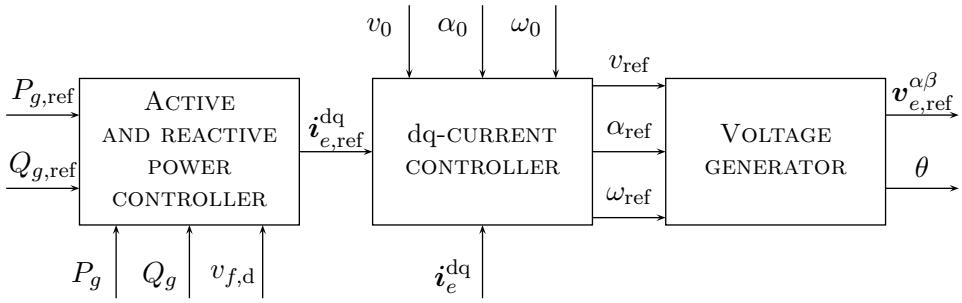

Figure 5.1 – Overview of the power controller.

forward signal to the dq-current controller.

The outputs are the capacitor voltage reference $\boldsymbol{v}_{e,\mathrm{ref}}^{\alpha\beta}$, and the reference frame for the dq-coordinate system, θ.

5.2 The dq reference frame

The dq-system originates from motor drive theory, where the d and q axis is dependent upon the flux field and the rotor position. For a normal motor only the q-current from the converter affects the output torque of the machine. In other words, the q-current determines the active power output, and the d-current gives the reactive power output. See for example [18] for a discussion of electrical machines and active and reactive power.

A converter connected to a grid has no physical rotor. The frequency of the grid provides the angular speed of the dq-system, but the phase can be chosen freely. In this thesis, the angle is chosen to be that of the reference of the capacitor voltage. That is, the reference vector of the inner voltage controller in the dq-frame is given by

$$\boldsymbol{v}_{\mathrm{ref}}^{\mathrm{dq}} = \begin{bmatrix} v_{\mathrm{ref}} \\ 0 \end{bmatrix}. \tag{5.1}$$

This means that unlike the motor drive, the d-current gives the active power output, and the q-current the reactive power output.

The reference vector in equation 5.1 is not the real capacitor voltage. The reference vector is changed by the inner voltage controller by the virtual impedance. Furthermore, the voltage shape controller does not regulate the capacitor voltage perfectly. This means that the relationship between d and q current components and the active and reactive power output is only approximate. However, the coupling is strong enough for the d component of the current to be called the active current, and for the q component of the current to be called the reactive current in this thesis.

5.3 Active and reactive power in the dq-system

For a general three phase system, instantaneous active and reactive power is given in the dq-frame as

$$P = v_{\mathrm{d}} i_{\mathrm{d}} + v_{\mathrm{q}} i_{\mathrm{q}}, \tag{5.2}$$

$$Q = v_{\mathrm{d}} i_{\mathrm{q}} - v_{\mathrm{q}} i_{\mathrm{d}}, \tag{5.3}$$

where P is the active power, and Q the reactive power. v_d, v_q, i_d, and i_q are the d and q components of the voltage and current, respectively.

As a side note it can be remarked that the definition of instantaneous reactive power has been somewhat contentious over the years. More recent papers on the subject (see e.g. [19] or [20]) refers to the instantaneous imaginary power introduced by Akagi [21], given by

$$q(t) = v_\alpha i_\beta - v_\beta i_\alpha. \tag{5.4}$$

This corresponds to the definition of the reactive power given here. From a geometrical point of view it can be worth noting that the reactive power in equation 5.2 corresponds to the cross product of the voltage vector and the current vector if they are extended to a third dimension.

As mentioned in the previous section, the reference frame for the dq-coordinate system have been chosen so the d-current gives active power output, and the q-current reactive power output. This is different from general motor theory, where the situation is opposite. Equation 5.3 shows that this swap of currents will cause the sign of Q to be changed as well.

The active and reactive power delivered to the capacitor from the converter is thus

$$P_e = v_{f,\mathrm{d}} i_{e,\mathrm{d}} + v_{f,\mathrm{q}} i_{e,\mathrm{q}}, \tag{5.5}$$
$$Q_e = v_{f,\mathrm{d}} i_{e,\mathrm{q}} - v_{f,\mathrm{q}} i_{e,\mathrm{d}}. \tag{5.6}$$

Likewise the active and reactive power delivered to the grid from the capacitor is

$$P_g = v_{f,\mathrm{d}} i_{g,\mathrm{d}} + v_{f,\mathrm{q}} i_{g,\mathrm{q}}, \tag{5.7}$$
$$Q_g = v_{f,\mathrm{d}} i_{g,\mathrm{q}} - v_{f,\mathrm{q}} i_{g,\mathrm{d}}. \tag{5.8}$$

For the capacitor, using equation A.34 gives

$$\boldsymbol{i}_f^{\mathrm{dq}} = \frac{y_f}{\omega_n} \left(\boldsymbol{\omega} \times \boldsymbol{v}_f^{\mathrm{dq}} + \dot{\boldsymbol{v}}_f^{\mathrm{dq}} \right) \tag{5.9}$$

Considering the steady state situation, i.e. $\dot{\boldsymbol{v}}_f^{\mathrm{dq}} = 0$, the capacitor current is given by

$$i_{f,d} = y_f v_{f,q}, \tag{5.10}$$
$$i_{f,q} = -y_f v_{f,d}. \tag{5.11}$$

Thus, as $\boldsymbol{i}_e^{\mathrm{dq}} = \boldsymbol{i}_g^{\mathrm{dq}} + \boldsymbol{i}_f^{\mathrm{dq}}$

$$P_e = v_{f,\mathrm{d}} i_{g,\mathrm{d}} + v_{f,\mathrm{q}} i_{g,\mathrm{q}} + y_f \left(v_{f,\mathrm{d}} v_{f,\mathrm{q}} - v_{f,\mathrm{q}} v_{f,\mathrm{d}}\right) = P_g, \tag{5.12}$$

$$Q_e = v_{f,\mathrm{d}} i_{g,\mathrm{q}} - v_{f,\mathrm{q}} i_{g,\mathrm{d}} - y_f \left(v_{f,\mathrm{d}} v_{f,\mathrm{d}} + v_{f,\mathrm{q}} v_{f,\mathrm{q}}\right) = Q_g - y_f \|\boldsymbol{v}_f^{\mathrm{dq}}\|_2^2. \tag{5.13}$$

This shows that the capacitor will not affect the active power in steady state, which is as expected. For a typical situation with a filter voltage amplitude of one and $y_f = 0.15$, the capacitor will subtract 15 % reactive power.

The inductance separating the capacitor from the grid is not included and can be considered part of the grid here. It will only affect the reactive power and can be handled similarly as the capacitance.

5.4 Voltage reference generator

The voltage reference generator is responsible for creating the reference for the inner voltage controller described in the previous chapter, given a frequency and amplitude reference. It corresponds in many ways to the rotor and magnetizing circuit of a machine.

The angle of the dq-frame is defined from the voltage reference. It is established using an integrator from the reference frequency. Using Euler's method to convert this integrator to a discrete model gives the difference equation*

$$\theta_k = \theta_{k-1} + T\omega_k \tag{5.14}$$

The time delay from the measurements to the output means that the dq-frame has rotated from the measurement until the reference output is in effect. For example, for a reference frequency of 50 Hz and a switching frequency of 8 kHz, the difference will be 2.25°. This rotation can be taken into account when converting to and from the dq-frame by changing the frame from θ_k to θ_{k+1} before calculating the reference.

Figure 5.2 shows a block diagram of the voltage reference generator. Here, v_{ref} is the voltage magnitude reference. The dq-coordinates of the voltage reference, $\boldsymbol{v}_{\mathrm{ref}}^{\mathrm{dq}}$, is given by setting v_{ref} as the d-component, and 0 as the q-component. In the figure a small angle, α_{ref}, which rotates the voltage reference vector, has been included. This can be used for extra tuning purposes.

*The infinitely increasing angle will create problems for a computer implementation. To avoid the numerical problems the angle is normally restricted to e.g. the range $\langle -\pi, \pi]$ by adding/subtracting a multiple of 2π.

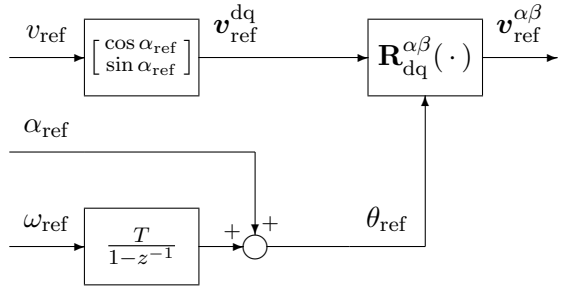

Figure 5.2 – Block diagram of the voltage reference generator.

ω_{ref} is the voltage frequency reference. α_{ref} is a phase adjustment term enabling immediate tuning of the phase. θ_{ref} is the dq-frame angle for the reference.

5.5 dq-current controller

A voltage amplitude difference or a phase shift between the capacitor voltage and the grid voltage will cause a current to flow. It is however not trivial how this difference decouples into a d and a q current. Effects like for example the dead-band, internal impedances of the IGBTs, and the tuning of the inner voltage controller will change this coupling.

5.5.1 Ideal impedance response

Let two three phase voltage vectors with a fixed difference in amplitude and phase be given by

$$\boldsymbol{v}_1^{abc} = v(1+\delta)\begin{bmatrix}\cos(\omega_n t)\\ \cos(\omega_n t - 120°)\\ \cos(\omega_n t - 240°)\end{bmatrix}, \tag{5.15}$$

$$\boldsymbol{v}_2^{abc} = v\begin{bmatrix}\cos(\omega_n t + \alpha)\\ \cos(\omega_n t + \alpha - 120°)\\ \cos(\omega_n t + \alpha - 240°)\end{bmatrix}. \tag{5.16}$$

δ gives the relative difference of the voltages, and α gives the difference in the angle between the first and the second voltage.

Now consider an ideal symmetric impedance with inductance $\frac{x}{\omega_n}$ and resistance r connected between the two voltages. Ohm's law gives the relation between the current and voltage vectors as

$$\frac{x}{\omega_n}\frac{d}{dt}\boldsymbol{i}^{abc} + r\boldsymbol{i}^{abc} = \boldsymbol{v}_1^{abc} - \boldsymbol{v}_2^{abc}. \tag{5.17}$$

Transforming the right side of equation 5.17 using the dq-transform with the dq-frame aligned to the phase of $\boldsymbol{v}_1^{abc}$ gives the voltage difference

$$\boldsymbol{v}_1^{\mathrm{dq}} - \boldsymbol{v}_2^{\mathrm{dq}} = v \begin{bmatrix} 1 + \delta - \cos\alpha \\ -\sin\alpha \end{bmatrix}. \tag{5.18}$$

Similarly, transforming the left side of equation 5.17 with the help of equation A.34 gives

$$r\boldsymbol{i}^{\mathrm{dq}} + \mathbf{R}_{\alpha\beta}^{\mathrm{dq}} \mathbf{T}_{abc}^{\alpha\beta} \frac{x}{\omega_n} \frac{d}{dt} \boldsymbol{i}^{abc} = r\boldsymbol{i}^{\mathrm{dq}} + \frac{x}{\omega_n} \left(\begin{bmatrix} i_{\mathrm{q}} \\ -i_{\mathrm{d}} \end{bmatrix} \omega_n + \frac{d}{dt} \boldsymbol{i}^{\mathrm{dq}} \right). \tag{5.19}$$

Combining the two sides and assuming a steady state system gives

$$\begin{bmatrix} r & x \\ -x & r \end{bmatrix} \boldsymbol{i}^{\mathrm{dq}} = v \begin{bmatrix} 1 + \delta - \cos\alpha \\ -\sin\alpha \end{bmatrix}. \tag{5.20}$$

Thus, the current response in the dq-frame can be given as

$$\boldsymbol{i}^{\mathrm{dq}} = \frac{v}{\sqrt{x^2 + r^2}} \boldsymbol{R}(\beta) \boldsymbol{\delta}_v^{\mathrm{dq}}, \tag{5.21}$$

where

$$\boldsymbol{R}(\beta) = \begin{bmatrix} \cos\beta & -\sin\beta \\ \sin\beta & \cos\beta \end{bmatrix}, \ \beta = \arctan\left(\frac{x}{r}\right), \tag{5.22}$$

$$\boldsymbol{\delta}_v^{\mathrm{dq}} = \begin{bmatrix} 1 + \delta - \cos\alpha \\ -\sin\alpha \end{bmatrix}. \tag{5.23}$$

The new angle β is a rotational term introduced by the relation between the resistance and the inductance of the impedance.

Now assume the phase difference to be small, i.e. $\sin\alpha \approx \alpha$ and $\cos\alpha \approx 1$. If the inductance is zero, i.e. $x = 0$, the rotational angle is $\beta = 0$ and the current response becomes

$$\boldsymbol{i}^{\mathrm{dq}} = \frac{v}{r} \begin{bmatrix} \delta \\ -\alpha \end{bmatrix}. \tag{5.24}$$

This means that for this case a voltage amplitude difference will cause a active power flow, and a difference in phase cause a reactive power flow. This is called an ohmic response.

If the resistance is zero instead and the impedance positive, i.e. $r = 0$, and $x > 0$ the rotational angle is $\beta = 90°$ and the current response becomes

$$\boldsymbol{i}^{\mathrm{dq}} = \frac{v}{x} \begin{bmatrix} \alpha \\ \delta \end{bmatrix}. \tag{5.25}$$

For this case, a difference in voltage amplitude gives a reactive power flow, and a difference in phase a active power flow. This is called an inductive response. If $x < 0$, $\beta = -90°$, the current response will change sign. This is called a capacitive response.

5.5.2 Mapping of active and reactive current

Instead of trying to calculate the converters' response to differences in the voltage amplitude or phase, the converter can be "mapped" empirically by setting a fixed phase shift or a fixed amplitude difference and measuring the resulting current components.

In this thesis, this is done using two converters. The DC-buses are interconnected and the outputs connected together through a transformator, separating them galvanically. One converter is set to run at a fixed frequency and amplitude, basically functioning as a signal generator to create a strong net. To further strengthen the voltage of this converter, the grid side inductor is bypassed, and the virtual impedance set to zero.

The other converter is configured to lock its phase to its capacitor voltage using the net observer. This converter can now be set to run at a fixed phase shift and a fixed amplitude difference. The currents are then measured in the dq-frame.

An automatic scan is run through a matrix of 21×21 different amplitudes and phases, creating 441 sampling points. The corresponding current response creates a "topographic map" of the current responses of the converter against a strong net. The absolute output phase and amplitude was set to values that reduced the output current to approximately zero before each scan, centering the map.

Two discontinuities are generally visible in a map. These are caused by a limited DC-voltage and the overcurrent protection (See section 1.5.3).

The DC-link voltage is 2 p.u. without load for the system used here. When the converter is loaded, i.e. transmitting power to the grid, it will drop even further. This will limit the maximum obtainable output voltage amplitude, and thus the maximum positive output difference available. Equation 1.5 gives the absolute maximum output voltage assuming space vector modulation and non-overmodulated mode. For the no-load situation where $v_{\mathrm{DC}} = 2$ p.u. the maximum output voltage is

$$v_{\max} = \frac{1}{\sqrt{3}} v_{\mathrm{DC}} = \frac{2}{\sqrt{3}} \approx 1.15. \tag{5.26}$$

Because of this limitation, the grid voltage is lowered to around 0.9 p.u. when running the automatic scan.

The overcurrent protection protects the converter and the load from excessive currents. It caps the output current of the individual phases to a maximum limit. The limit for the system used here is set to 2.25 p.u..

Figure 5.3 shows a contour map of $\boldsymbol{i}_e^{\mathrm{dq}}$ when the virtual impedance have been turned off. The blue lines are the contours of $i_{e,\mathrm{d}}$, and the green lines are the contours of $i_{e,\mathrm{q}}$. The discontinuity caused by the limited DC-voltage is visible in the right of the plot.

Red dotted lines have been included to indicate the total magnitude of the current at 1 p.u. and 2 p.u.. This magnitude is given by the length of the current vector

$$\|\boldsymbol{i}_e^{\mathrm{dq}}\|_2 = \sqrt{i_{e,\mathrm{d}}^2 + i_{e,\mathrm{q}}^2}. \tag{5.27}$$

The discontinuity caused by the overcurrent protection is visible just outside the 2 p.u. current magnitude line.

Figure 5.4 shows a map of the converter's current response for a fixed virtual impedance of $k_z = 0.05$. Comparing this map to the one in figure 5.3 shows that the impedance lessens the current response of the converter's for differences in the grid voltage, as it should. It is also rotated somewhat towards a more ohmic response.

Figure 5.5 shows a map for the converter when running with a time-varying virtual impedance of $\tilde{k}_z = 0.1$. Comparing this to the one in 5.4 shows a much more relaxed response for phase errors, and a harder response for amplitude errors. Figure 5.6 shows the same map as figure 5.5, but with extended phase difference range.

5.5.3 Decoupling the current feedback

If the system had a mainly inductive response, the phase could be used directly to control the active current, and the amplitude could be used to control the reactive current. For a mainly ohmic response, the regulation can be done similarly, but with the amplitude and phase swapped.

The mapping information from the previous section shows that the converter system have a response which are somewhere between inductive or ohmic. Using the mapping information, a rotation transformation can be found which significantly decouples the current vector into an amplitude and phase part.

A decoupling can be found using least square optimization. Let an error function be given by

$$J = \sum_k \left(\begin{bmatrix} v_k \\ \alpha_k \end{bmatrix} - \boldsymbol{F}\left(\boldsymbol{i}_{e,k}^{\mathrm{dq}}, \boldsymbol{\psi} \right) \right)^2, \tag{5.28}$$

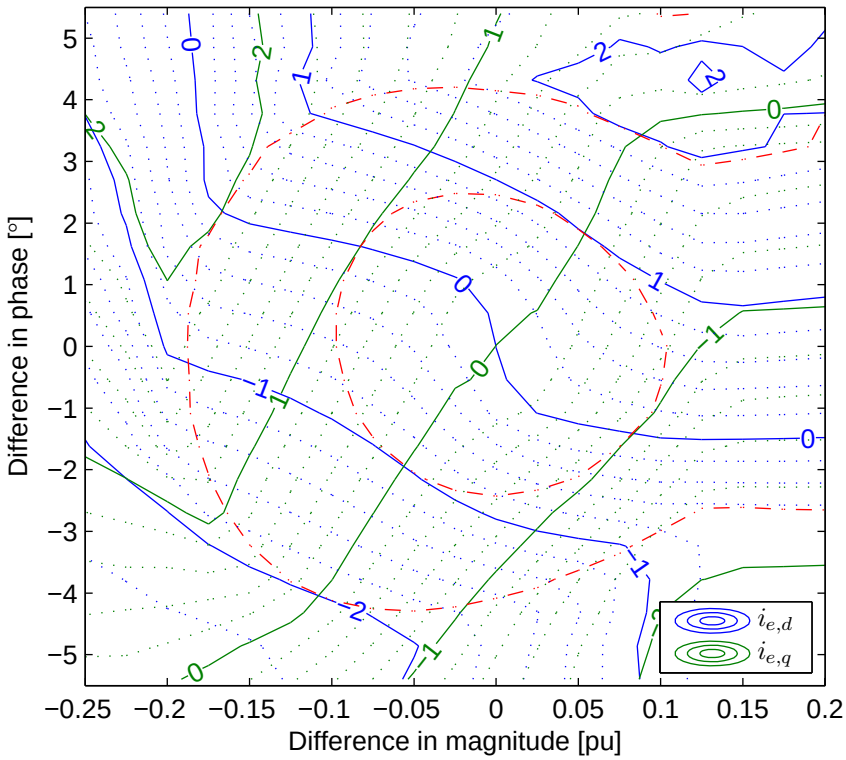

Figure 5.3 – Contour map of measurements of the converter's current response for differences in amplitude and phase with no virtual impedance. The blue lines are the contours of $i_{e,\mathrm{d}}$, and the green lines are the contours of $i_{e,\mathrm{q}}$. In addition, two red dotted lines have been added to show where the converter's current magnitude is 1 p.u. and 2 p.u.. The output current protection is clearly visible just outside the 2 p.u. line. Furthermore, the maximum obtainable positive magnitude difference was limited by the DC-link voltage, as can be seen at the right edge of the plot.

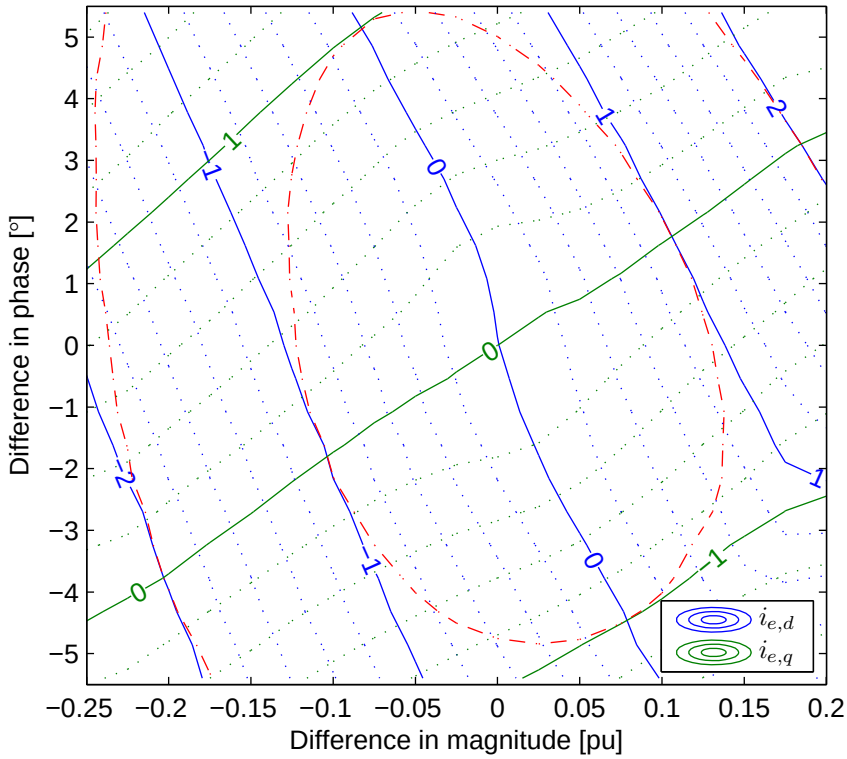

Figure 5.4 – Contour map of measurements of the converter's current response for differences in amplitude and phase with a constant virtual impedance. The blue lines are the contours of $i_{e,\mathrm{d}}$, and the green lines are the contours of $i_{e,\mathrm{q}}$. In addition, two red dotted lines have been added to show where the converter's current magnitude is 1 p.u. and 2 p.u.. The maximum obtainable positive magnitude difference was limited by the DC-link voltage, as can be seen at the lower right corner of the plot.

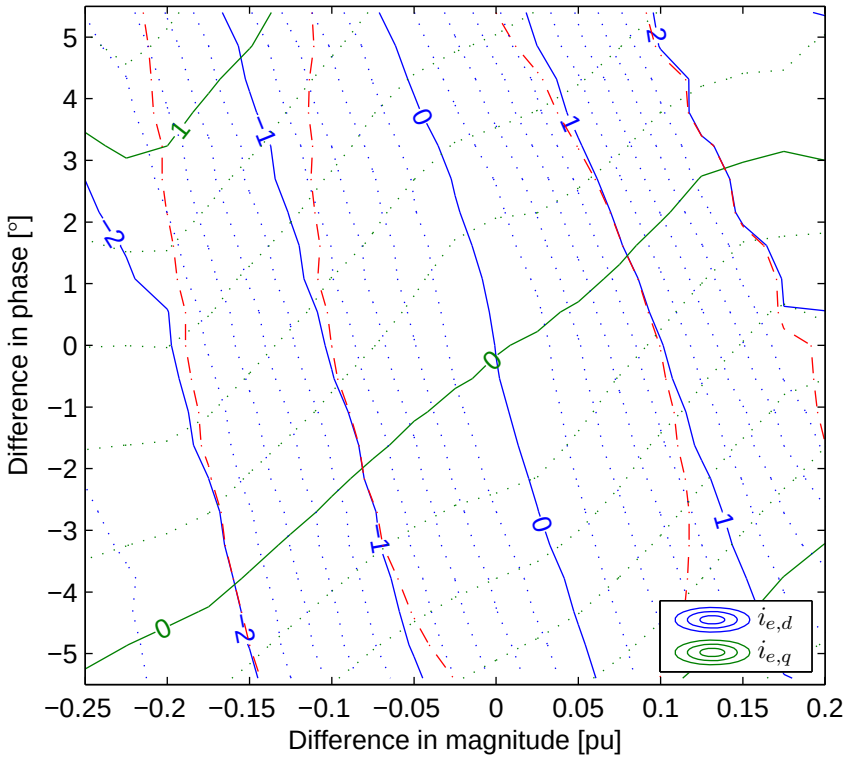

Figure 5.5 – Contour map of measurements of the converter's current response for differences in amplitude and phase with a time-variant virtual impedance. The blue lines are the contours of $i_{e,\mathrm{d}}$, and the green lines are the contours of $i_{e,\mathrm{q}}$. In addition, two red dotted lines have been added to show where the converter's current magnitude is 1 p.u. and 2 p.u.. The effects of the output current protection is visible just outside the 2 p.u. line at the left and right edges.

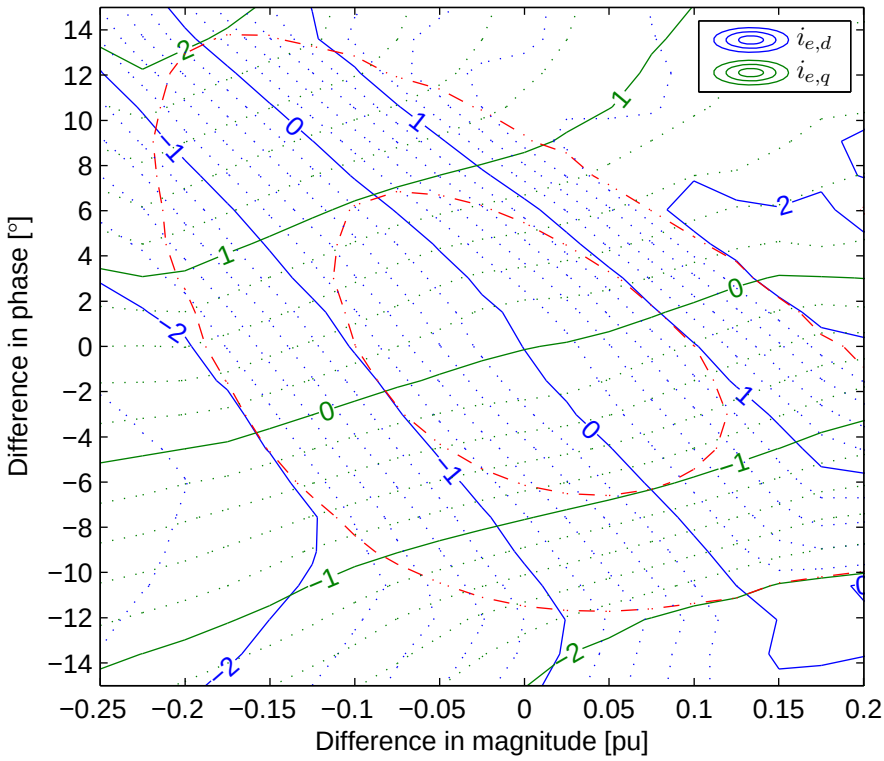

Figure 5.6 – Contour map of measurements of the converter's current response for differences in amplitude and phase with a time-variant virtual impedance with extended phase range. The blue lines are the contours of $i_{e,\mathrm{d}}$, and the green lines are the contours of $i_{e,\mathrm{q}}$. In addition, two red dotted lines have been added to show where the converter current magnitude is 1 p.u. and 2 p.u.. The effects of the output current protection is visible just outside the 2 p.u. line. The maximum obtainable positive magnitude difference was limited by the DC-link voltage, as can be seen at the right edge of the plot.

where v_k and α_k is the amplitude and phase difference for sample point k, $\boldsymbol{i}_{e,k}^{\mathrm{dq}}$ is the measured current response for the same sample point, $\boldsymbol{F}(\,\cdot\,,\cdot\,)$ is a candidate best fit function with $\boldsymbol{\psi}$ the parameters of the best fit function to optimize.

A best fit function candidate is

$$\boldsymbol{F}(\boldsymbol{i}_e^{\mathrm{dq}}, \boldsymbol{\psi}) = \begin{bmatrix} \gamma_m & 0 \\ 0 & \gamma_\theta \end{bmatrix} \boldsymbol{R}(\beta)\boldsymbol{i}_e^{\mathrm{dq}} + \begin{bmatrix} v_0 \\ \alpha_0 \end{bmatrix}, \tag{5.29}$$

$$\boldsymbol{\psi} = \begin{bmatrix} \gamma_m & \gamma_\theta & v_0 & \alpha_0 & \beta \end{bmatrix}^{\mathrm{T}}, \tag{5.30}$$

where γ_m and γ_θ are scaling constants, $\boldsymbol{R}(\beta)$ is the usual rotational matrix

$$\boldsymbol{R}(\beta) = \begin{bmatrix} \cos(\beta) & -\sin(\beta) \\ \sin(\beta) & \cos(\beta) \end{bmatrix}, \tag{5.31}$$

and v_0 and α_0 the amplitude and phase offset giving a zero current response.

Optimizing the error function J for the time varying impedance of $\tilde{k} = 0.05$ for all the points where $\|\boldsymbol{i}_e^{\mathrm{dq}}\| \leq 1$ using a numerical optimization function like e.g. `lsqnonlin` in Matlab gives a result of

$$\begin{aligned} \gamma_m &= 0.1203, \quad \gamma_\theta = 0.01645, \\ v_0 &= 0.8750, \quad \alpha_0 = -2.565^\circ, \\ \beta &= 43.01^\circ \end{aligned} \tag{5.32}$$

Define a new $m\theta$-coordinate system using

$$\boldsymbol{x}^{m\theta} = \mathbf{R}_{\mathrm{dq}}^{m\theta}\boldsymbol{x}^{\mathrm{dq}} \tag{5.33}$$

where $\mathbf{R}_{\mathrm{dq}}^{m\theta}$ is a transformation matrix transforming a vector in the dq-coordinate system to the $m\theta$-coordinate system. It is given as the rotation matrix $\boldsymbol{R}(\beta)$ in equation 5.31. $\boldsymbol{x}^{\mathrm{dq}}$ is any vector in the dq-coordinate system, and $\boldsymbol{x}^{m\theta}$ the corresponding vector in the new $m\theta$-coordinate system.

The current response in this coordinate system is given by $\boldsymbol{i}_e^{m\theta} = \mathbf{R}_{\mathrm{dq}}^{m\theta}\boldsymbol{i}_e^{\mathrm{dq}}$. This current vector is rotated so a change in the amplitude will be strongly coupled with a change in the first vector component, $i_{e,m}$. This component is called the amplitude current. A change in the phase will be strongly coupled with a change in the second vector component $i_{e,\theta}$. This component is called the phase current.

To summarize, the relationship between the amplitude and phase and the output current of the converter can be approximated as

$$\begin{bmatrix} v \\ \alpha \end{bmatrix} \approx \boldsymbol{S}^{m\theta}\mathbf{R}_{\mathrm{dq}}^{m\theta}\boldsymbol{i}_{e,\mathrm{ref}}^{\mathrm{dq}} + \begin{bmatrix} v_0 \\ \alpha_0 \end{bmatrix}, \tag{5.34}$$

where

$$\boldsymbol{S}^{m\theta} = \begin{bmatrix} \gamma_m & 0 \\ 0 & \gamma_\theta \end{bmatrix}. \tag{5.35}$$

Equation 5.32 gives the parameters for the case where $\tilde{k} = 0.05$.

5.5.4 The dq-current controller

The feed forward rule given in equation 5.34 is approximate and will also vary a great deal depending upon e.g. the grid impedance. To lower the error between the reference current and the real current, a feedback control is needed.

Using the results of the last section, a simple proportional controller with feedforward using the amplitude and phase currents is

$$\begin{bmatrix} v_{\text{ref}} \\ \alpha_{\text{ref}} \end{bmatrix} = \boldsymbol{S}^{m\theta} \boldsymbol{i}_e^{m\theta} + \boldsymbol{K}^{m\theta} \left(\boldsymbol{i}_{e,\text{ref}}^{m\theta} - \boldsymbol{i}_e^{m\theta} \right) + \begin{bmatrix} v_0 \\ \alpha_0 \end{bmatrix} \tag{5.36}$$

where

$$\boldsymbol{K}^{m\theta} = \begin{bmatrix} k_m & 0 \\ 0 & k_\theta \end{bmatrix} \tag{5.37}$$

is the feedback gain matrix.

Note that a difference in frequency between the grids will cause a continously rising or descending phase as the two voltages drifts apart in phase. To avoid drifting apart and be able to synchronize to the external net, a feedback is also needed for the frequency reference, ω_{ref}

$$\omega_{\text{ref}} = \omega_0 + k_\omega \left(i_{e,\text{ref},\alpha} - i_{e,\alpha} \right) \tag{5.38}$$

This feedback will synchronize the converter to a frequency giving a static error for $i_{e,\alpha}$ related to the difference of ω_0 and the grid frequency. Figure 5.7 shows a block diagram of the controller.

A converter using this controller can work as a standalone unit, setting ω_{ref} to the nominal frequency and v_0 to the nominal output voltage. Loads will cause static deviations from these nominal settings depending on the size of the proportional gains of the controller.

The droop caused by this controller structure can be used to share a load between two or more converters without any further communication than the local output current. This internal, rapid response droop enables the load sharing to also work for transients and non-linear loads.

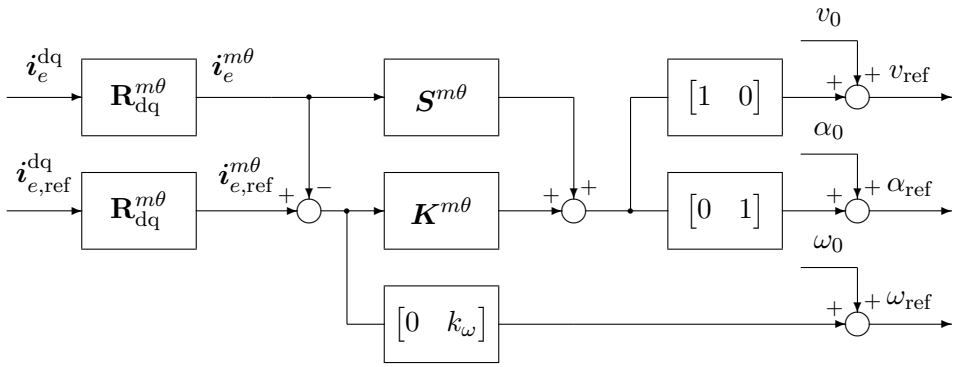

Figure 5.7 – Block diagram of the dq-current controller.

5.6 Power controller

The active and reactive power from the controller can be regulated using the dq-current controller. The d-component of the current is used to control the active power, and the q-component the reactive power.

The dq-current controller uses the converter current, not the grid current. However, equation 5.12 and equation 5.13 shows the relations between the active and reactive power from the converter. The power delivered to the grid is thus:

$$P_g = v_{f,\mathrm{d}} i_{e,\mathrm{d}} + v_{f,\mathrm{q}} i_{e,\mathrm{q}}, \tag{5.39}$$

$$Q_g = v_{f,\mathrm{d}} i_{e,\mathrm{q}} - v_{f,\mathrm{q}} i_{e,\mathrm{d}} + y_f \|\boldsymbol{v}_f^{\mathrm{dq}}\|_2^2. \tag{5.40}$$

As the q-component of the capacitor voltage vector is small it can be approximated as zero, i.e. $v_{f,\mathrm{q}} \approx 0$. The active and reactive power delivered to the grid from the capacitor can then be approximated as

$$P_g \approx v_{f,\mathrm{d}} i_{e,\mathrm{d}}, \tag{5.41}$$

$$Q_g \approx v_{f,\mathrm{d}} \left(i_{e,\mathrm{q}} + y_f v_{f,\mathrm{d}}\right). \tag{5.42}$$

An active power controller and a reactive power controller using feedforward and a relatively slow integrator to avoid static deviations are

$$i_{e,\mathrm{ref,d}} = \frac{P_{g,\mathrm{ref}}}{v_{f,\mathrm{d}}} + \frac{k_P}{1 - z^{-1}} \left(P_{g,\mathrm{ref}} - P_g\right), \tag{5.43}$$

$$i_{e,\mathrm{ref,q}} = \frac{Q_{g,\mathrm{ref}}}{v_{f,\mathrm{d}}} - i_{0,\mathrm{q}} + \frac{k_Q}{1 - z^{-1}} \left(Q_{g,\mathrm{ref}} - Q_g\right), \tag{5.44}$$

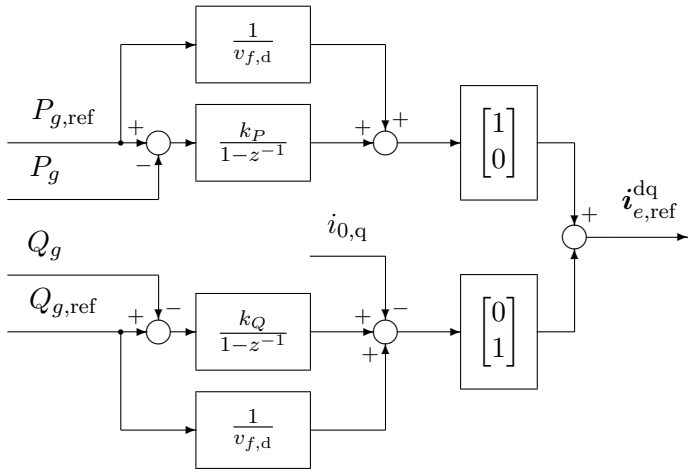

Figure 5.8 – Block diagram of the active and reactive power controller.

where

$$i_{0,\mathrm{q}} = y_f v_{f,\mathrm{d}}. \tag{5.45}$$

$i_{0,\mathrm{q}}$ is the reactive current needed for the capacitor in steady state. Figure 5.8 shows a block diagram of the active and reactive power controller.

Note that special care must be taken when $v_{f,\mathrm{d}}$ is small, as the feed forward signal will become exceedingly large. This follows from the low grid voltage which limits the ability to manipulate the power. One way to limit the current is to use

$$\underline{v}_{f,\mathrm{d}} = \max\left(v_{f,\mathrm{d}}, v_{\min}\right) \tag{5.46}$$

instead of $v_{f,\mathrm{d}}$ in the controller equations. Setting for example $v_{\min} = 0.5$ will limit the current to 2 p.u. for an output power of 1 p.u..

Figure 5.9 shows a plot of the measured active and reactive power responses for different steps in the active and reactive power references. The power measurements were low pass filtered with a bandwidth of 12.5 Hz and two notch filters for 50 Hz and 100 Hz to remove any harmonics caused by unsymmetries. The controller gains was set to

$$k_m = 0.1, \qquad k_\theta = 0.63, \qquad k_\omega = 0.13 \tag{5.47}$$

$$k_P = 0.002, \qquad k_Q = 0.002 \tag{5.48}$$

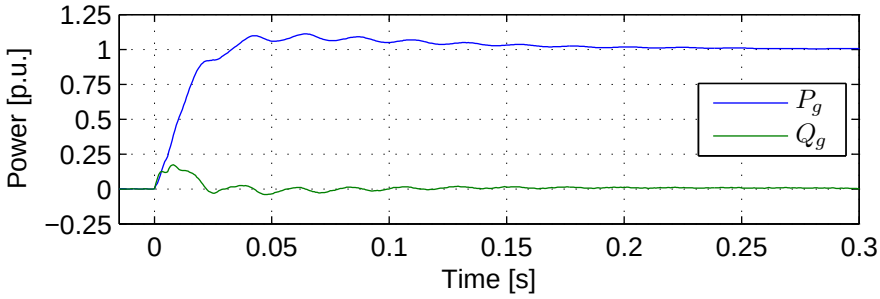

(a) A step from 0 to 1 in the active power reference.

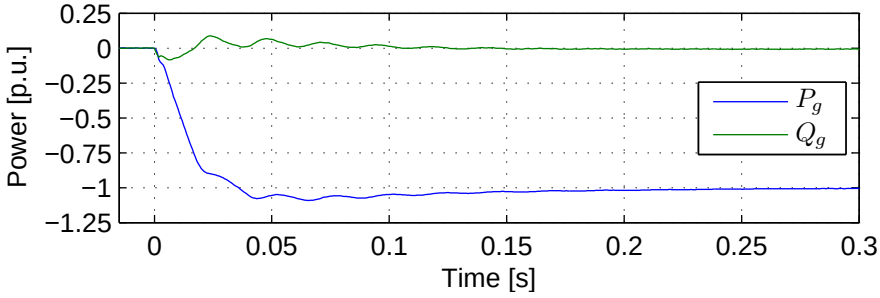

(b) A step from 0 to −1 in the active power reference.

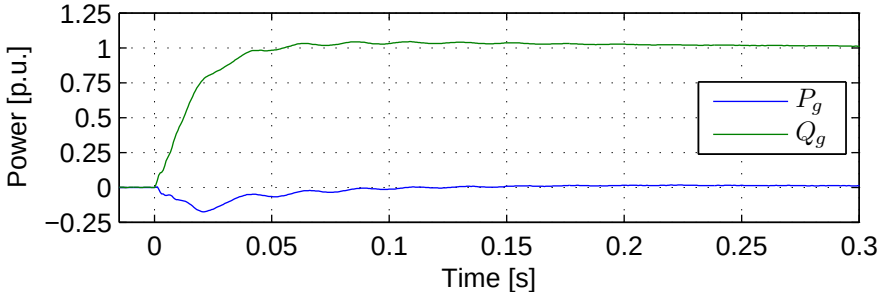

(c) A step from 0 to 1 in the reactive power reference.

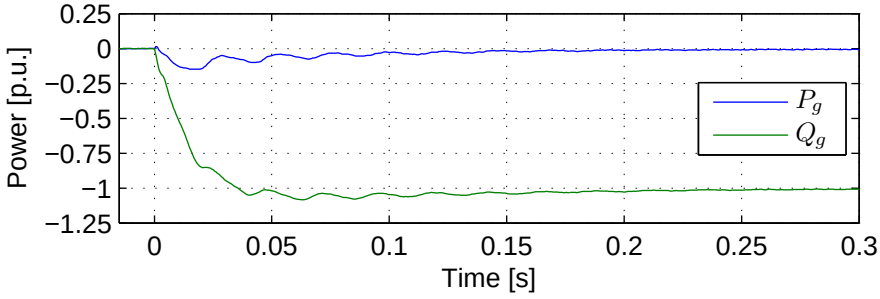

(d) A step from 0 to −1 in the reactive power reference.

Figure 5.9 – Measurements of active and reactive power responses for steps in the active or reactive power reference.

CHAPTER 6

Grid control

This chapter uses the active and reactive power control introduced in the last chapter to create an explicit droop control for load sharing. It also discusses issues related to running in parallel with a main grid and in islanding mode. Distributed converters running in parallel creating a small grid is often called a minigrid or microgrid.

Guerrero [22] splits the control of a microgrid into three control levels. A *primary control*, which is the droop control used to share load between converters. A *secondary control*, responsible for removing any steady state errors introduced by the droop control. And last a *tertiary control* concerning more global responsibilities using e.g. economic data to decide import/export of energy for the microgrid. The controller given in this thesis falls into the first category, but secondary control is briefly discussed in section 6.3.1 on page 80.

6.1 Droop control

Traditionally (see e.g. [23]), large power producers in a grid have power droop dependent on the grid frequency to share the load. This is a direct consequence of the nature of the synchronous generators. A synchronous generator will slow down when a load drawing active power is connected, and generate a lower amplitude if a load drawing reactive power is connected.

Emulating amplitude droop and frequency droop using a pulse width modulated converter to share loads is a known technique. Numerous papers on droop control for load sharing for linear loads without extra communications exists in the literature, see e.g. [24].

For non-linear loads, like for example a diode rectifier, an inductive impedance is not ideal. Compared to linear loads which only generates

a ground harmonic current, non-linear loads generate higher harmonics in their load current. The inductive impedance means that these higher harmonics will have a much higher attenuation compared to the ground harmonic. This will in turn limit the voltage of the DC-link of the rectifier as the top of the grid voltage is reduced. To improve the response of the converter to non-linear load, a more ohmic response can be used instead of a purely inductive for these higher harmonics.

Controllers using virtual impedance which can potentially get better response for nonlinear loads have been introduced relatively recently, see [2, 25–29].

The dq-current controller introduced in the previous chapter has already an inherent amplitude and frequency droop from its virtual impedance. The rapid response of this droop also enable sharing of non-linear loads and transients.

It is often desireable to have better control over the droop characteristics of the converter for steady state linear loads. This can be done by setting the references to the active and reactive power regulator depending on the current state of the grid voltage magnitude and frequency.

A general linear droop control is given as

$$P_{g,\mathrm{ref}} = P_{g,0} + k_{pm}\delta_m + k_{p\omega}\delta_\omega, \tag{6.1}$$

$$Q_{g,\mathrm{ref}} = Q_{g,0} + k_{qm}\delta_m + k_{q\omega}\delta_\omega, \tag{6.2}$$

where

$$\delta_m = \frac{v_0 - v_{\mathrm{meas}}}{v_0}, \tag{6.3}$$

$$\delta_\omega = \frac{\omega_0 - \omega_{\mathrm{meas}}}{\omega_0}. \tag{6.4}$$

Here, $P_{g,\mathrm{ref}}$ and $Q_{g,\mathrm{ref}}$ is the active and reactive power reference, respectively. $P_{g,0}$ and $Q_{g,0}$ is the wanted active and reactive power input when both the grid voltage and grid frequency is nominal. k_{pm} and k_{qm} is the relative droop from the voltage difference to the active power and reactive power, respectively. $k_{p\omega}$ and $k_{q\omega}$ is the droop from the frequency difference to the active power and reactive power. δ_m is the relative difference of the nominal voltage magnitude and the grid voltage magnitude, and δ_ω is the relative difference of the nominal grid frequency and the grid frequency. The power references are limited to a configurable minimum/maximum value, not shown in the equations here.

As the grid voltage observer is relatively slow, this droop control will also be slow. For fast transients, the rapid internal droop will be dominant.

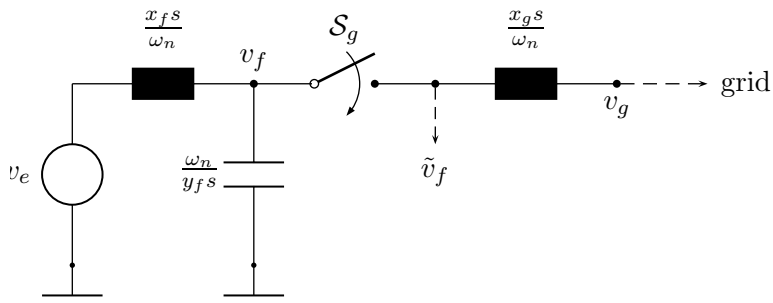

Figure 6.1 – Connecting the converter to a grid.

6.2 Running in parallel with a grid

The normal operation of a grid converter is running in parallel with a strong main grid. Examples of a converter running in parallel with a grid is shown in the next chapter.

6.2.1 Connecting to and disconnecting from a grid

A contactor switch is used to split the filter from the grid when the converter is off. This avoids exitations of the resonance frequency of the LCL-filter, which is now not actively damped. It can also be used to separate the converter from the grid in case of emergency trips or maintenance.

The measurements of the filter voltages can be moved to the grid side of the switch to avoid extra voltage sensors for the grid voltage. This enables the converter to synchronize to the external grid before closing the switch. Figure 6.1 shows the switch position in the LCL-filter*. The voltage measurement point labeled $\tilde{v}_f$ is shown on the far side of the switch.

To reduce transients at connection, the virtual impedance of the inner voltage regulator can be set to a high value before gradually being reduced to its nominal value. This is called a "soft" connection.

A similar soft disconnection can be used to avoid both sudden transients and even blackouts. If the grid is very weak, a gradual increase of the impedance can be used to see if the grid voltage magnitude falls below its required minimum voltage or the grid frequency becomes out of bounds. If it does, the disconnection procedure is aborted to avoid a blackout.

*A single phase representation has been used instead of a three phase in the figure to reduce the figure complexity.

6.2.2 Attenuation of subharmonic oscillations

The drooping characteristics can in many ways be seen as controller feedback gains. Steep droop responses where small changes cause a large current response introduces large feedback gains in the open loop function. This can cause oscillations in the voltage frequency and magnitude. A virtual impedance can be used to dampen these oscillations. To keep a reasonable response for nonlinear loads, the time varying impedance is useful as the oscillations are usually most prominent for the frequency.

6.3 Islanding mode

The droop control enables several converters to run both with and without a main grid. Local converters still supplying power to the local grid when the main grid is disabled are said to be running in islanding mode. Hoff [30] has examined issues and algorithms surronding distributed power generation and islanding modes in detail.

6.3.1 Supervisor controller

To have a stable grid in islanding mode requires that the power delivered to the grid by the converters equals the power used by any load connected to the same grid. The amplitude and frequency droop characteristics of the converters enables them to share this load without any further communication.

Continuous deviations from the voltage magnitude and frequency can be a problem in some situations. These deviations are caused by the droop characteristics of the converter.

If the load is relatively constant, the grid can be tuned for this load and the voltage can be fine tuned by a large single power source using integral action. However, this is often neither desireable nor feasible. In these cases a central controller is needed.

This controller will be responsible for the long term voltage amplitude and frequency. It can also be responsible for tuning the load sharing between the different controllers. As this is a slow process, communication can be done over a relatively low bandwidth communication medium.

The supervisor controller can also be used to synchronize the islanded grid to an external grid before connecting them together.

6.3.2 Experimental verification of load sharing

Figure 6.2 shows the responses of two individual converters running in islanding mode in parallel when an ohmic load is connected. The power measurements were low pass filtered with a bandwidth of 12.5 Hz and two notch filters for 50 Hz and 100 Hz to remove any harmonics caused by unsymmetries. The droop control of the two converters are set to

$$v_0 = 1, \qquad \omega_0 = 314.15, \tag{6.5}$$

$$P_{g,0} = 0, \qquad Q_{g,0} = 0, \tag{6.6}$$

$$k_{pm} = 20, \qquad k_{p\omega} = -20, \tag{6.7}$$

$$k_{qm} = -8, \qquad k_{q\omega} = 50. \tag{6.8}$$

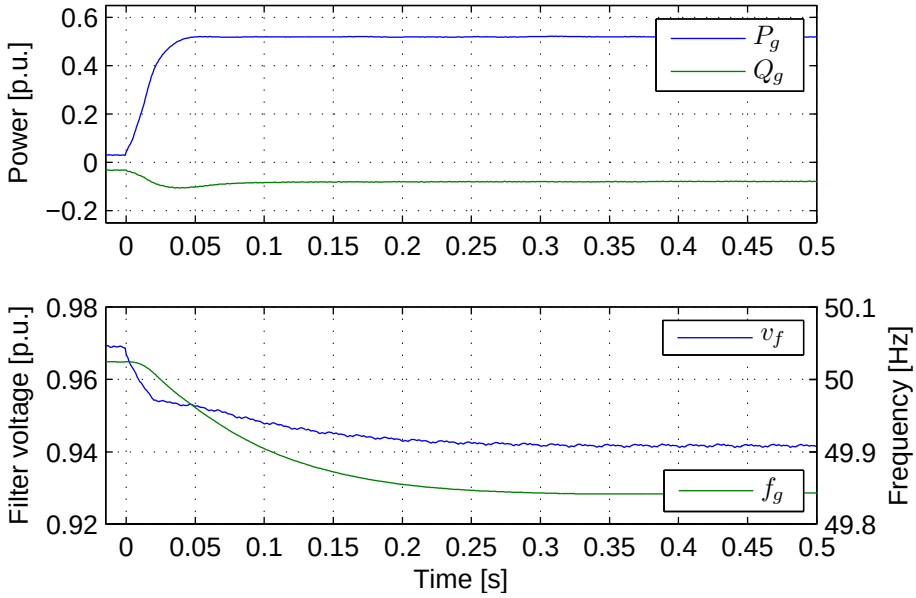

(a) Converter 1

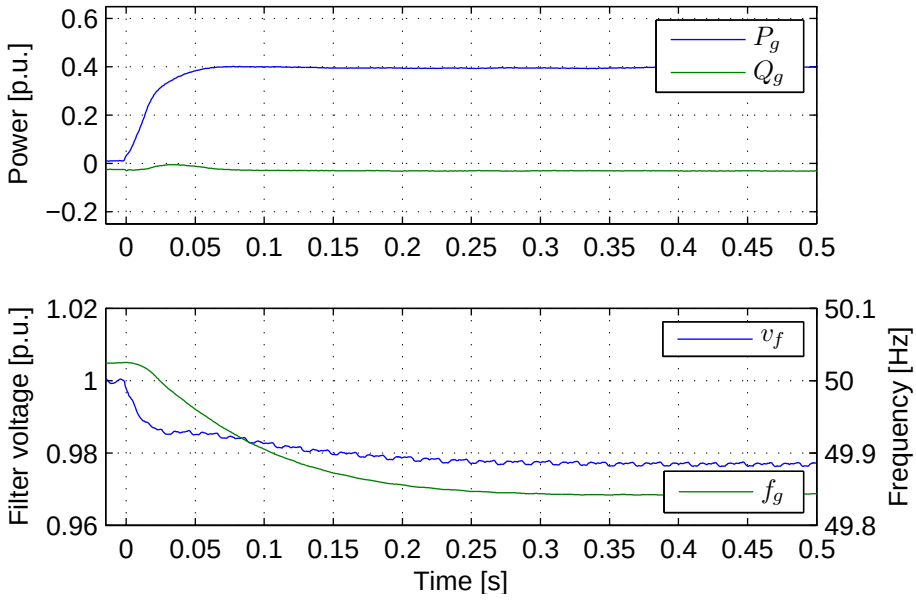

(b) Converter 2

Figure 6.2 – Measurements of two individual converters running in parallel when connecting an ohmic load. The difference in voltage magnitudes is caused by the 230 : 240-transformer which provides the galvanic separation between the converters.

CHAPTER 7

Power system guidelines

The power system guidelines for connecting to a grid is given by the transmission system operator (TSO). These guidelines are called grid codes.

In Norway the TSO is Statnett. Statnett has recently added guidelines for wind farms greater than 10 MVA in their grid code. This chapter outlines the guidelines presented in the document "Veiledende systemkrav til anlegg tilknyttet regional- og sentralnettet i Norge"* [1].

An experiment is done with the grid connected pulse width modulated converter introduced in this thesis. This shows the converter operation during a dip in the grid voltage.

7.1 Normal operation

The controller of the wind farm must have the following functions:

- Output power limitation. It shall be possible to limit the output power to a reference between 20 % to 100 % of rated power.
- Ramp rate limitation. It shall be possible to limit the ramp rate of the output power to a reference between 10 % to 100 % of rated power per minute.
- System protection. It shall be possible to regulate the output power from rated power to zero, i.e. stop, in 30 s.
- Frequency control. The output power shall respond to frequency deviation. It shall be possible to adjust the frequency droop between 2 % to 8 %.

*Translation: "Guideline system requirements to installations connected to the Norwegian regional and main transmission grid."

Table 7.1 – Operational requirements of wind farm output for deviations in frequency.

Frequency band	Operation requirements
$47 - 47.5$ Hz	Reduced operation for at least 20 s.
$47.5 - 49$ Hz	Continuous reduced operation.
$49 - 50.5$ Hz	Continuous normal operation.
$50.5 - 51$ Hz	Reduced operation for at least 30 min.
$51 - 53$ Hz	Reduced operation for at least 3 min.

The wind farm is required to operate normally for a certain band of frequencies and amplitudes of the grid voltage. Table 7.1 summarizes the operational requirements of the wind farms output for deviations in the grid frequency.

For deviations in the grid voltage amplitude, the active power output of the wind farm shall not be reduced when the grid voltage is within $90 - 110$ % of the normal voltage amplitude. In this operation the wind farm shall also be able to operate with a power factor of $\cos\phi = \pm 0.91$ referred the wind farm point of grid connection. Reduced reactive capability is accepted at lower grid voltages.

7.1.1 Verifying droop control

The droop control of the grid connected converter is set to a strictly inductive droop control with the droop controller parameters set as

$$k_{pv} = 0, \qquad k_{p\omega} = 12.5, \tag{7.1}$$

$$k_{qv} = -9, \qquad k_{q\omega} = 0. \tag{7.2}$$

The converter is connected directly to a synchronous machine with controllable frequency and field magnetizing current. Figure 7.1 shows the power responses for differences in grid voltage frequency, and figure 7.2 shows the power responses for differences in grid voltage magnitude.

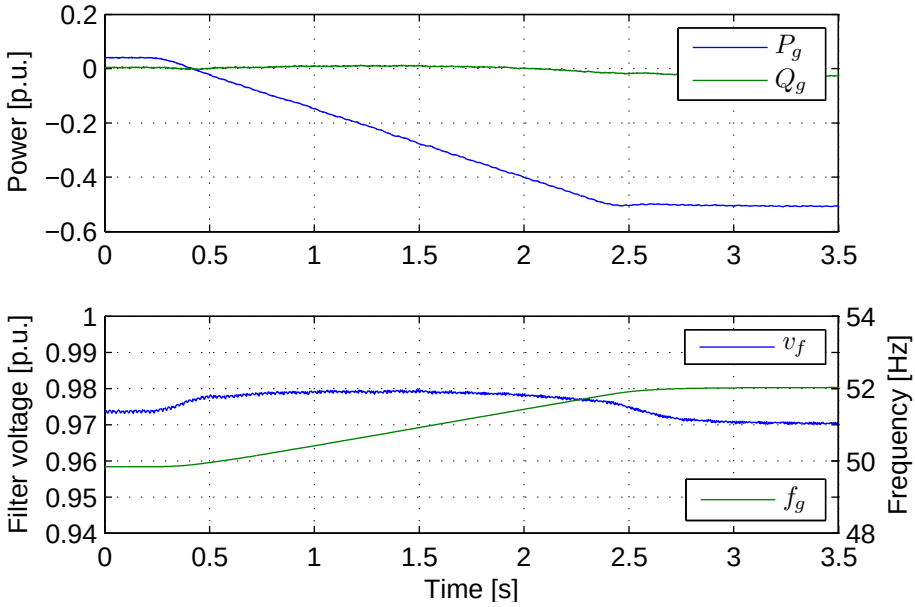

(a) Frequency up

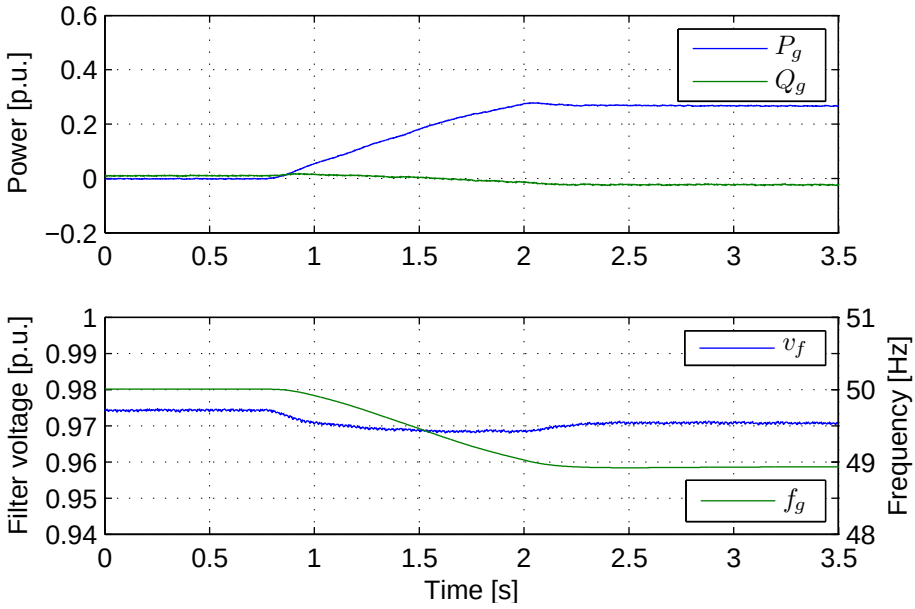

(b) Frequency down

Figure 7.1 – Measurements of power responses with inductive droop control for changes in frequency.

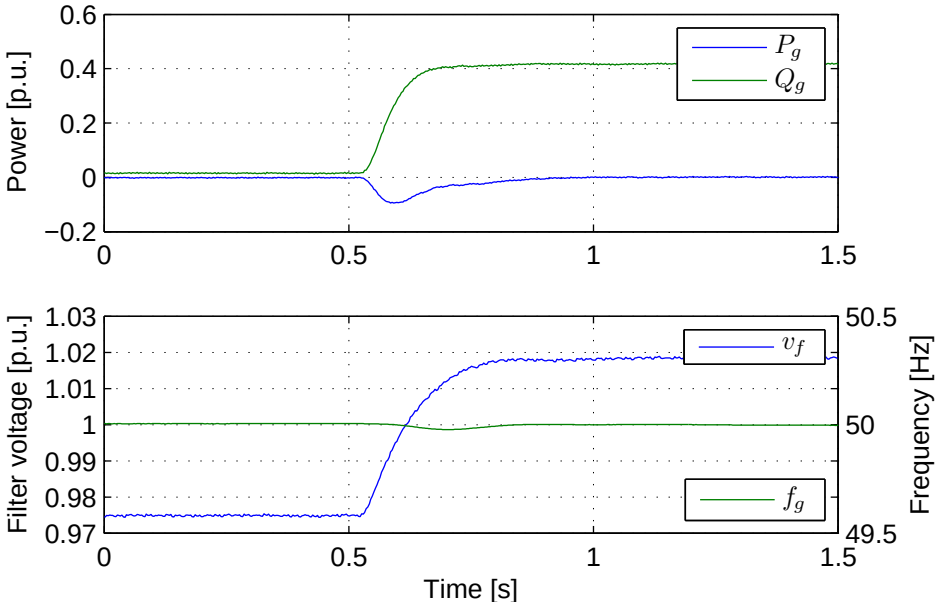

(a) Voltage magnitude up

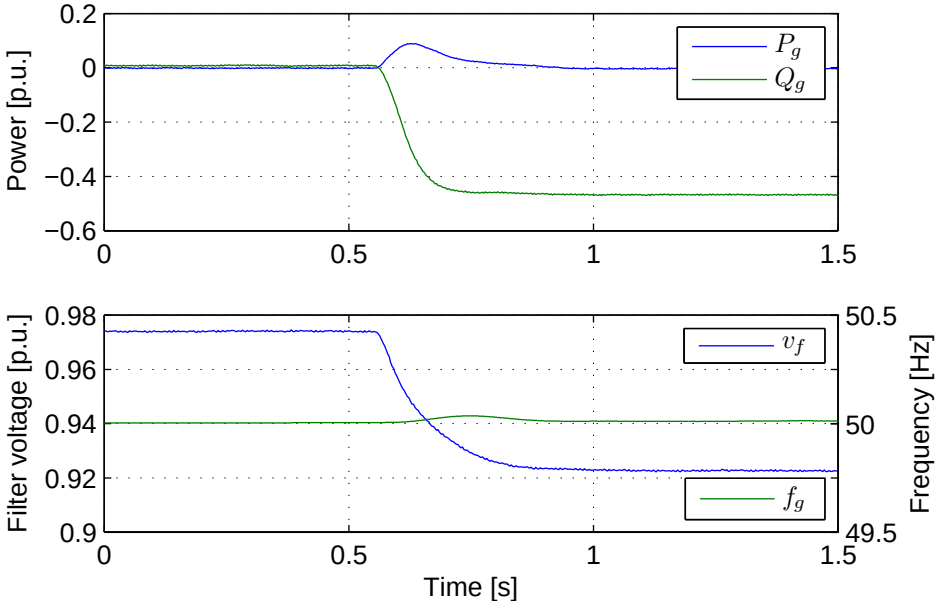

(b) Voltage magnitude down

Figure 7.2 – Measurements of power responses with inductive droop control for changes in voltage magnitude.

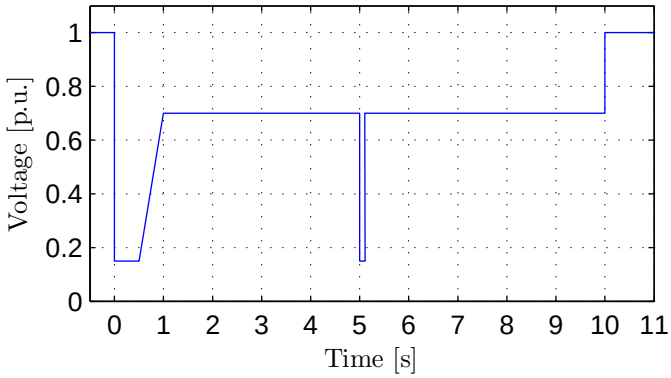

Figure 7.3 – Voltage dip specification from wind farm specification document

7.2 Toleration limits during net faults

For wind farms with voltages below 132 kV, the wind farm shall endure a fault giving approximately symmetrical voltages as shown in figure 7.3.

In addition to the guidelines, IEC 61400-21 [31] is a standard giving a uniform methodology to ensure consistency and accuracy in presentation, testing and assessment of power quality characteristics of grid connected wind turbines. Of particlar interest here is the detailed test procedures for voltage dips.

It specifies testing the converter for a 400 ms dips of 90 % and 50 % voltage while supplying 20 % and 100 % rated power. Test should be done for both phase to phase and full three phase short circuits.

The test setup used the inductors of one of the converter filters connected to the main grid. Figure 7.4 shows a simplified line-phase outline of the test setup. The dashed lines mark where the converter is connected for the different voltage dips.

Experiments was done short circuiting with 400 ms dips to 87.5 %, 50 %, and 25 % of nominal voltage. The reactive power delivered to the grid was limited to -1 p.u., -0.7 p.u., and -0.5 p.u., respectively.

See figures 7.5 to 7.9 on pages 89–93 for experiments done for a voltage dip to 87.5 %. Figure 7.5 shows the voltage dip when no converter is connected for both the full three phase short cirucit and the phase to phase short circuit. Figure 7.6 and figure 7.7 gives the response for the converter for a full three phase short circuit when running at 20 % and 100 % of rated power, respectively. Similarly, figure 7.8 and figure 7.9 gives the response

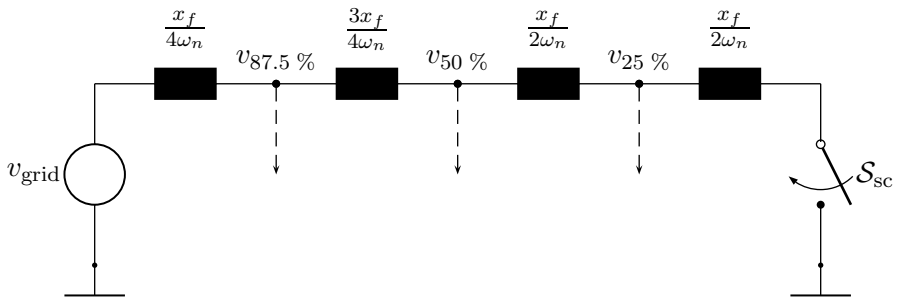

Figure 7.4 – Outline of experimental setup for voltage dips

for a phase to phase short circuit. The power measurements were low pass filtered with a bandwidth of 12.5 Hz and two notch filters for 50 Hz and 100 Hz to remove any harmonics caused by unsymmetries. The voltage and frequency measurement are those estimated by the voltage observer.

Figures 7.10 to 7.14 on pages 94–98 show similar results for experiments done for a voltage dip to 50 %, and figures 7.16 to 7.19 on pages 100–103 show the results for experiments done for a voltage dip to 25 %.

In addition, experiments for a 3 s dip was done for the dip to 25 %. See figures 7.20 to 7.23 on pages 104–107.

For these larger dips, the overcurrent protection is readily visible at the peaks of the current $i_{g,a}$ giving it a "jagged" look, particularly for the phase to phase short circuits. This protection interferes with the decoupling of the current as it limits the converter response and makes it more ohmic. This in turn gives a poorer response from the controller, as it does not adjust its parameters accordingly. The response could be improved if a overcurrent protection detection was included.

The large currents running in the short circuit limited the period of the obtainable dip to 3 s for the setup in figure 7.4. To obtain a longer lasting dip, the converter was connected directly to the synchronous generator and the grid short circuited through inductances of $\frac{x_f}{\omega_n}$. The resulting response for both a phase to phase and full three phase short circuit is shown in figures 7.24 to 7.25 on pages 108–109.

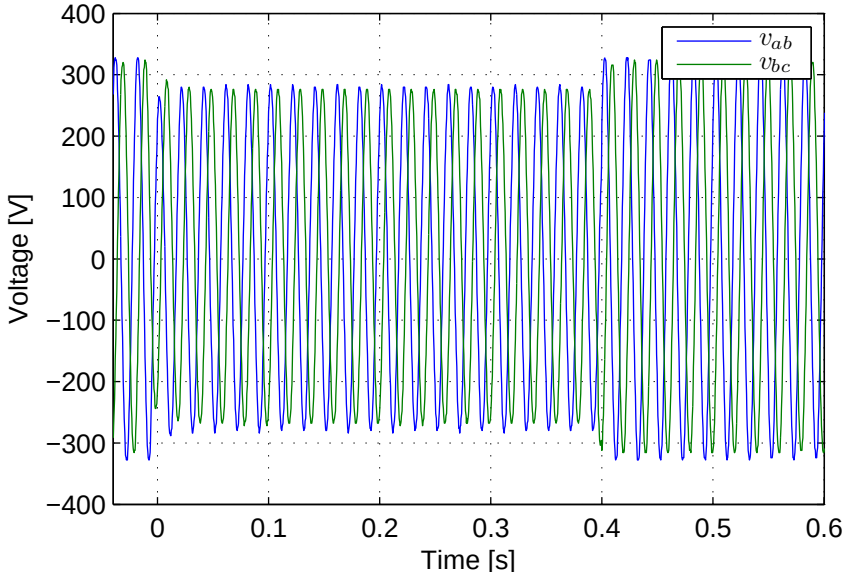

(a) Full three phase short circuit

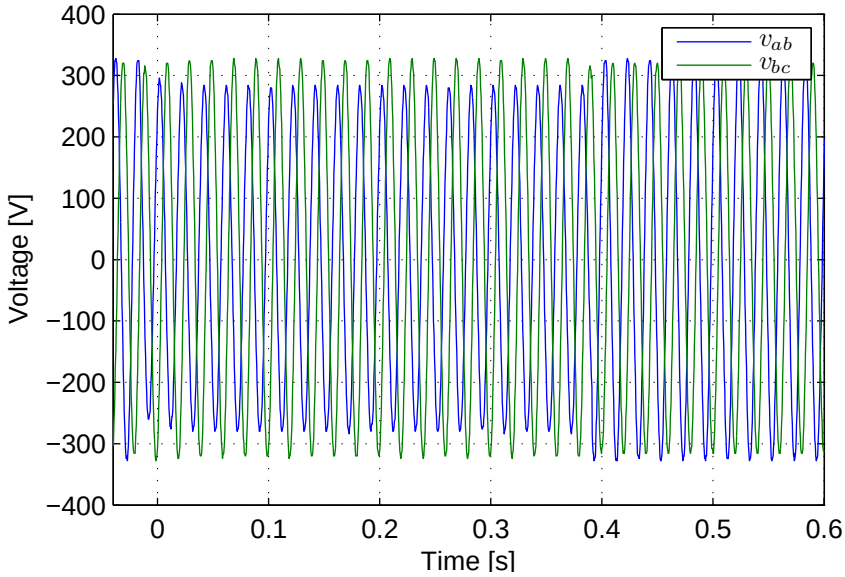

(b) Phase a to phase b short circuit

Figure 7.5 – Oscilloscope measurements of short circuits to 87.5 % voltage of a strong grid without any converter connected.

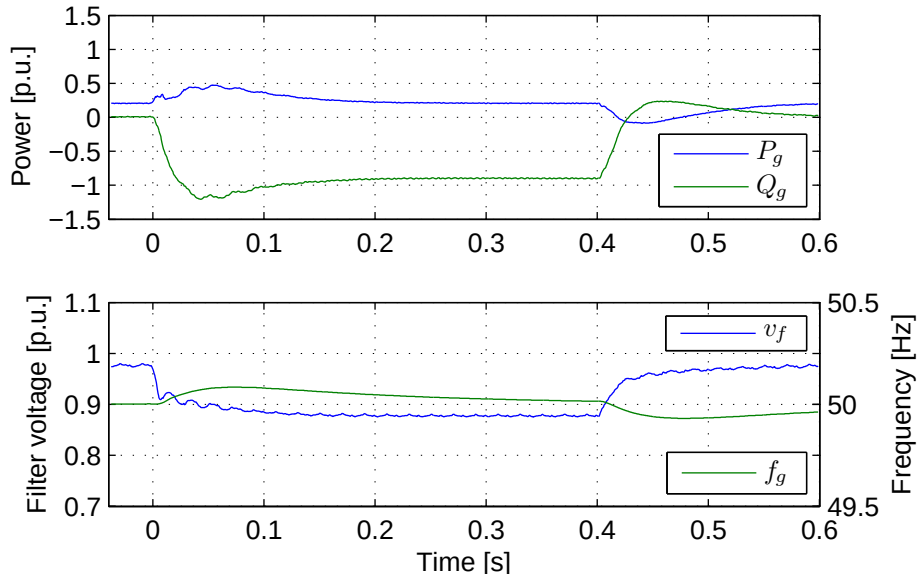

(a) Converter measurments

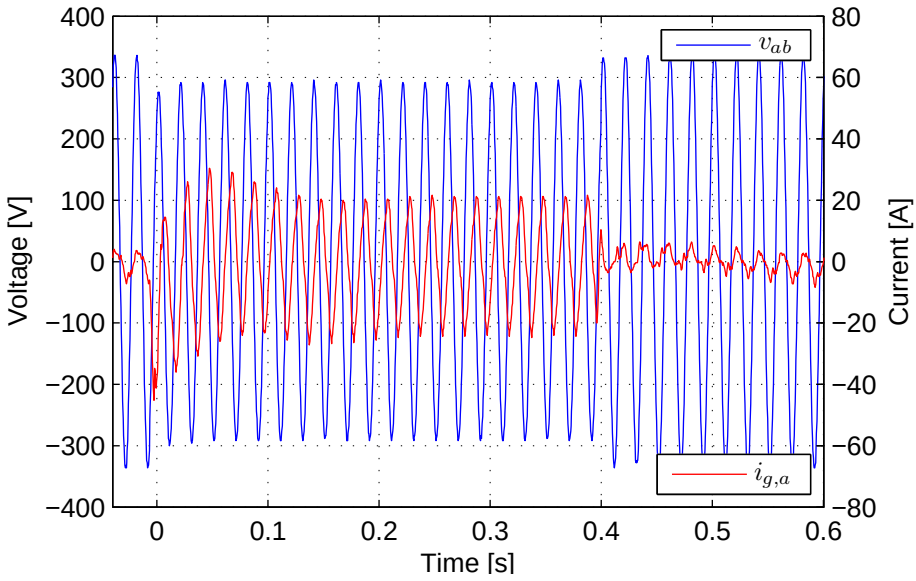

(b) Oscilloscope measurements

Figure 7.6 – Full three phase short circuit to 87.5 % voltage of a strong grid with a converter connected supplying 20 % active power.

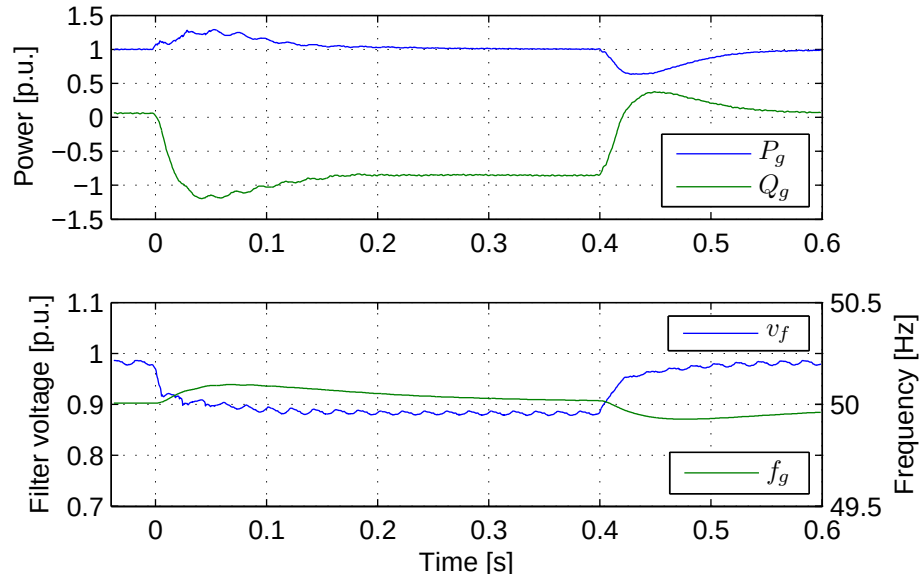

(a) Converter measurments

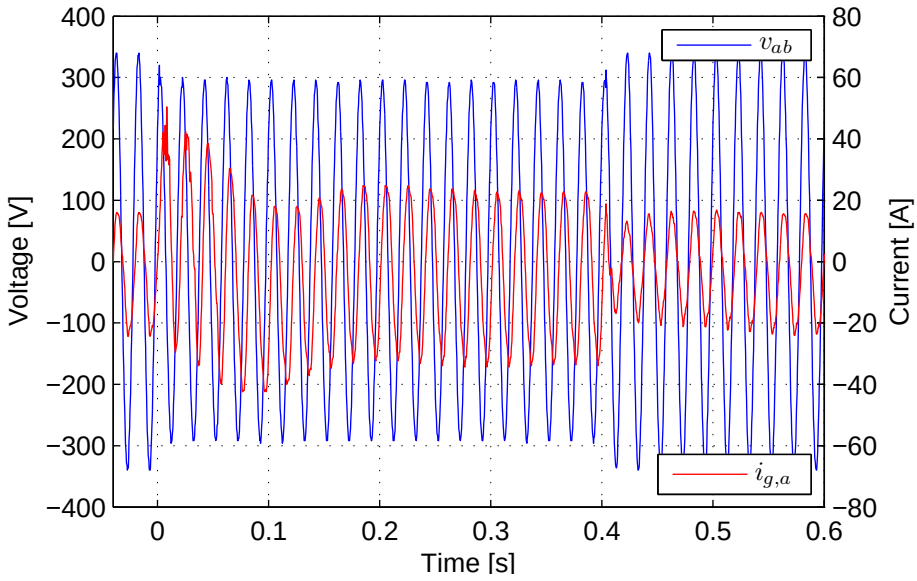

(b) Oscilloscope measurements

Figure 7.7 – Full three phase short circuit to 87.5 % voltage of a strong grid with a converter connected supplying 100 % active power.

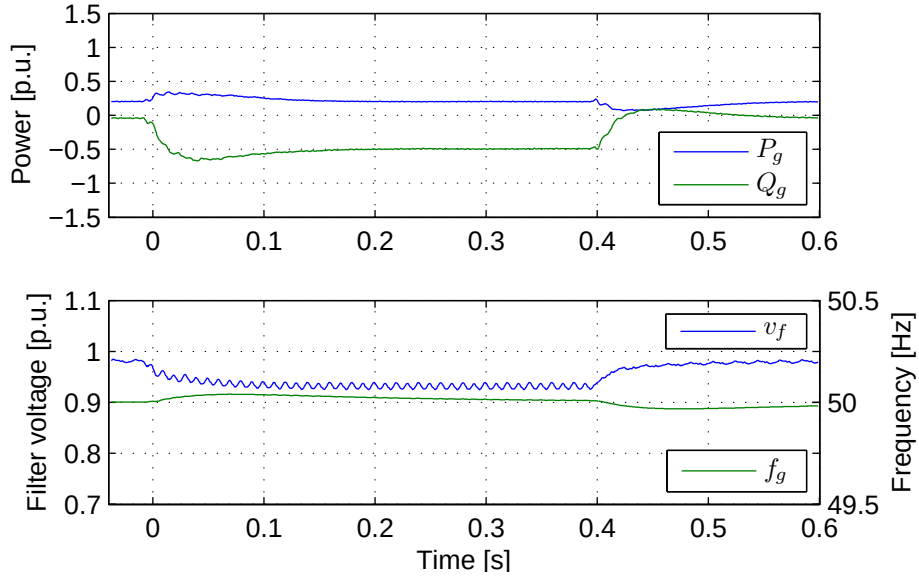

(a) Converter measurments

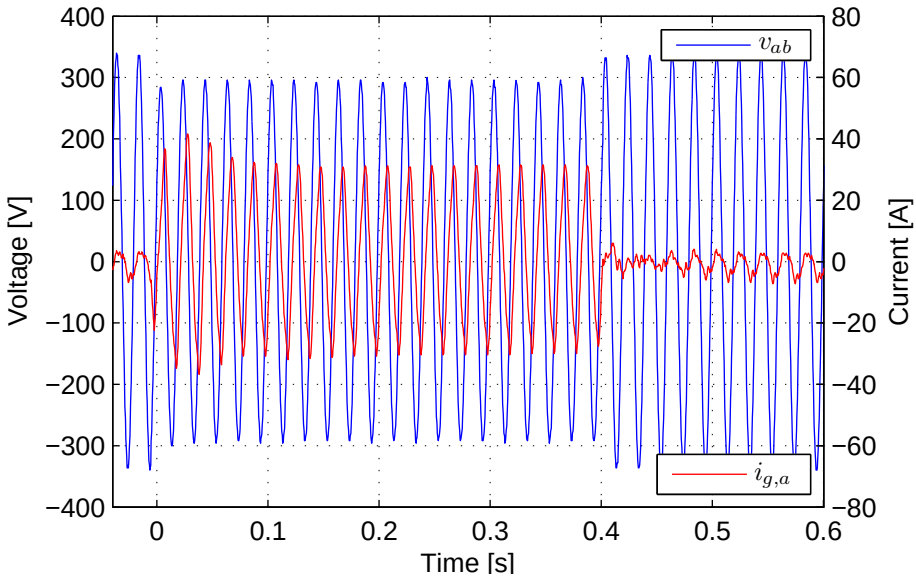

(b) Oscilloscope measurements

Figure 7.8 – Phase a and phase b short circuit to 87.5 % voltage of a strong grid with a converter connected supplying 20 % active power.

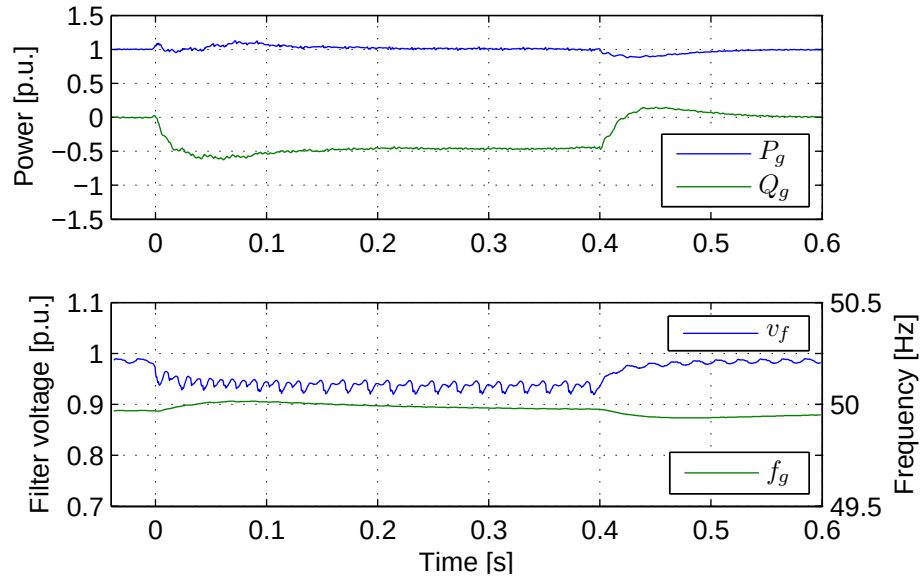

(a) Converter measurments

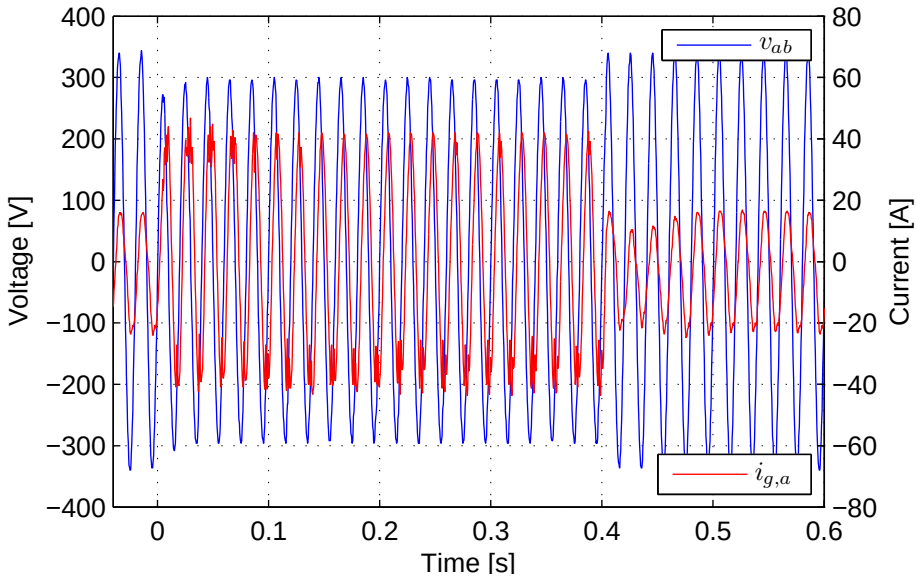

(b) Oscilloscope measurements

Figure 7.9 – Phase a and phase b short circuit to 87.5 % voltage of a strong grid with a converter connected supplying 100 % active power.

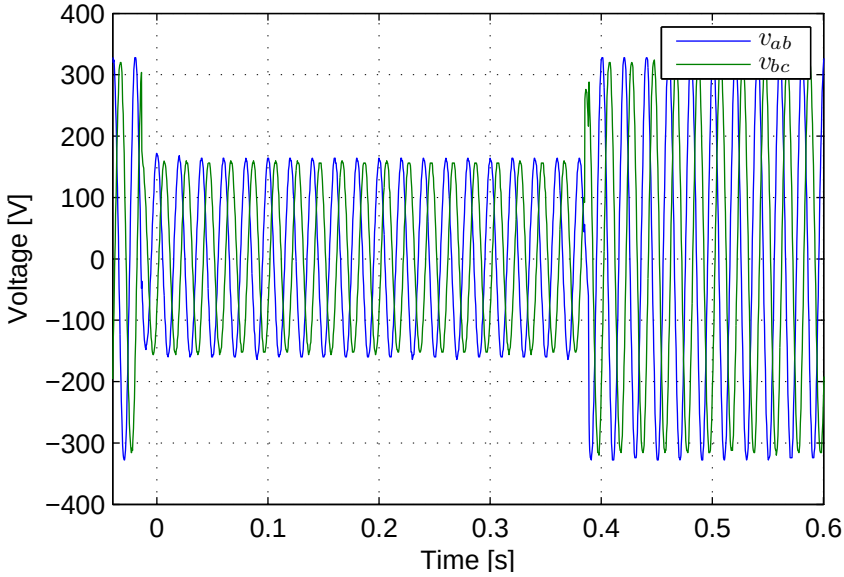

(a) Full three phase short circuit

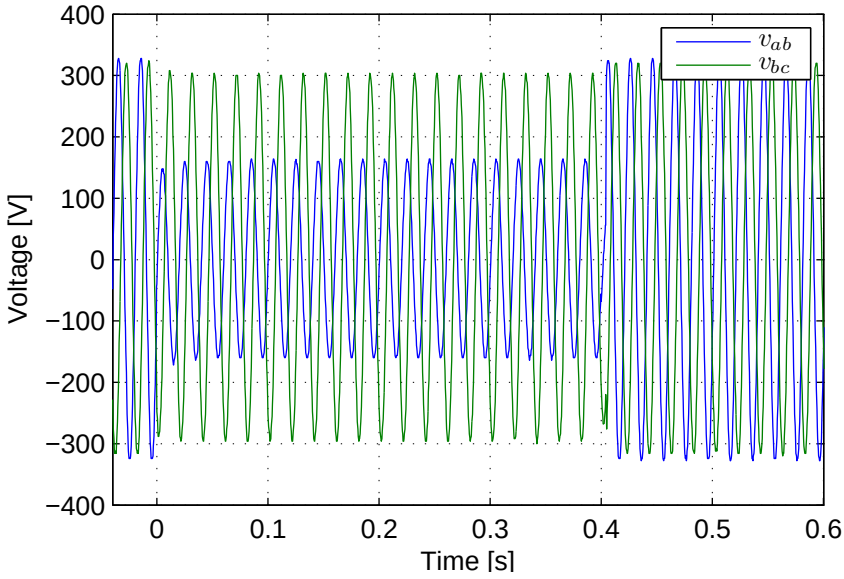

(b) Phase a to phase b short circuit

Figure 7.10 – Oscilloscope measurements of short circuits to 50 % voltage of a strong grid without any converter connected.

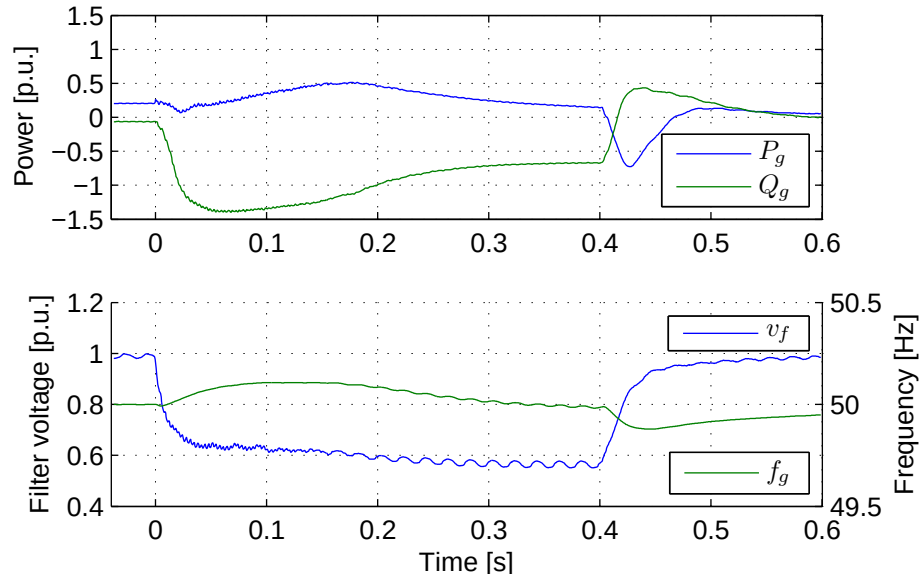

(a) Converter measurments

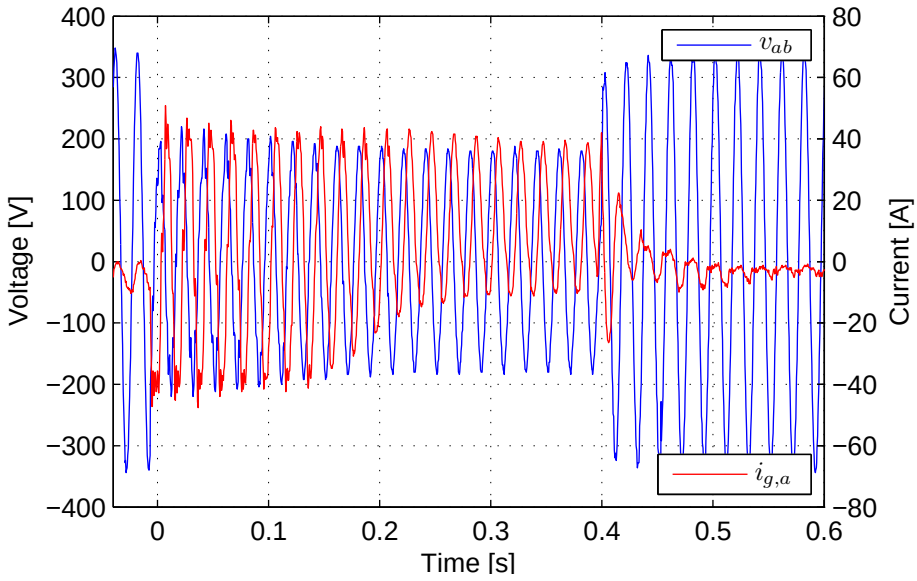

(b) Oscilloscope measurements

Figure 7.11 – Full three phase short circuit to 50 % voltage of a strong grid with a converter connected supplying 20 % active power.

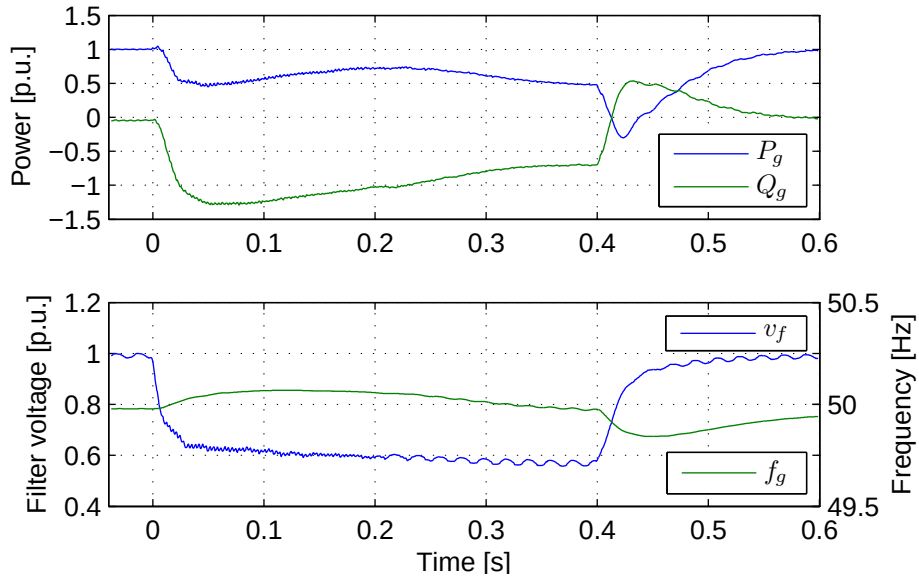

(a) Converter measurments

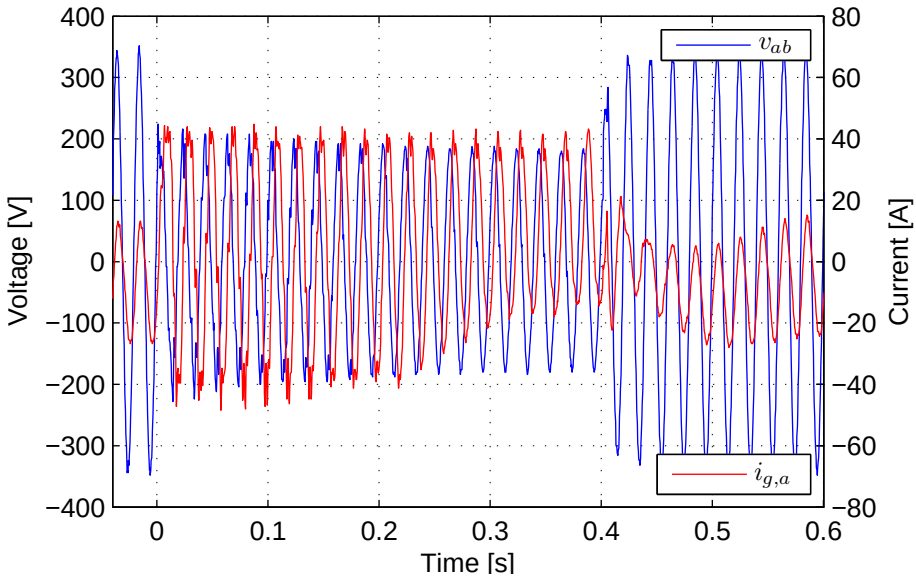

(b) Oscilloscope measurements

Figure 7.12 – Full three phase short circuit to 50 % voltage of a strong grid with a converter connected supplying 100 % active power.

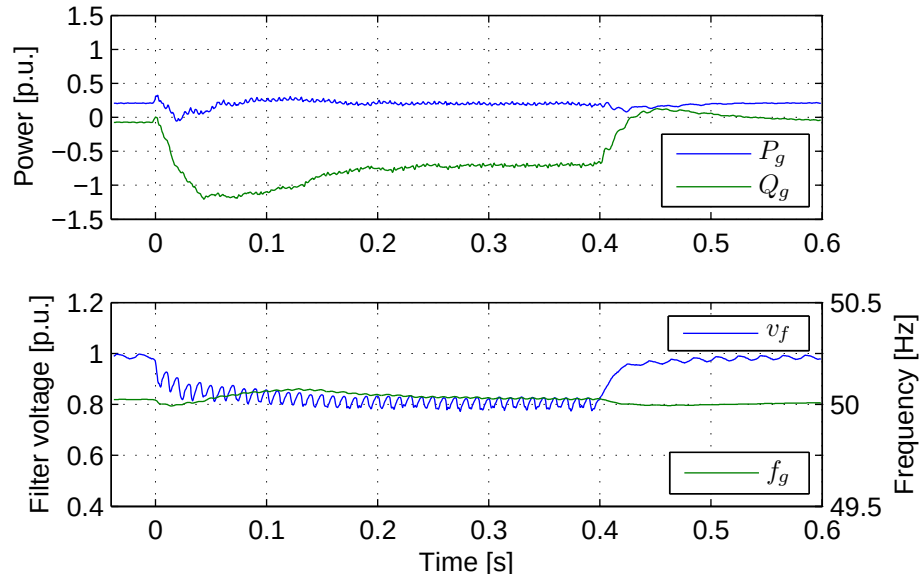

(a) Converter measurments

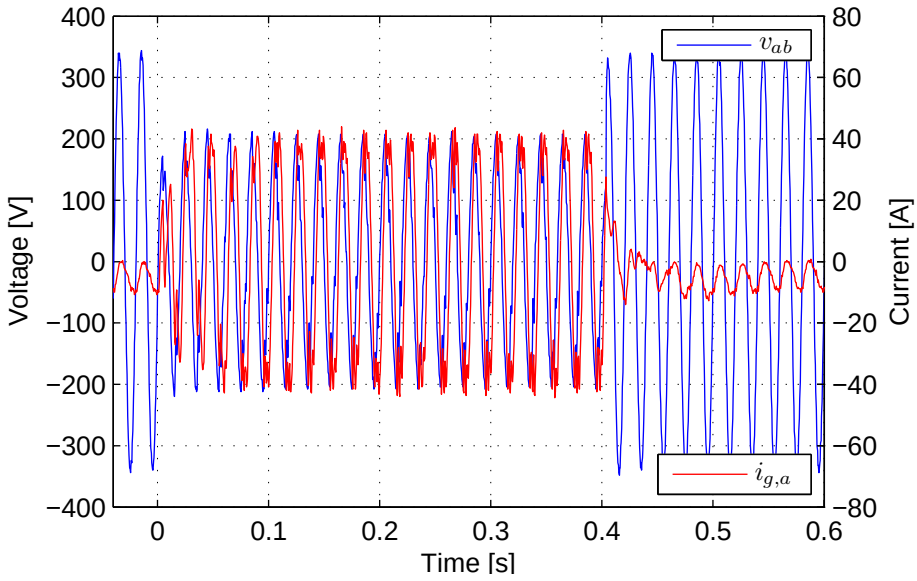

(b) Oscilloscope measurements

Figure 7.13 – Phase a and phase b short circuit to 50 % voltage of a strong grid with a converter connected supplying 20 % active power.

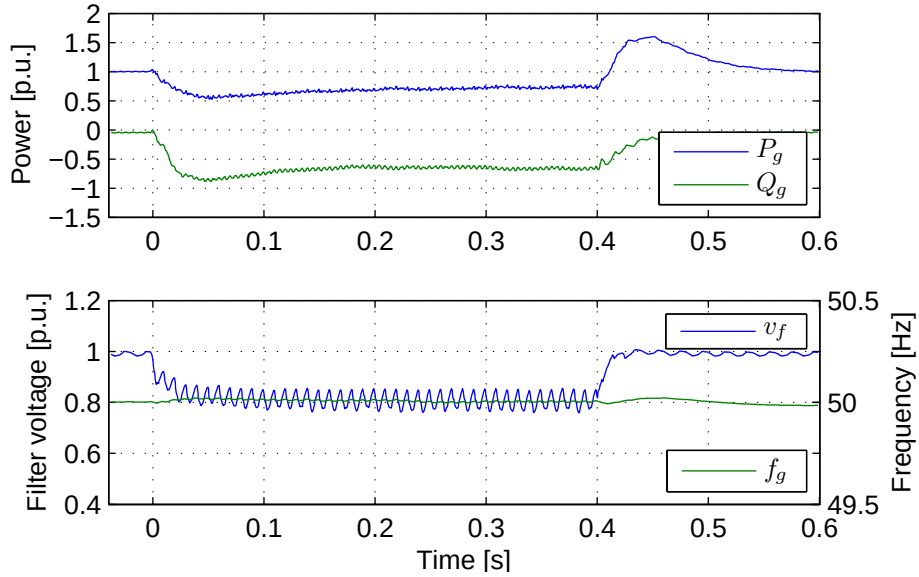

(a) Converter measurments

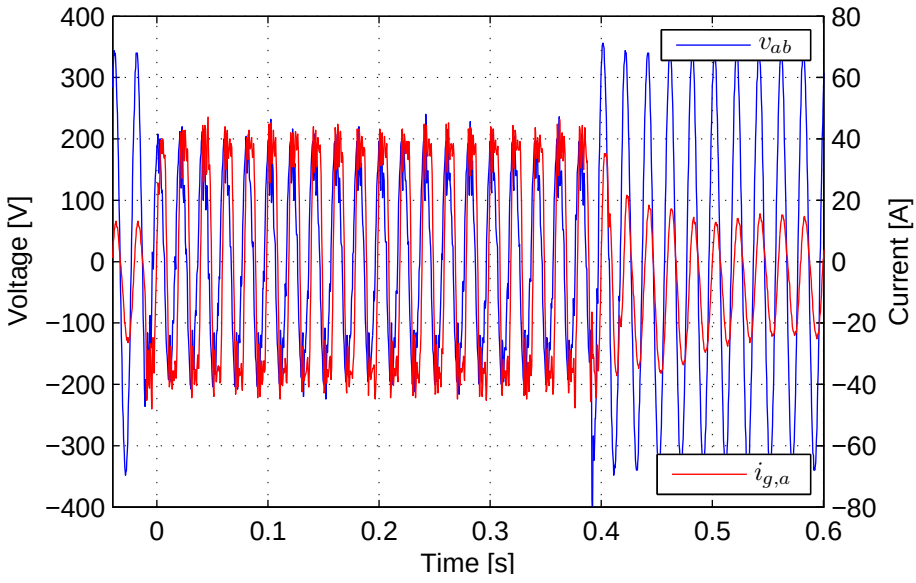

(b) Oscilloscope measurements

Figure 7.14 – Phase a and phase b short circuit to 50 % voltage of a strong grid with a converter connected supplying 100 % active power.

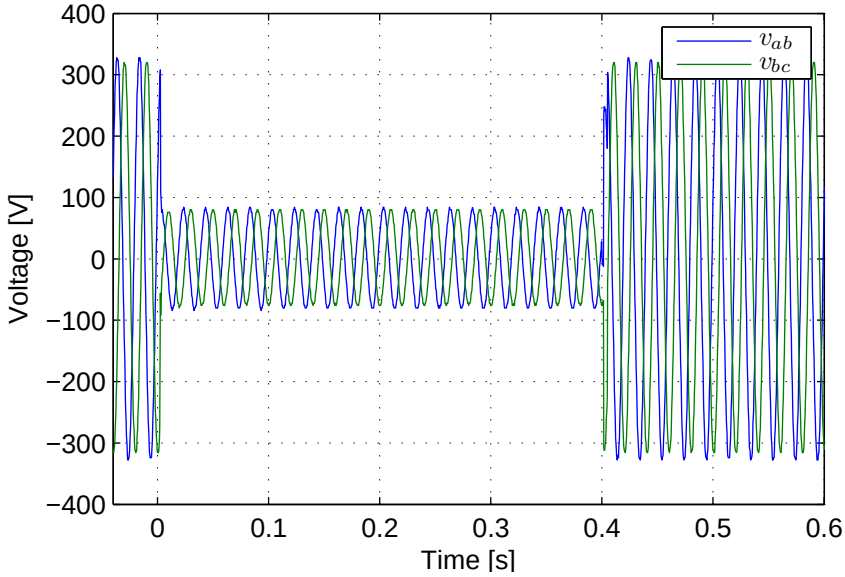

(a) Full three phase short circuit

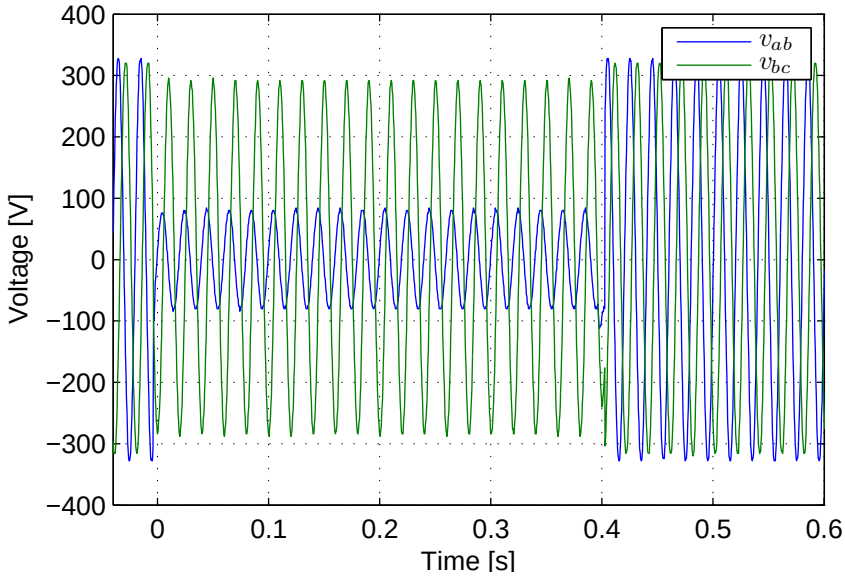

(b) Phase a to phase b short circuit

Figure 7.15 – Oscilloscope measurements of short circuits to 25 % voltage of a strong grid without any converter connected.

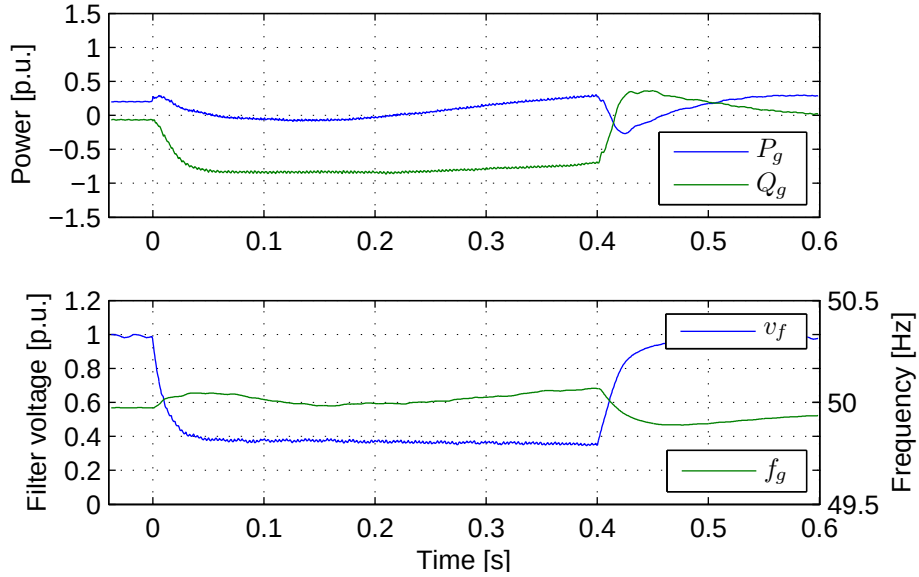

(a) Converter measurments

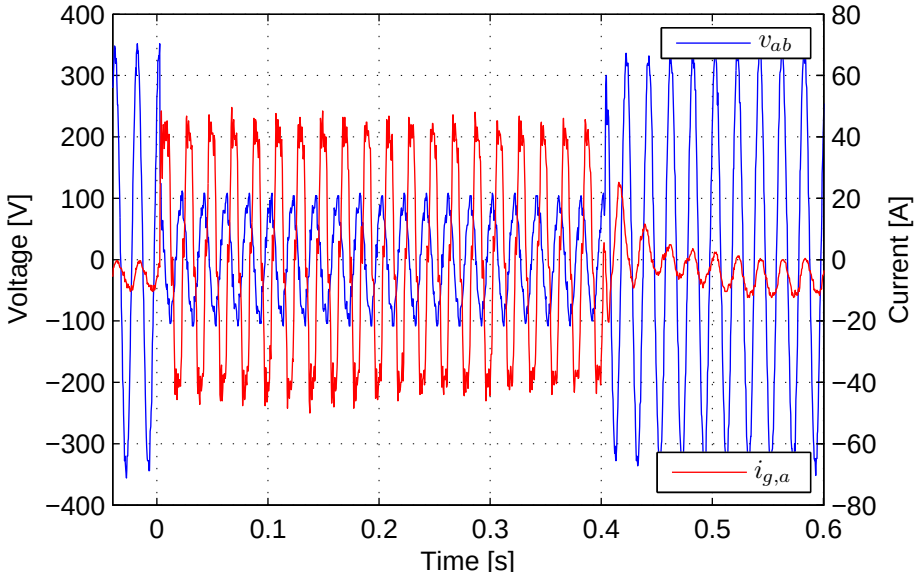

(b) Oscilloscope measurements

Figure 7.16 – Full three phase short circuit to 25 % voltage of a strong grid with a converter connected supplying 20 % active power.

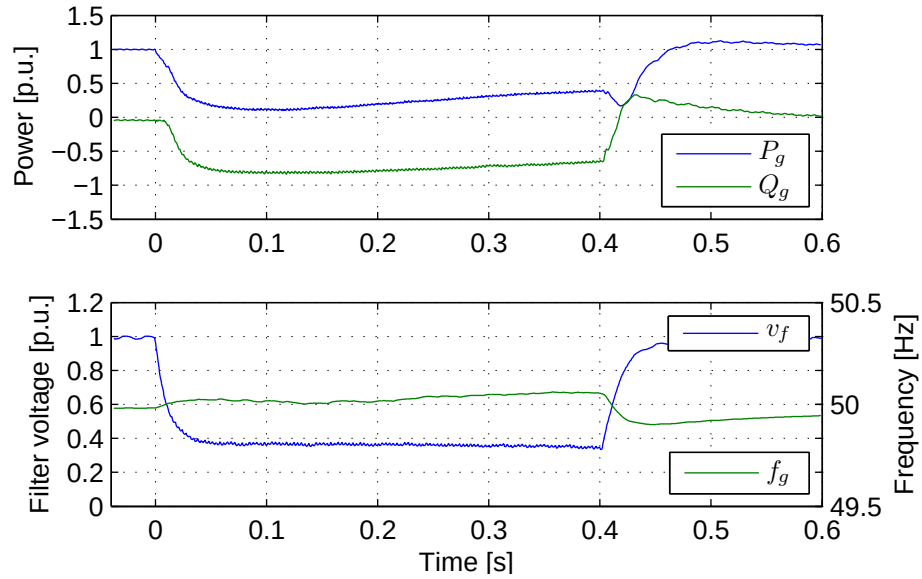

(a) Converter measurments

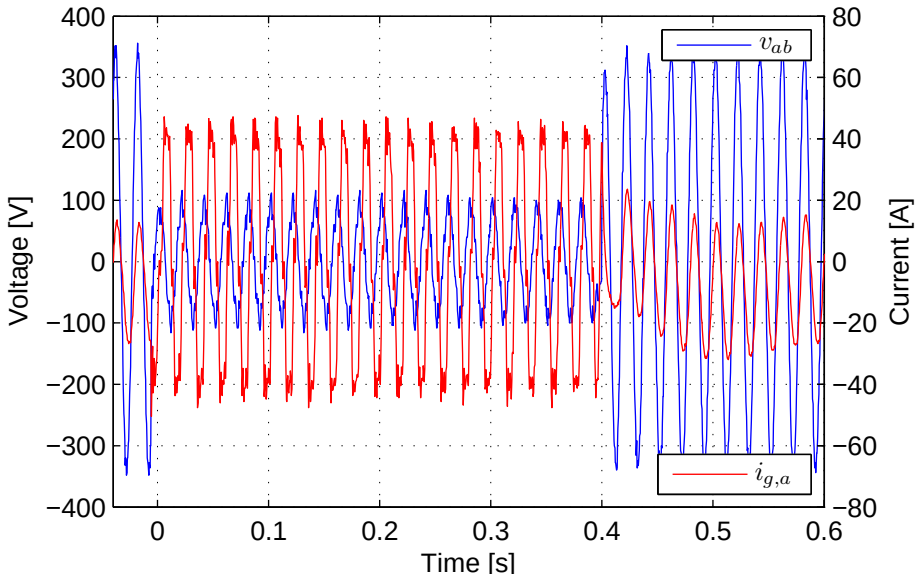

(b) Oscilloscope measurements

Figure 7.17 – Full three phase short circuit to 25 % voltage of a strong grid with a converter connected supplying 100 % active power.

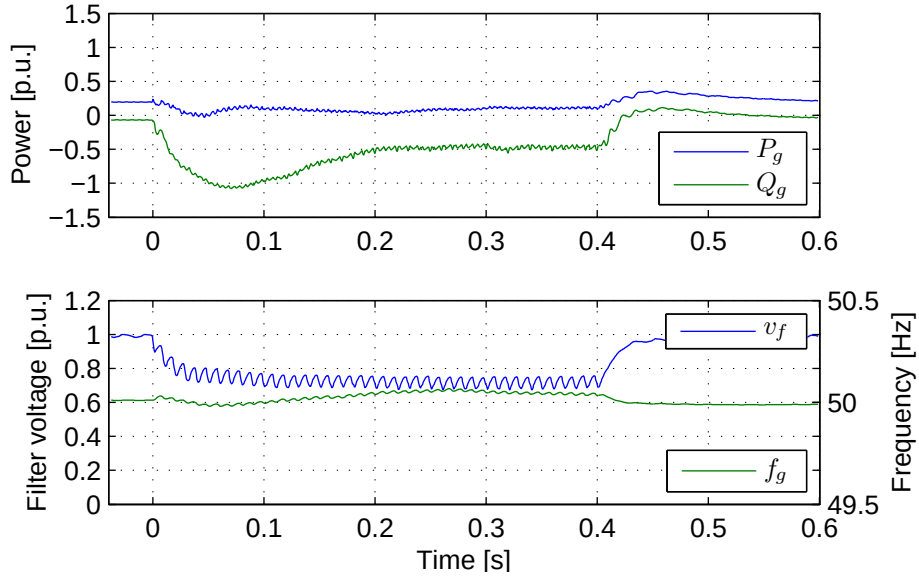

(a) Converter measurments

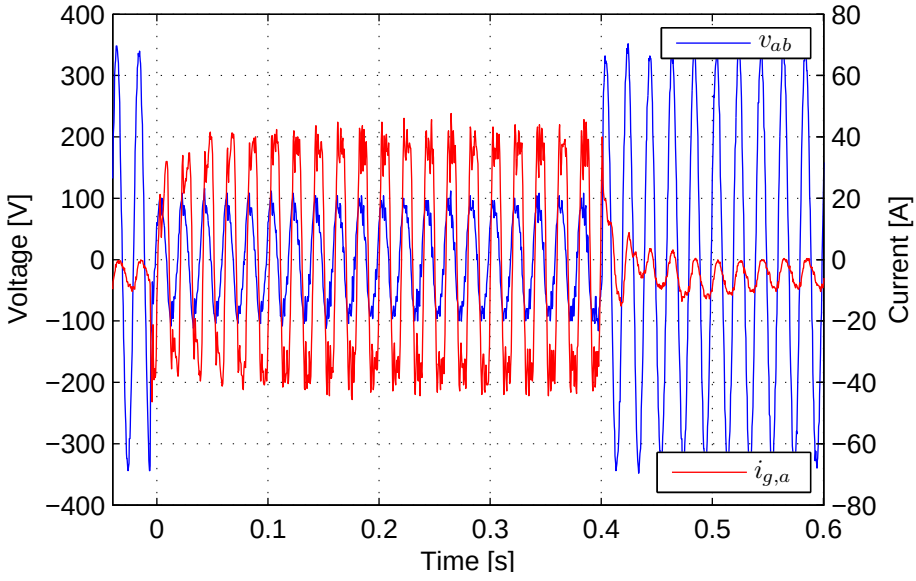

(b) Oscilloscope measurements

Figure 7.18 – Phase a and phase b short circuit to 25 % voltage of a strong grid with a converter connected supplying 20 % active power.

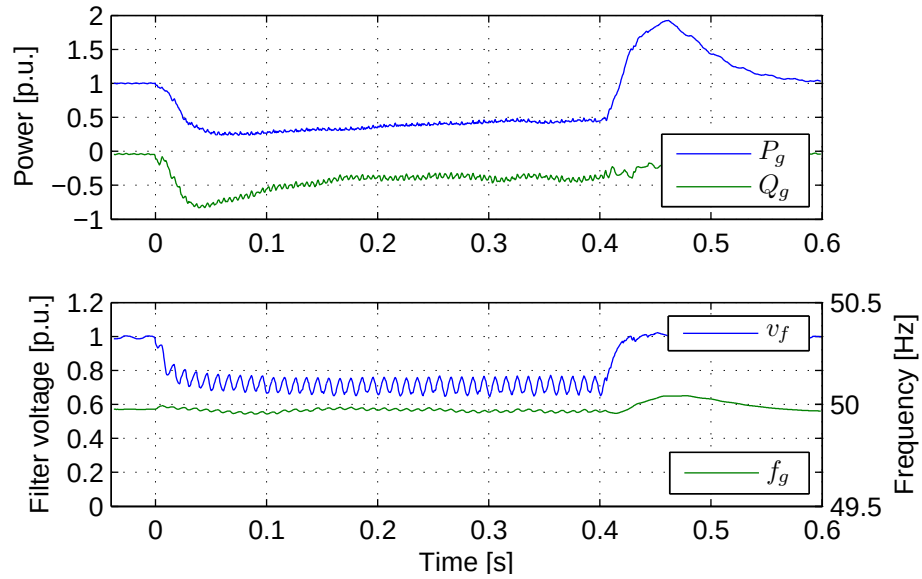

(a) Converter measurments

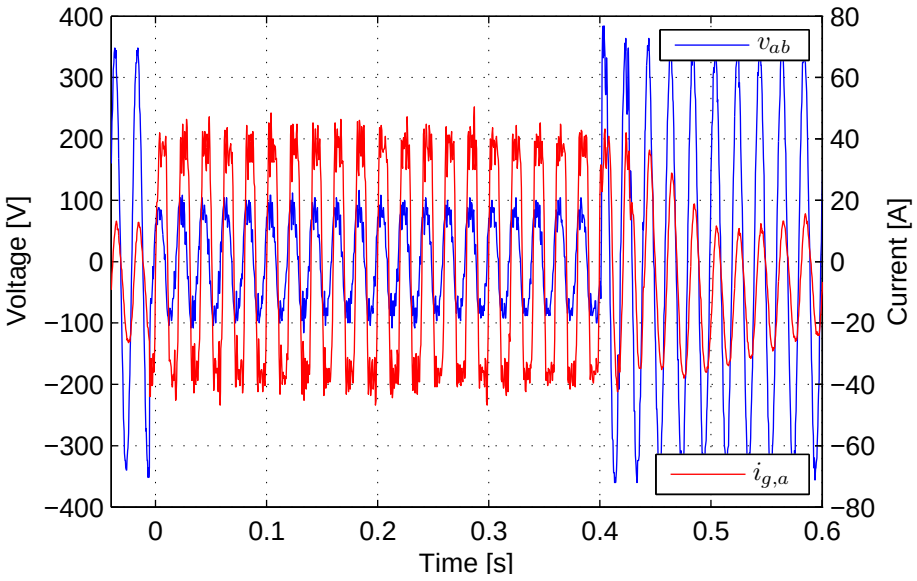

(b) Oscilloscope measurements

Figure 7.19 – Phase a and phase b short circuit to 25 % voltage of a strong grid with a converter connected supplying 100 % active power.

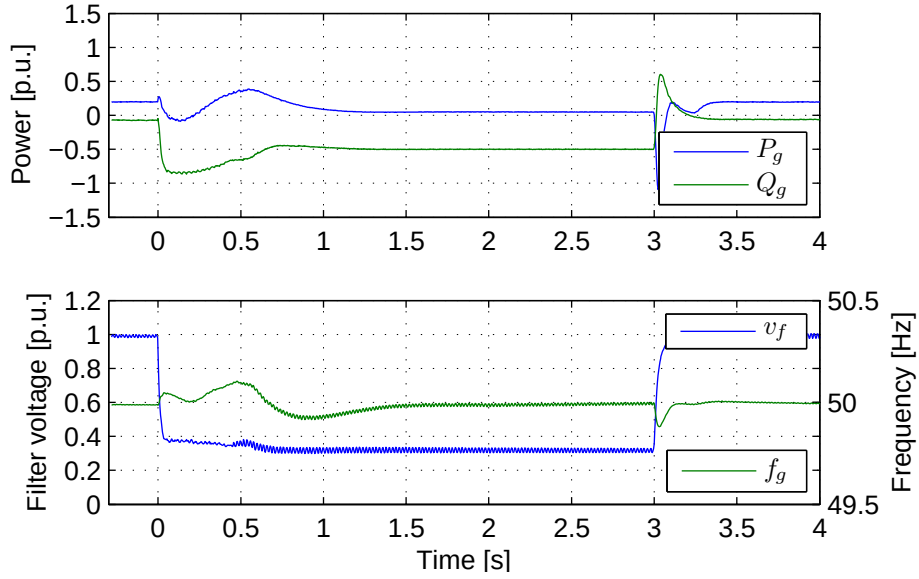

(a) Converter measurments

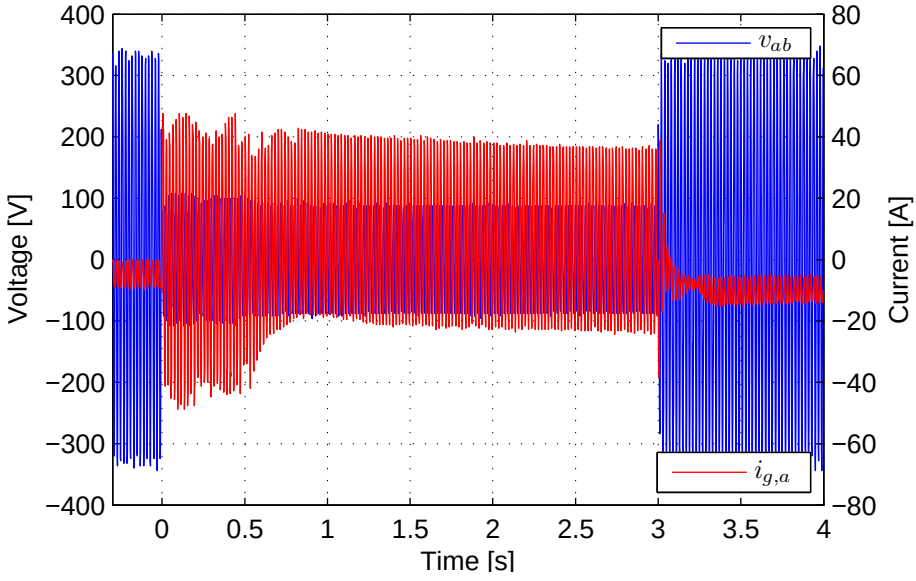

(b) Oscilloscope measurements

Figure 7.20 – Full three phase short circuit to 25 % voltage of a strong grid for 3 s with a converter connected supplying 20 % active power.

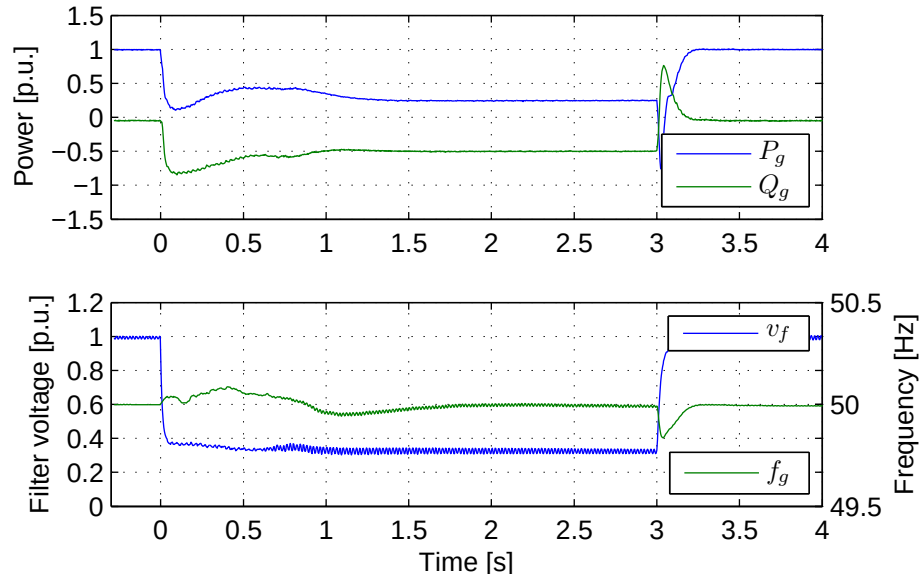

(a) Converter measurments

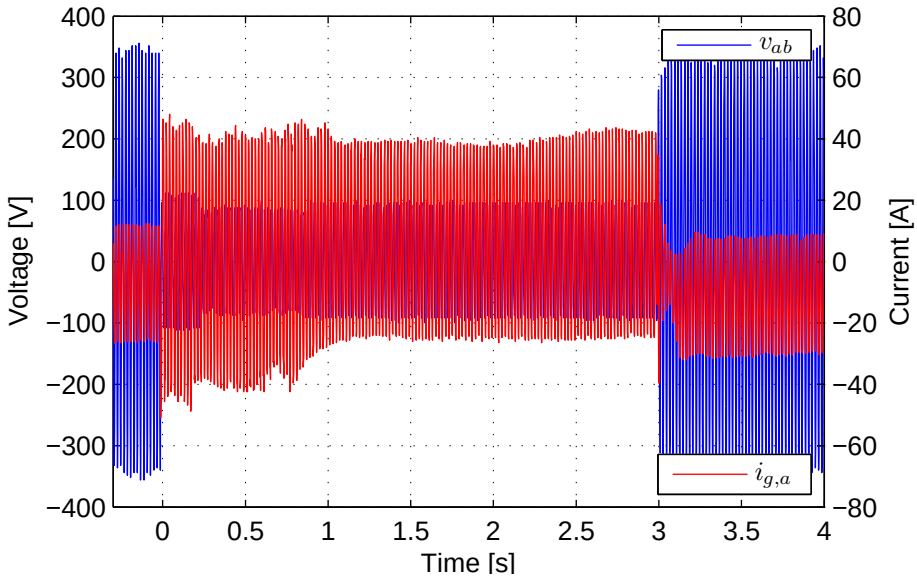

(b) Oscilloscope measurements

Figure 7.21 – Full three phase short circuit to 25 % voltage of a strong grid for 3 s with a converter connected supplying 100 % active power.

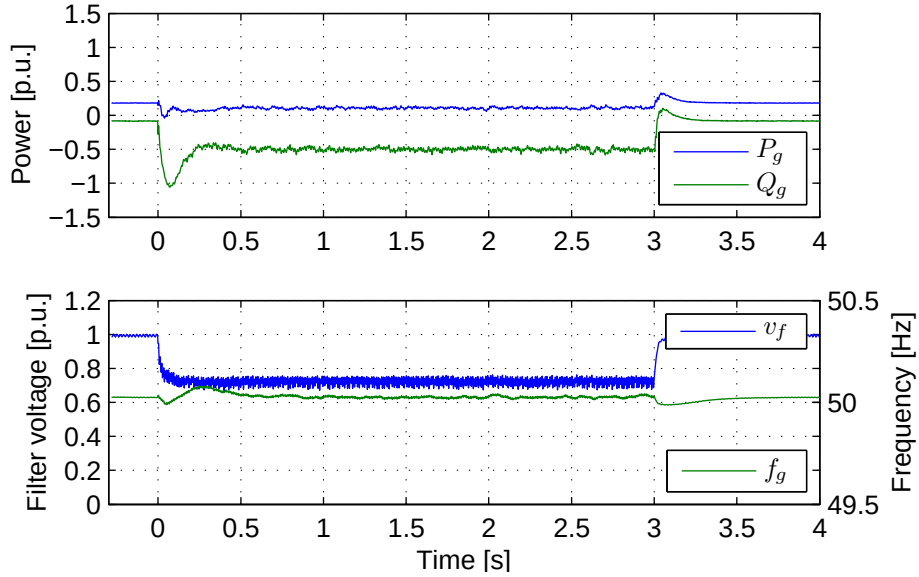

(a) Converter measurments

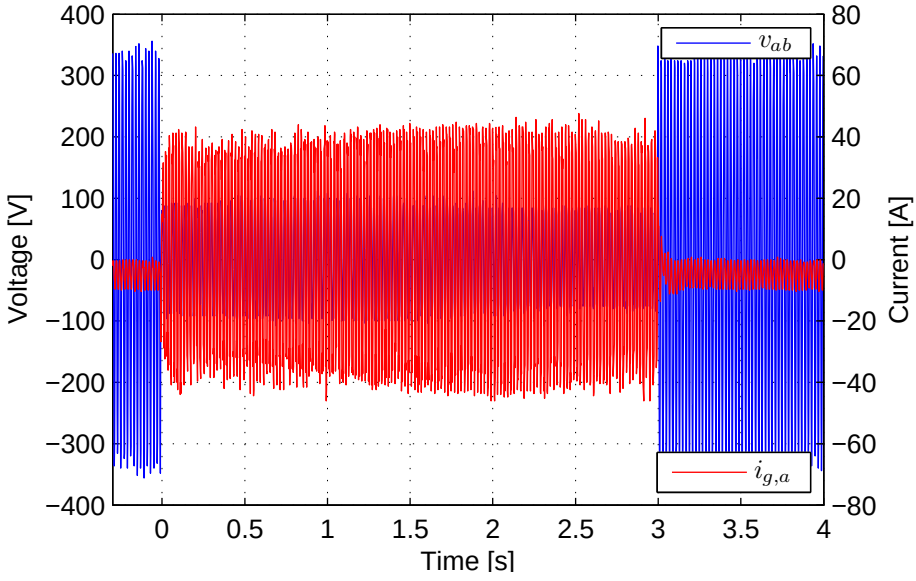

(b) Oscilloscope measurements

Figure 7.22 – Phase a and phase b short circuit to 25 % voltage of a strong grid for 3 s with a converter connected supplying 20 % active power.

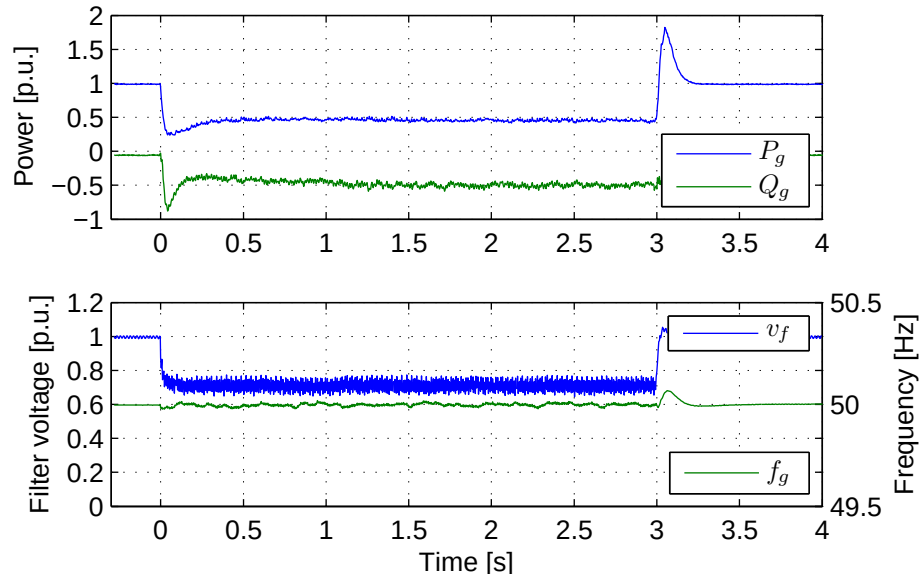

(a) Converter measurments

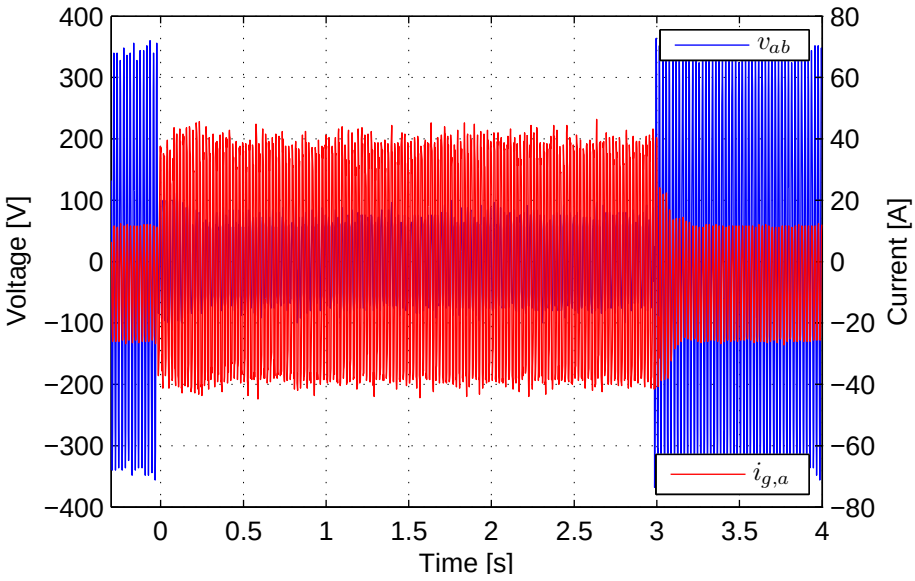

(b) Oscilloscope measurements

Figure 7.23 – Phase a and phase b short circuit to 25 % voltage of a strong grid for 3 s with a converter connected supplying 100 % active power.

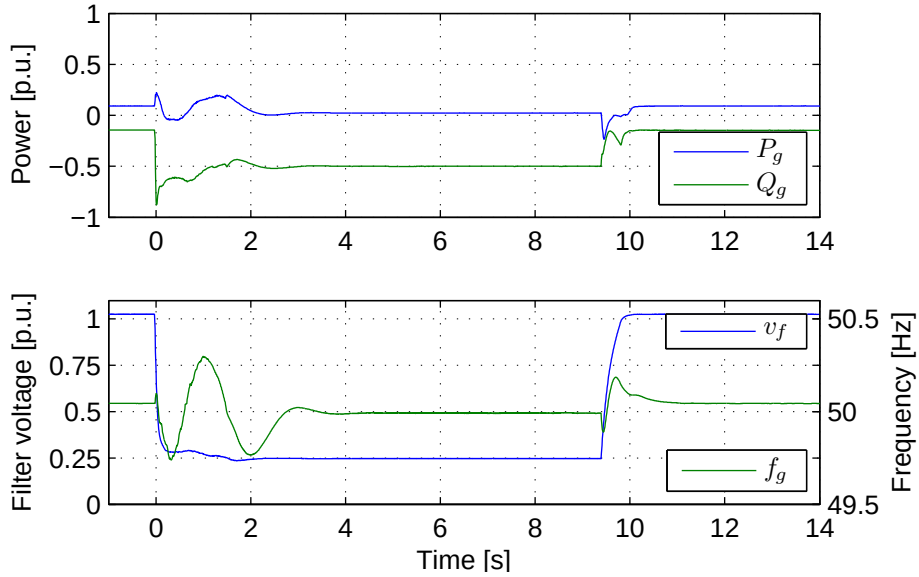

(a) Converter measurments

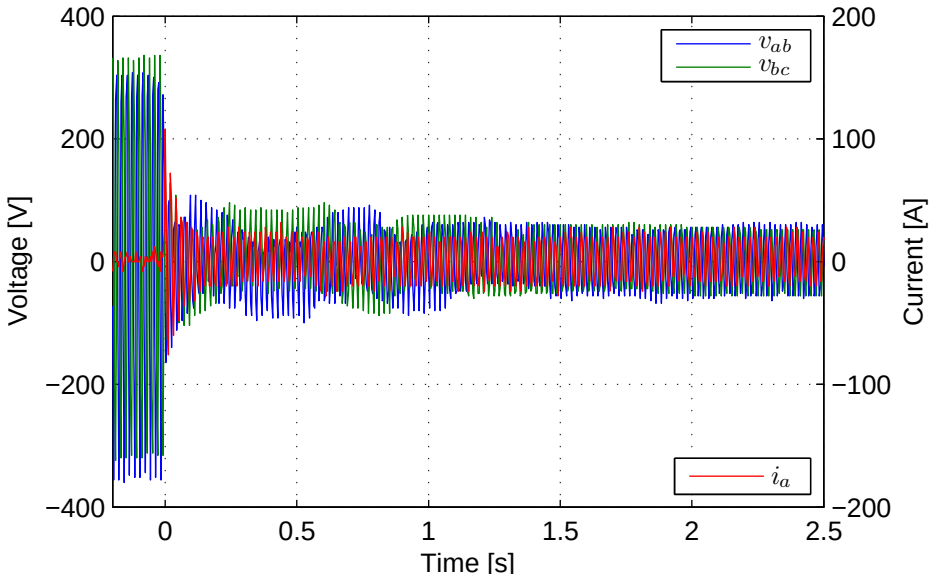

(b) Oscilloscope measurements

Figure 7.24 – Full short circuit of a weak synchronous generator grid voltage with converter connected supplying 10 % active power.

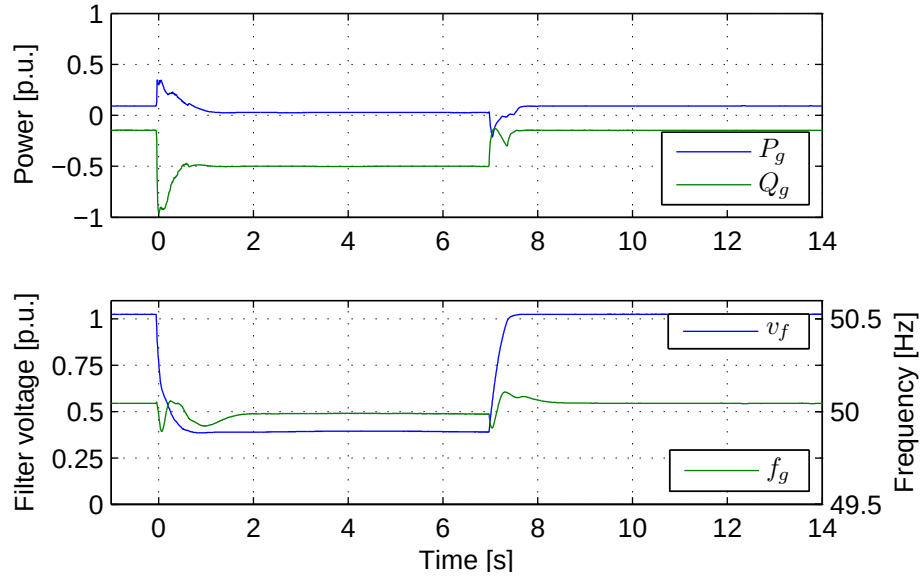

(a) Converter measurments

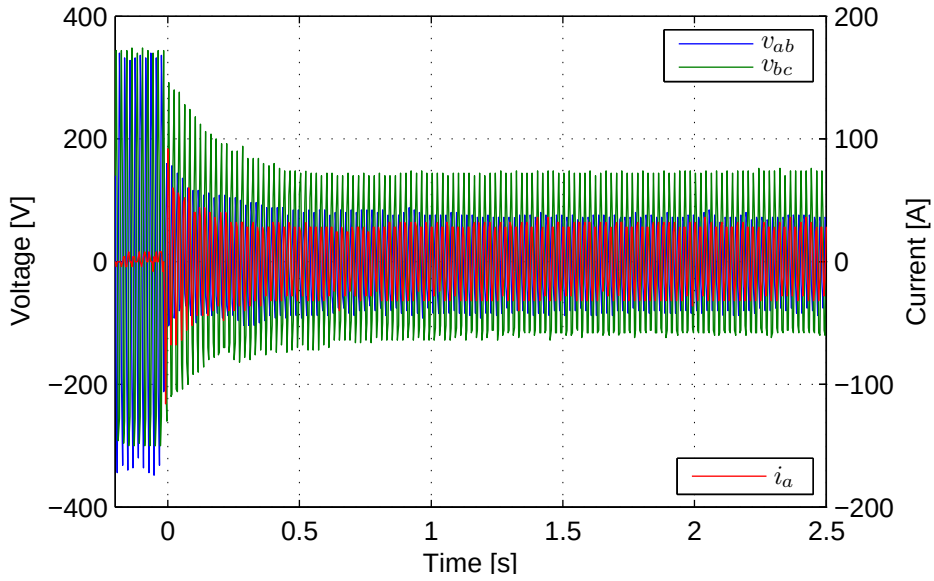

(b) Oscilloscope measurements

Figure 7.25 – Phase-to-phase short circuit of a weak synchronous generator grid voltage with converter connected supplying 10 % active power.

CHAPTER 8

Conclusions

This chapter presents a summary of the thesis with conclusions. It also proposes future work.

8.1 Summary

In this thesis a controller for a voltage controlled three phase pulse width modulated converter has been presented.

Chapter 1 introduces the grid converter controller and chapter 2 presents the laboratory setup for a test system which is used to illustrate the concepts introduced in later chapters.

A voltage observer for observing both magnitude and frequency of a three phase voltage is given in chapter 3. This observer can be used for synchronization to an external grid, or for running phase locked against a strong grid. It can even be used for synchronization over a low bandwidth communication channel.

Chapter 4 presents the inner voltage regulator which regulates the capacitor filter voltage. This chapter introduces the virtual impedance, in particular the interperiodic time-variant virtual impedance. An active damping feedback and a voltage shape controller is also presented.

Active and reactive power control is discussed in chapter 5. The current response of the converter to differences in magnitude and phase compared to a grid voltage is used to decouple the current into a magnitude part and a phase part. This decoupled response is used to implement a current regulator, which in turn is used to control the power delivered by the converter.

Chapter 6 uses the active and reactive power control to implement a general droop control and discusses issues conserning grid control.

Finally, chapter 7 presents experiments giving evidence that the proposed controller can be made to work according to the new grid codes for small-scale plants.

8.2 Proposed future work

The pulse width modulated converter is a very versatile component, implying a wast field of opportunities for further study.

As DSPs and microcontrollers become more powerful, available computing power becomes less of a limiting factor for control of the converter. The bandwidth of the controller is thus limited by the IGBTs and their maximum switching frequency.

The increase of computing capabilities enables the use of more numerically taxing control algorithms. More advanced algorithms using e.g. estimators, multivariable feedback and higher order controllers can increase the bandwidth compared to more classically designed algorithms for a given switching frequency. In particular, implementing multivariable frequency based algorithms based on for example H_∞ or μ-optimal controllers, which are typically very numerically intensive, has become feasible.

Another way to increase the bandwidth is to use several pulse width modulated bridges connected in parallel or serial configurations. These can use e.g. an interleaved switching pattern. Another possibility is to use fast, relatively low current IGBTs with high switching frequency to correct and help shape the output of slower high current IGBTs which uses a low switching frequency. The idea here is that control of the higher harmonics only need a small fraction of the power needed to output the fundamental frequency.

For the converter in this thesis, the inner voltage regulator was designed using classical, continuous cybernetic tools. Other possibilties, such as e.g. discrete tools based on ARMAX control, could potentially give better performance, particularly for the active damping. Also, investigating hybrid filters using both passive and active damping could prove interesting.

This thesis has only examined the performance of the controller in case of a limited voltage dip. If the dip goes all the way to zero, no information of the phase of the grid is available. The frequency can be expected to be approximately the same as it was before the short circuit, so the voltage observer presented in chapter 3 can be used setting the phase error to zero. However, if the short circuit lasts for a period of time, the converter and the grid will drift apart. To get a softer start if the grid voltage returns, the virtual impedance can be gradually increased while the grid is short

circuited.

Currently no short circuit detection has been implemented. Such a detection mechanism, particularly for the phase-to-phase short circuits, can improve the response for dips and short circuits by updating the internal parameters for the controllers.

To avoid the sharp cut-off created by the overcurrent protection for large currents the virtual impedance can be made non-linear. This non-linear response would increase the impedance for large currents limiting the current more smoothly.

It is the author's belief that the concept of the virtual impedance can be developed substantially further. The interperiodic time dependent virtual impedance introduced in this thesis is only one of many tools which can be used to shape the apparent source impedance of a converter.

Bibliography

[1] *Veiledende systemkrav for tilknytning til sentralnettet i Norge*, Statnett, Norway, 2006, document id 328582. [Online]. Available: http://www.statnett.no/default.aspx?ChannelID=1416

[2] T. Skjellnes, A. Skjellnes, and L. E. Norum, "Load sharing for parallel inverters without communication," *Proc. NORPIE'02*, 12-15 August 2002.

[3] D. G. Holmes and T. A. Lipo, *Pulse width modulation for power converters: Principles and Practice.* Wiley-IEEE press, 2003.

[4] *IEEE recommended practices and requirements for harmonic control in electrical power systems*, 12 Apr 1993, IEEE Std 519-1992.

[5] V. Pradeep, A. Kolwalar, and R. Teichmann, "Optimized filter design for IEEE 519 compliant grid connected inverters," *India International Conference on Power Electronics*, 2004.

[6] W. Gullvik, "Modeling, analysis and control of active front end (AFE) converter," Ph.D. dissertation, Norwegian University of Science and Technology, Department of Electric Power Engineering, Trondheim, Norway, October 2007.

[7] L. Harnefors and H.-P. Nee, "A general algorithm for speed and position estimation of ac motors," *Industrial Electronics, IEEE Transactions on*, vol. 47, no. 1, pp. 77–83, Feb. 2000.

[8] T. Wang, Z. Ye, G. Sinha, and X. Yuan, "Output filter design for a grid-interconnected three-phase inverter," *Power Electronics Specialist Conference, 2003. PESC '03. 2003 IEEE 34th Annual*, vol. 2, pp. 779–784 vol.2, 15-19 June 2003.

[9] I. J. Gabe, J. R. Massing, V. F. Montagner, and H. Pinheiro, "Stability analysis of grid-connected voltage source inverters with LCL-filters using partial state feedback," *Proc. EPE*, 2-5 September 2007.

[10] P. Dahono, "A control method for DC-DC converter that has an LCL output filter based on new virtual capacitor and resistor concepts," *Power Electronics Specialists Conference, 2004. PESC 04. 2004 IEEE 35th Annual*, vol. 1, pp. 36–42 Vol.1, 20-25 June 2004.

[11] O. Mo, M. Hernes, and K. Ljøkelsøy, "Active damping of oscillations in LC-filter for line connected, current controlled, PWM voltage source converters," *Proc. EPE*, 2-4 September 2003.

[12] E. Twining and D. Holmes, "Grid current regulation of a three-phase voltage source inverter with an LCL input filter," *Power Electronics Specialists Conference, 2002. pesc 02. 2002 IEEE 33rd Annual*, vol. 3, pp. 1189–1194 vol.3, 2002.

[13] V. Blasko and V. Kaura, "A novel control to actively damp resonance in input LC filter of a three phase voltage source converter," *Applied Power Electronics Conference and Exposition, 1996. APEC '96. Conference Proceedings 1996., Eleventh Annual*, vol. 2, pp. 545–551 vol.2, 3-7 Mar 1996.

[14] W. Gullvik, L. Norum, and R. Nilsen, "Active damping of resonance oscillations in LCL-filters base on virtual flux and virtual resistor," *Proc. EPE*, 2-5 September 2007.

[15] M. Malinowski, M. Kazmierkowski, S. Hansen, F. Blaabjerg, and G. Marques, "Virtual-flux-based direct power control of three-phase PWM rectifiers," *Industry Applications, IEEE Transactions on*, vol. 37, no. 4, pp. 1019–1027, Jul/Aug 2001.

[16] E. W. Weisstein, "Stable polynomial," *MathWorld – A Wolfram Web Resource*, 21 Sep. 2000. [Online]. Available: http://mathworld.wolfram.com/StablePolynomial.html

[17] S. Strelitz, "On the Routh-Hurwitz problem," *Amer. Math. Monthly*, no. 84, pp. 542–544 vol.2, 1977.

[18] A. E. Fitzgerald, J. Charles Kingsley, and S. D. Umans, *Electric machinery*, 5th ed. McGraw-Hill, 1995.

[19] J. L. Willems, "A new interpretation of the Akagi-Nabae power components for nonsinusoidal three-phase situations," *Instrumentation and Measurement, IEEE Transactions on*, vol. 41, no. 4, pp. 523–527, Aug 1992.

[20] F. Z. Peng, L. M. Tolbert, and Z. Qian, "Definitions and compensation of non-active current in power systems," *Power Electronics Specialists Conference, 2002. pesc 02. 2002 IEEE 33rd Annual*, vol. 4, pp. 1779–1784, 2002.

[21] H. Akagi, Y. Kanazawa, and A. Nabae, "Instantaneous reactive power compensators comprising switching devices without energy storage components," *Industry Applications, IEEE Transactions on*, vol. 20, pp. 625–630, May/June 1984.

[22] J. M. Guerrero, J. C. Vásquez, J. Matas, J. L. Sosa, and L. G. de Vicuñja, "Parallel operation of uninterruptible power supply systems in microgrids," *Proc. EPE*, 2-5 September 2007.

[23] A. Hagemann, *Elektriske anlegg for sterkstrøm.* Trondheim, Norway: NTH, 1966.

[24] M. Chandorkar, D. Divan, and R. Adapa, "Control of parallel connected inverters in standalone AC supply systems," *Industry Applications, IEEE Transactions on*, vol. 29, no. 1, pp. 136–143, Jan/Feb 1993.

[25] E. A. A. Coelho, P. C. Cortizo, and P. F. D. Garcia, "Small-signal stability for parallel-connected inverters in stand-alone AC supply systems," *Industry Applications, IEEE Transactions on*, vol. 38, no. 2, pp. 533–542, Mar/Apr 2002.

[26] S. Chiang and J. Chang, "Parallel control of the UPS inverters with frequency-dependent droop scheme," *Power Electronics Specialists Conference, 2001. PESC. 2001 IEEE 32nd Annual*, vol. 2, pp. 957–961 vol.2, 2001.

[27] J. M. Guerrero, L. G. de Vicuñja, M. Castilla, and J. Miret, "A wireless controller to enhance dynamic performance of parallel inverters in distributed generation systems," *Power Electronics, IEEE Transactions on*, vol. 19, no. 5, pp. 1205–1213, Sept. 2004.

[28] E. S. Hoff, T. Skjellnes, and L. E. Norum, "Paralleled three-phase inverters," *Proc. NORPIE'04*, 14-16 June 2004.

[29] K. D. Brabandere, B. Bolsens, J. V. den Keybus, A. Woyte, J. Driesen, and R. Belmans, "A voltage and frequency droop control method for parallel inverters," *Power Electronics, IEEE Transactions on*, vol. 22, no. 4, pp. 1107–1115, July 2007.

[30] E. S. Hoff, "Distributed generation - power electronic converters, communication and control," Ph.D. dissertation, Norwegian University of Science and Technology, Department of Electric Power Engineering, Trondheim, Norway, April 2007.

[31] *Standards for measurements and testing of wind turbine power quality*, IEC61400-21.

[32] G. Paap, "Symmetrical components in the time domain and their application to power network calculations," *Power Systems, IEEE Transactions on*, vol. 15, no. 2, pp. 522–528, May 2000.

[33] C. L. Fortescue, "Method of symmetrical coordinates applied to the solution of polyphase networks," *Trans. AIEE, pt. II*, vol. 37, pp. 1027–1140, 1918.

[34] A. V. Oppenheim, A. S. Willsky, and I. T. Young, *Signals and systems.* Prentice-Hall, 1983.

[35] O. Egeland and J. T. Gravdahl, *Modeling and Simulation for Automatic Control.* Trondheim, Norway: Marine Cybernetics, 2002.

[36] S. Skogestad and I. Postlethwaite, *Multivariable Feedback Control, Analysis and Design.* Baffins Lane, Chichester: John Wiley & Sons Ltd., 1997.

[37] E. Kreyszig, *Advanced Engineering Mathematics*, 7th ed. John Wiley & Sons, Inc., 1993.

APPENDIX A

Mathematical tools

This chapter presents a few mathematical tools that are used through this thesis.

A.1 On three-phase systems

Both the grid side converter and the motor drive is three-phase systems. This section investigates transformations between different coordinate systems.

The history of the $\alpha\beta$ and dq-transformation presented here can according to Paap [32] be traced back to a paper presented in 1918 by Fortescue [33] when he introduced the symmetrical component transform as a decomposition of complex steady-state phasors.

Note that the scaling of some of the transformations given in this chapter differ from the scaling sometimes found in litterature, e.g. the paper mentioned above by Paap. This scaling has been chosen because peak values are preferred over RMS values in this thesis.

A.1.1 Phase-to-phase to line voltage conversion

Sometimes a conversion from phase-to-phase measurements to line voltages are necessary, or vice versa. The conversion to phase-to-phase measurements is simple:

$$\boldsymbol{x}^{\Delta} = \begin{bmatrix} x_{bc} \\ x_{ca} \\ x_{ab} \end{bmatrix} = \begin{bmatrix} x_b - x_c \\ x_c - x_a \\ x_a - x_b \end{bmatrix} = \begin{bmatrix} 0 & 1 & -1 \\ -1 & 0 & 1 \\ 1 & -1 & 0 \end{bmatrix} \begin{bmatrix} x_a \\ x_b \\ x_c \end{bmatrix} = \mathbf{T}^{\Delta}_{abc} \boldsymbol{x}^{abc}. \quad \text{(A.1)}$$

The sign and order of the elements in $\boldsymbol{x}^{\Delta}$ are chosen so that the transformation matrix $\mathbf{T}^{\Delta}_{abc}$ is skew-symmetric. Furthermore, it is the negated

cross-product matrix of the vector $\boldsymbol{q}^{abc} = \begin{bmatrix}1 & 1 & 1\end{bmatrix}^{\mathrm{T}}$, i.e.

$$\boldsymbol{x}^{\Delta} = -\boldsymbol{q}^{abc} \times \boldsymbol{x}^{abc}. \tag{A.2}$$

The matrix $\mathbf{T}^{\Delta}_{abc}$ is linearly dependent with a rank of 2. In particular

$$x_{bc} + x_{ca} + x_{ab} = 0. \tag{A.3}$$

The linear dependence of the transformation matrix means that it can not be inverted. However, premultiplying with the cross product of $\boldsymbol{q}^{abc}$ and using Lagrange's formula*, it can be easily verified that:

$$\boldsymbol{x}^{abc} = \frac{1}{3}\boldsymbol{q}^{abc} \times \boldsymbol{x}^{\Delta} + \boldsymbol{q}^{abc} x_0, \tag{A.4}$$

where

$$x_0 = \frac{\boldsymbol{q}^{abc} \cdot \boldsymbol{x}^{abc}}{\boldsymbol{q}^{abc} \cdot \boldsymbol{q}^{abc}} = \frac{x_a + x_b + x_c}{3}. \tag{A.5}$$

In matrix form this becomes

$$\boldsymbol{x}^{abc} - \boldsymbol{q}^{abc} x_0 = \mathbf{T}^{abc}_{\Delta} \boldsymbol{x}^{\Delta} = \frac{1}{3}\left(\mathbf{T}^{\Delta}_{abc}\right)^{\mathrm{T}} \boldsymbol{x}^{\Delta} = \frac{1}{3}\begin{bmatrix} 0 & -1 & 1 \\ 1 & 0 & -1 \\ -1 & 1 & 0 \end{bmatrix}\begin{bmatrix} x_{bc} \\ x_{ca} \\ x_{ab} \end{bmatrix}. \tag{A.6}$$

The linear dependence means that only two measurements are needed. The following equations summarizes the relationships between the line and phase measurements:

$$x_a - x_0 = \frac{-x_{bc} - 2x_{ca}}{3} = \frac{x_{bc} + 2x_{ab}}{3} = \frac{-x_{ca} + x_{ab}}{3} \tag{A.7}$$

$$x_b - x_0 = \frac{2x_{bc} + x_{ca}}{3} = \frac{x_{bc} - x_{ab}}{3} = \frac{-x_{ca} - 2x_{ab}}{3} \tag{A.8}$$

$$x_c - x_0 = \frac{-x_{bc} + x_{ca}}{3} = \frac{-2x_{bc} - x_{ab}}{3} = \frac{2x_{ca} + x_{ab}}{3}. \tag{A.9}$$

A.1.2 The $\alpha\beta$ transform

The well known $\alpha\beta$ transform, often called the Clarke transform, is useful for three phase systems. Its basic property is that it decouples three similar sinusoidal signals separated by 120° into two sinusoidal signals separated by 90°. More general periodic signals are investigated below.

*Lagrange's formula: $\boldsymbol{r} \times (\boldsymbol{s} \times \boldsymbol{t}) = \boldsymbol{s}\,(\boldsymbol{r} \cdot \boldsymbol{t}) - \boldsymbol{t}\,(\boldsymbol{r} \cdot \boldsymbol{s})$.

The $\alpha\beta 0$ transform can be given as

$$\boldsymbol{x}^{\alpha\beta 0} = \begin{bmatrix} x_\alpha \\ x_\beta \\ x_0 \end{bmatrix} = \mathbf{T}_{abc}^{\alpha\beta 0} \boldsymbol{x}^{abc} = \frac{1}{3} \begin{bmatrix} 2 & -1 & -1 \\ 0 & \sqrt{3} & -\sqrt{3} \\ 1 & 1 & 1 \end{bmatrix} \begin{bmatrix} x_a \\ x_b \\ x_c \end{bmatrix}. \tag{A.10}$$

The inverse transformation can be calculated from the inverse of $\mathbf{T}_{abc}^{\alpha\beta 0}$:

$$\boldsymbol{x}^{abc} = \mathbf{T}_{\alpha\beta 0}^{abc} \boldsymbol{x}^{\alpha\beta 0} = \mathbf{T}_{abc}^{\alpha\beta 0 \, -1} \boldsymbol{x}^{\alpha\beta 0} = \frac{1}{2} \begin{bmatrix} 2 & 0 & 2 \\ -1 & \sqrt{3} & 2 \\ -1 & -\sqrt{3} & 2 \end{bmatrix} \boldsymbol{x}^{\alpha\beta 0}. \tag{A.11}$$

The third vector component of the transformed vector, x_0, is called the null component of the system. It is the average of the three phases and is often zero or simply ignored. This thesis uses the name $\alpha\beta 0$ transform if the null component is included, as opposed to the name $\alpha\beta$ transform if the null component is ignored.

If the null component is known to be zero, or subtracted from the values before transformation, then $x_a + x_b + x_c = 0$. This relation can be used to remove one of the elements:

$$\begin{bmatrix} x_\alpha \\ x_\beta \end{bmatrix} = \begin{bmatrix} 1 & 0 \\ \frac{1}{\sqrt{3}} & \frac{2}{\sqrt{3}} \end{bmatrix} \begin{bmatrix} x_a \\ x_b \end{bmatrix} = \begin{bmatrix} 1 & 0 \\ -\frac{1}{\sqrt{3}} & -\frac{2}{\sqrt{3}} \end{bmatrix} \begin{bmatrix} x_a \\ x_c \end{bmatrix} = \begin{bmatrix} -1 & -1 \\ \frac{1}{\sqrt{3}} & -\frac{1}{\sqrt{3}} \end{bmatrix} \begin{bmatrix} x_b \\ x_c \end{bmatrix}. \tag{A.12}$$

The inverse is of course equation A.11 without the null-component:

$$\begin{bmatrix} x_a \\ x_b \\ x_c \end{bmatrix} = \begin{bmatrix} 1 & 0 \\ -\frac{1}{2} & \frac{\sqrt{3}}{2} \\ -\frac{1}{2} & -\frac{\sqrt{3}}{2} \end{bmatrix} \begin{bmatrix} x_\alpha \\ x_\beta \end{bmatrix}. \tag{A.13}$$

The $\boldsymbol{x}^{\alpha\beta}$-vector can also be found directly from phase-to-phase measurements:

$$\begin{bmatrix} x_\alpha \\ x_\beta \end{bmatrix} = \begin{bmatrix} \frac{x_{ab} - x_{ca}}{3} \\ \frac{2x_{bc} - x_{ca} - x_{ab}}{3\sqrt{3}} \end{bmatrix} = \begin{bmatrix} -\frac{2x_{ca} + x_{bc}}{3} \\ \frac{x_{bc}}{\sqrt{3}} \end{bmatrix} = \begin{bmatrix} \frac{2x_{ab} + x_{bc}}{3} \\ \frac{x_{bc}}{\sqrt{3}} \end{bmatrix} = \begin{bmatrix} \frac{x_{ab} - x_{ca}}{3} \\ -\frac{x_{ab} + x_{ca}}{\sqrt{3}} \end{bmatrix}. \tag{A.14}$$

General periodic signal

A more thorough investigation of the $\alpha\beta 0$-transform gives further insight into its usefulness. Let $f(t)$ be a piecewise smooth and continuous, period-

ical signal of period T. The fourier series expansion of $f(t)$ is

$$f(t) = \frac{1}{2}a_0 + \sum_{n=1}^{\infty} \left(a_n \cos\left(\omega_n t\right) + b_n \sin\left(\omega_n t\right)\right) \tag{A.15}$$

where

$$\omega_n = \frac{2\pi n}{T}, \tag{A.16}$$

$$a_n = \frac{2}{T}\int_0^{\mathrm{T}} f(\tau)\cos\left(\omega_n \tau\right) d\tau, \tag{A.17}$$

$$b_n = \frac{2}{T}\int_0^{\mathrm{T}} f(\tau)\sin\left(\omega_n \tau\right) d\tau. \tag{A.18}$$

Using the fourier series expansion, split $f(t)$ into the sum of three functions

$$f(t) = f_0(t) + f_p(t) + f_n(t), \tag{A.19}$$

where $f_0(t)$ contains every third harmonic starting from the 0. harmonic (the DC-average), $f_p(t)$ every third harmonic starting from the 1. harmonic (the fundamental harmonic), and $f_n(t)$ every third harmonic starting from the 2. harmonic.

Let $\boldsymbol{x}^{abc}$ be a three phase vector defined as

$$\boldsymbol{x}^{abc} = \begin{bmatrix} x_a \\ x_b \\ x_c \end{bmatrix} = \begin{bmatrix} f(t) \\ f(t - \frac{T}{3}) \\ f(t - \frac{2T}{3}) \end{bmatrix}. \tag{A.20}$$

Then it can be shown that (see appendix B)

$$\boldsymbol{x}^{\alpha\beta 0} = \begin{bmatrix} x_\alpha \\ x_\beta \\ x_0 \end{bmatrix} = \begin{bmatrix} f_p(t) + f_n(t) \\ f_p^{90^\circ}(t) - f_n^{90^\circ}(t) \\ f_0(t) \end{bmatrix}. \tag{A.21}$$

The superscript $(\,\cdot\,)^{90^\circ}$ denotes a transform shifting all the harmonics 90°, i.e.

$$\begin{aligned} g^{90^\circ}(t) &= \frac{1}{2}a_0 + \sum_{n=1}^{\infty} \left(a_n \cos\left(\omega_n t - \frac{\pi}{2}\right) + b_n \sin\left(\omega_n t - \frac{\pi}{2}\right)\right) \\ &= \frac{1}{2}a_0 + \sum_{n=1}^{\infty} \left(-b_n \cos\left(\omega_n t\right) + a_n \sin\left(\omega_n t\right)\right), \end{aligned} \tag{A.22}$$

where a_n and b_n are the fourier series coefficients of $g(t)$.

A.1.3 The dq transform

The dq transform, sometimes called the Park transform, is the $\alpha\beta$ transform followed by a rotation. The rotation gives an accelerated coordinate system where symmetric sinusoidal three phase signals with a frequency equal to the rotation rate are transformed into constant signals.

Like the $\alpha\beta$ transform, the null component is often not needed. This thesis uses the name dq0 transform if the null component is included, and dq transform if the null component is ignored.

The dq0 transform of a vector $\boldsymbol{x}$ is given as

$$\begin{aligned}\boldsymbol{x}^{\mathrm{dq0}} &= \mathbf{T}^{\mathrm{dq0}}_{abc}\boldsymbol{x}^{abc} = \mathbf{R}^{\mathrm{dq0}}_{\alpha\beta0}\mathbf{T}^{\alpha\beta0}_{abc}\boldsymbol{x}^{abc} \\ &= \begin{bmatrix} \cos\omega t & \sin\omega t & 0 \\ -\sin\omega t & \cos\omega t & 0 \\ 0 & 0 & 1 \end{bmatrix} \left(\frac{1}{3} \begin{bmatrix} 2 & -1 & -1 \\ 0 & \sqrt{3} & -\sqrt{3} \\ 1 & 1 & 1 \end{bmatrix} \right) \boldsymbol{x}^{abc} \\ &= \begin{bmatrix} \frac{2}{3}\cos\omega t & \frac{2}{3}\cos\left(\omega t - 120°\right) & \frac{2}{3}\cos\left(\omega t - 240°\right) \\ -\frac{2}{3}\sin\omega t & -\frac{2}{3}\sin\left(\omega t - 120°\right) & -\frac{2}{3}\sin\left(\omega t - 240°\right) \\ \frac{1}{3} & \frac{1}{3} & \frac{1}{3} \end{bmatrix} \boldsymbol{x}^{abc}.\end{aligned} \tag{A.23}$$

The inverse trasformation is given as

$$\begin{aligned}\boldsymbol{x}^{abc} &= \mathbf{T}^{abc}_{\mathrm{dq0}}\boldsymbol{x}^{\mathrm{dq0}} = \mathbf{T}^{abc}_{\alpha\beta0}\mathbf{R}^{\alpha\beta0}_{\mathrm{dq0}}\boldsymbol{x}^{\mathrm{dq0}} \\ &= \begin{bmatrix} 1 & 0 & 1 \\ -\frac{1}{2} & \frac{\sqrt{3}}{2} & 1 \\ -\frac{1}{2} & -\frac{\sqrt{3}}{2} & 1 \end{bmatrix} \begin{bmatrix} \cos\omega t & -\sin\omega t & 0 \\ \sin\omega t & \cos\omega t & 0 \\ 0 & 0 & 1 \end{bmatrix} \boldsymbol{x}^{\mathrm{dq0}} \\ &= \begin{bmatrix} \cos\omega t & -\sin\omega t & 1 \\ \cos\left(\omega t - 120°\right) & -\sin\left(\omega t - 120°\right) & 1 \\ \cos\left(\omega t - 240°\right) & -\sin\left(\omega t - 240°\right) & 1 \end{bmatrix} \boldsymbol{x}^{\mathrm{dq0}}.\end{aligned} \tag{A.24}$$

If $x_a + x_b + x_c = 0$, this can be inserted into the transform to give

$$\begin{bmatrix} x_d \\ x_q \end{bmatrix} = \frac{2\sqrt{3}}{3} \begin{bmatrix} \cos\left(\omega t - 60°\right) & \sin\omega t \\ -\sin\left(\omega t - 60°\right) & \cos\omega t \end{bmatrix} \begin{bmatrix} x_a \\ x_b \end{bmatrix} \tag{A.25}$$

$$= \frac{2\sqrt{3}}{3} \begin{bmatrix} \cos\left(\omega t + 60°\right) & -\sin\omega t \\ -\sin\left(\omega t - 60°\right) & -\cos\omega t \end{bmatrix} \begin{bmatrix} x_a \\ x_c \end{bmatrix} \tag{A.26}$$

$$= \frac{2\sqrt{3}}{3} \begin{bmatrix} -\cos\left(\omega t + 60°\right) & -\cos\left(\omega t - 60°\right) \\ \sin\left(\omega t + 60°\right) & \sin\left(\omega t - 60°\right) \end{bmatrix} \begin{bmatrix} x_b \\ x_c \end{bmatrix}. \tag{A.27}$$

Time derivates

The dq-coordinate system uses a rotating reference frame. This means that time derivates of variables in this coordinate system gets a cross coupling factor which is not present in the $\alpha\beta$-coordinate system. This coupling factor can be compared to the fictitious centrifugal force in a rotating mechanical system.

The relationship between a time derivate variable in the $\alpha\beta$-coordinate system and one in the dq-coordinate system is

$$\dot{\boldsymbol{x}}^{\alpha\beta0} = \frac{d}{dt}\left(\mathbf{R}_{\mathrm{dq0}}^{\alpha\beta0}\boldsymbol{x}^{\mathrm{dq0}}\right) = \begin{bmatrix} -x_\beta \\ x_\alpha \\ 0 \end{bmatrix}\dot{\theta} + \mathbf{R}_{\mathrm{dq0}}^{\alpha\beta0}\dot{\boldsymbol{x}}^{\mathrm{dq0}}, \tag{A.28}$$

$$\dot{\boldsymbol{x}}^{\mathrm{dq0}} = \frac{d}{dt}\left(\mathbf{R}_{\alpha\beta0}^{\mathrm{dq0}}\boldsymbol{x}^{\alpha\beta0}\right) = \begin{bmatrix} x_q \\ -x_d \\ 0 \end{bmatrix}\dot{\theta} + \mathbf{R}_{\alpha\beta0}^{\mathrm{dq0}}\dot{\boldsymbol{x}}^{\alpha\beta0}. \tag{A.29}$$

Note that if $\theta = \omega t$ for a constant ω, then $\dot{\theta} = \omega$.

Keeping with the comparison with a mechanical system, the relationship can also be written

$$\dot{\boldsymbol{x}}^{\alpha\beta0} = \boldsymbol{\omega} \times \boldsymbol{x}^{\alpha\beta0} + \mathbf{R}_{\mathrm{dq0}}^{\alpha\beta0}\dot{\boldsymbol{x}}^{\mathrm{dq0}}, \tag{A.30}$$

$$\dot{\boldsymbol{x}}^{\mathrm{dq0}} = -\boldsymbol{\omega} \times \boldsymbol{x}^{\mathrm{dq0}} + \mathbf{R}_{\alpha\beta0}^{\mathrm{dq0}}\dot{\boldsymbol{x}}^{\alpha\beta0}, \tag{A.31}$$

where:

$$\boldsymbol{\omega} = \begin{bmatrix} 0 & 0 & \dot{\theta} \end{bmatrix}^{\mathrm{T}}. \tag{A.32}$$

A useful relationship can be found for the case where

$$\boldsymbol{y}^{\alpha\beta0} = k\dot{\boldsymbol{x}}^{\alpha\beta0}, \tag{A.33}$$

where k is a scalar. Then

$$\boldsymbol{y}^{\mathrm{dq0}} = k\left(\boldsymbol{\omega} \times \boldsymbol{x}^{\mathrm{dq0}} + \dot{\boldsymbol{x}}^{\mathrm{dq0}}\right) = k\left(\begin{bmatrix} x_q \\ -x_d \\ 0 \end{bmatrix}\dot{\theta} + \dot{\boldsymbol{x}}^{\mathrm{dq0}}\right). \tag{A.34}$$

A.2 On discrete and continuous systems

The converter is composed of a mix of discrete and continuous systems. This section investigates approximations and conversions between discrete and continuous systems, as well as some discrete filters.

For a proper introduction to the relationship between discrete and continuous system, see any digital signal processing book (e.g. [34]). This introduction should include but not be limited to the z-transform, the Nyquist criterion, the Nyquist frequency and aliasing phenomenons.

For easy implementation in software, the difference equations[†] are given. The difference equation gives the next output signal as a function of the previous output signals and current and previous input signals

$$y_k = f(y_{k-1}, y_{k-2}, \dots, u_k, u_{k-1}, \dots) \tag{A.35}$$

The symbol y_k is used for the output signal for time-step k, and u_k is used for the input signal for the same time-step. Special care has been taken in the form of these equations to have both speed of calculation and more importantly to avoid loss of precision when using fixed point math.

A.2.1 Simple continuous to discrete conversion

If the sampling frequency is sufficiently high compared to the time responses of the discrete system, the continuous transfer function in the s-plane can be converted to a discrete transfer function in the z-plane by replacing the variable s with $\frac{1-z^{-1}}{T}$. T is the sampling period.

This method utilizes Euler's method (see e.g. [35]), which approximates the differential of a signal with the difference between the two time steps.

Another approximation which can be used to convert a continuous system to a discrete system is the bilinear transform. It replaces s with $\frac{2}{T}\frac{1-z^{-1}}{1+z^{-1}}$. Low pass filters implemented with this approximation has much better attenuation around the Nyquist frequency of the filter, but adds some complexity.

A discrete low pass filter

Euler's method can be used to discretize the simple, well known, continuous low pass filter

$$F_c(s) = \frac{1}{\frac{s}{\omega_f} + 1}. \tag{A.36}$$

The bandwidth of this low pass filter is given by ω_f. Inserting $s = \frac{1-z^{-1}}{T}$ gives the discrete version as

$$F_d(z) = F_c(\tfrac{1-z^{-1}}{T}) = \frac{1}{\frac{1-z^{-1}}{T\omega_f} + 1} = \frac{k_f}{1-(1-k_f)z^{-1}}, \tag{A.37}$$

[†]Also called a recurrence relation.

where

$$k_f = \frac{1}{1 + \frac{1}{T\omega_f}}. \tag{A.38}$$

A very simple difference equation for this low pass filter is

$$y_k = y_{k-1} + k_f(u_k - y_{k-1}) \tag{A.39}$$

Here, y_k is the filtered signal at time step k, and u_k is the signal to be filtered. Note that the filter is frozen if k_f is set to zero, and disabled (i.e. $y_k = u_{k-1}$) if k_f is set to one.

The difference equation A.39 has been formatted so it can be calculated very quickly by a processor. It is even possible to exchange the multiplication with a bit shift if k_f is 2^{-n} for an integer n. Note however that if the processor is a digital signal processor (DSP), the multiplication can typically be done just as fast or even faster than a bit shift.

Using the bilinear transform instead for the same continuous lowpass filter in equation A.36 gives

$$F_b(z) = F_c(\tfrac{2}{T}\tfrac{1-z^{-1}}{1+z^{-1}}) = \frac{\frac{k_b}{2}(1 + z^{-1})}{1 - (1 - k_b)z^{-1}}, \tag{A.40}$$

where

$$k_b = \frac{2}{1 + \frac{2}{T\omega_f}}. \tag{A.41}$$

The difference equation for the low pass filter using the bilinear transform is

$$y_k = y_{k-1} + k_b(\tfrac{u_k + u_{k-1}}{2} - y_{k-1}) \tag{A.42}$$

It can be easily seen that it is not possible to completely disable this filter by setting k_b to one, like the other filter in equation A.39.

A discrete high pass filter

Using Euler's method on the continuous high pass filter

$$F_c(s) = \frac{\frac{s}{\omega_f}}{\frac{s}{\omega_f} + 1}. \tag{A.43}$$

gives

$$F_d(z) = F_c(\tfrac{1-z^{-1}}{T}) = k_f \frac{1 - z^{-1}}{1 - k_f z^{-1}}, \tag{A.44}$$

where

$$k_f = \frac{1}{1 + T\omega_f}. \tag{A.45}$$

The difference equation is

$$y_k = k_f(y_{k-1} + u_k - u_{k-1}). \tag{A.46}$$

Note that setting $k_f = 1$ will not disable the filter completely, as the initial value of the filter y_0 will be retained. Numerical errors could also compound if floating points methods are used to calculate the equation. If the filter can be configured with $k_f = 1$, a test for this special case should be used.

This discrete filter will give a lower response than the continuous filter, especially if the bandwidth frequency is near the Nyquist frequency. It can therefore often be useful to boost the gain of the discrete filter so it equals 1 for the Nyquist frequency. Solving

$$|k_b F_d(\mathrm{e}^{-\mathrm{j}\pi})| = 1 \tag{A.47}$$

gives

$$k_b = \frac{k_f + 1}{2k_f}. \tag{A.48}$$

This gives a new alternative highpass filter

$$F'_d(z) = \frac{k_f + 1}{2} \frac{1 - z^{-1}}{1 - k_f z^{-1}}, \tag{A.49}$$

which have the difference equation

$$y_k = k_f \left(y_{k-1} + \frac{u_k - u_{k-1}}{2} \right) + \frac{u_k - u_{k-1}}{2}. \tag{A.50}$$

A.2.2 A discrete notch filter

A notch filter is used to remove unwanted frequencies in a relatively narrow band from a signal. A 2. order, discrete notch filter can be written as

$$F_n(z) = \alpha \frac{1 - 2\cos(\omega_N T)z^{-1} + z^{-2}}{1 - 2\alpha\cos(\omega_N T)z^{-1} + (2\alpha - 1)z^{-2}} \tag{A.51}$$

where ω_N is the frequency of the notch peak, T the sampling period, and α is a constant giving the width of the notch.

A difference equation suitable for a software implementation is

$$y_k = y_{k-2} + \alpha \left(u_k - 2u_{k-1} + u_{k-2} + 2(y_{k-1} - y_{k-2}) + k_\omega(u_{k-1} - y_{k-1}) \right) \tag{A.52}$$

where

$$k_\omega = 2\left(1 - \cos(\omega_N T)\right) \approx (\omega_N T)^2 \text{ for small } \omega_N T. \tag{A.53}$$

Note the need for high numeric precision of the constant k_ω if the notch frequency is much smaller than the sampling frequency.

A.2.3 The frequency response of a time delayed pulse

Let $f(t)$ describe a time delayed pulse

$$f(t) = u(t - t_1) - u(t - t_2) \tag{A.54}$$

where $u(t)$ is the Heaviside function. t_1 is the time delay for the rising edge of the pulse, and t_2 the time delay for the falling edge. The Laplace transform of $f(t)$ is

$$F(s) = \frac{\mathrm{e}^{-st_1} - \mathrm{e}^{-st_2}}{s}. \tag{A.55}$$

This can be rewritten as

$$F(s) = \mathrm{e}^{-s\tau}\frac{\mathrm{e}^{\frac{st_w}{2}} - \mathrm{e}^{-\frac{st_w}{2}}}{s}, \tag{A.56}$$

where

$$\tau = \frac{t_1 + t_2}{2}, \tag{A.57}$$

$$t_w = t_2 - t_1. \tag{A.58}$$

This gives the frequency response of the time delayed pulse

$$F(\mathrm{j}\omega) = t_w \mathrm{e}^{-\mathrm{j}\omega\tau}\frac{\sin(\frac{t_w\omega}{2})}{\frac{t_w\omega}{2}}. \tag{A.59}$$

The frequency response of a time delayed pulse can thus be separated into a time delay and a gain part.

A.2.4 Padé approximation of a time delay

When connecting discrete and continuous systems it is often convenient to approximate a time delay with a linear transfer function. In a continuous system, the transfer function of a time delay of length τ is given by

$$g_{\mathrm{td}}(s) = \mathrm{e}^{-\tau s}. \tag{A.60}$$

Table A.1 – Padé approximations of $\mathrm{e}^{-\tau s}$.

Order	Approximation
1.	$\frac{1-\frac{1}{2}\tau s}{1+\frac{1}{2}\tau s}$
2.	$\frac{1-\frac{1}{2}\tau s+\frac{1}{12}(\tau s)^2}{1+\frac{1}{2}\tau s+\frac{1}{12}(\tau s)^2}$
3.	$\frac{1-\frac{1}{2}\tau s+\frac{1}{10}(\tau s)^2-\frac{1}{120}(\tau s)^3}{1+\frac{1}{2}\tau s+\frac{1}{10}(\tau s)^2+\frac{1}{120}(\tau s)^3}$
4.	$\frac{1-\frac{1}{2}\tau s+\frac{3}{28}(\tau s)^2-\frac{1}{84}(\tau s)^3+\frac{1}{1680}(\tau s)^4}{1+\frac{1}{2}\tau s+\frac{3}{28}(\tau s)^2+\frac{1}{84}(\tau s)^3+\frac{1}{1680}(\tau s)^4}$
5.	$\frac{1-\frac{1}{2}\tau s+\frac{1}{9}(\tau s)^2-\frac{1}{72}(\tau s)^3+\frac{1}{1008}(\tau s)^4-\frac{1}{30240}(\tau s)^5}{1+\frac{1}{2}\tau s+\frac{1}{9}(\tau s)^2+\frac{1}{72}(\tau s)^3+\frac{1}{1008}(\tau s)^4+\frac{1}{30240}(\tau s)^5}$

This time delay can be approximated using a Padé approximation of n'th order

$$g_{\mathrm{td}}(s) \approx g_{\mathrm{p,n}}(s) = \frac{\sum_{k=0}^{n} c_k(-\tau s)^k}{\sum_{k=0}^{n} c_k(\tau s)^k}, \tag{A.61}$$

where

$$c_k = \frac{(2n-k)!n!}{2n!k!(n-k)!}, \quad k = 0, 1, \cdots, n. \tag{A.62}$$

See table A.1 for the Padé approximations up to the fifth order. Another possibility is to chain n first order approximations in series, see e.g. [36]

$$g_{\mathrm{td}}(s) \approx g_{\mathrm{c,n}}(s) = \frac{\left(1-\frac{1}{2n}\tau s\right)^n}{\left(1+\frac{1}{2n}\tau s\right)^n}. \tag{A.63}$$

The approximations introduces errors in the phase which increases with increasing frequency. Figure A.1 shows the phase error plotted against a normalized per unit frequency $s\tau = \mathrm{j}2\pi\lambda$, i.e. $\omega = \frac{2\pi\lambda}{\tau}$. The solid line gives normal Padé approximations from the first to the fifth order. The dashed lines gives the chained approximations from the second to the fifth order. Note that the frequency axis is linear, and not logarithmic. The figure shows that the chained approximation gets rapidly worse than their Padé counterparts for higher orders.

It is however possible to mitigate the error somewhat for a low order approximation if the approximation is only needed for a specific part of the frequency spectrum. This is done by introducing a "frequency shift" factor in the approximation to make the phase error zero for a specific

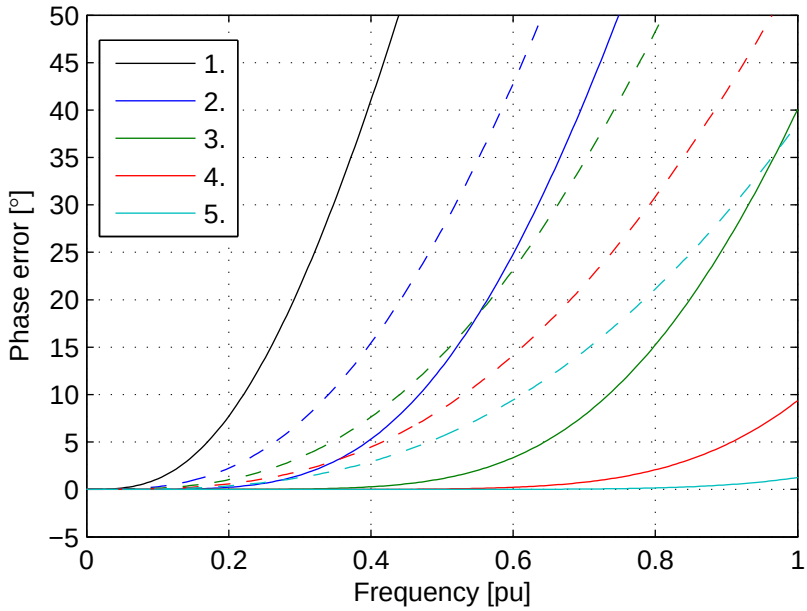

Figure A.1 – Phase errors of the Padé approximations of $\mathrm{e}^{-\mathrm{j}\lambda}$ for orders one through five. Higher orders give better approximations. The solid lines are the approximations given in table A.1, and the dashed lines are the chained first order approximations.

frequency. Instead of approximating the transfer function in equation A.60, the approximation is done for a transfer function

$$g_{\mathrm{fs}}(s) = \mathrm{e}^{-\tau\gamma s}. \tag{A.64}$$

A new factor γ called the frequency shift factor has been multiplied to the time delay in equation A.60.

As a special case, a simple analytic expression can be found for γ for the first order approximation

$$\mathrm{e}^{-\mathrm{j}2\pi\lambda_0} = \frac{1 - \mathrm{j}\gamma\pi\lambda_0}{1 + \mathrm{j}\gamma\pi\lambda_0}. \tag{A.65}$$

Solving this equation with respect for γ gives

$$\gamma = \frac{\tan(\pi\lambda_0)}{\pi\lambda_0}. \tag{A.66}$$

The limitation of the phase of the transfer function means this expression is only valid for $\lambda_0 \in \left[0, \frac{1}{2}\right]$.

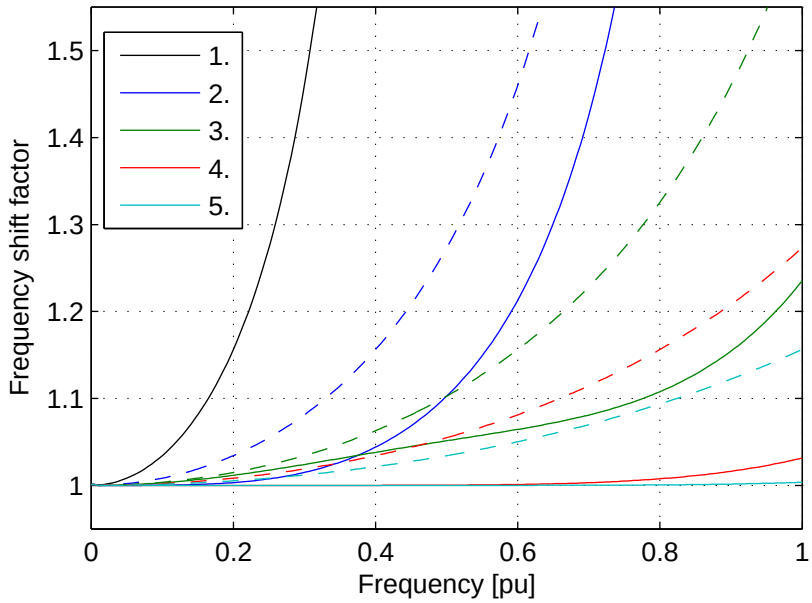

Figure A.2 – Frequency shift factor used in equation A.64 for phase correction of approximations of $e^{-j\lambda}$. Higher orders have lesser shifts. The solid lines are the approximations given in table A.1, and the dashed lines are the chained first order approximations.

For higher orders a numerical equation solver was used to create figure A.2. It shows the factor γ plotted against the normalized per unit frequency necessary to obtain zero error for a specific frequency. The maximum obtainable phase shift adjustment is limited as the approximations are rational transfer functions.

APPENDIX B

On the $\alpha\beta 0$-transformation of a periodic signal

This appendix calculates the $\alpha\beta 0$-transformation of a timeshifted three phase periodic vector.

Let $f(t)$ be a piecewise smooth and continuous, periodical function of period T. The vector to be transformed into the $\alpha\beta 0$-coordinate system is defined as

$$\boldsymbol{x}^{abc}(t) = \begin{bmatrix} f(t) \\ f(t-\frac{T}{3}) \\ f(t-\frac{2T}{3}) \end{bmatrix}. \tag{B.1}$$

First, consider the fourier series expansion of $f(t)$, which can be written as [37]

$$f(t) = \frac{1}{2}a_0 + \sum_{n=1}^{\infty} \left(a_n \cos\left(\omega_n t\right) + b_n \sin\left(\omega_n t\right)\right), \tag{B.2}$$

where

$$\omega_n = \frac{2\pi n}{T}, \tag{B.3}$$

$$a_n = \frac{2}{T}\int_0^T f(\tau)\cos\left(\omega_n \tau\right) d\tau, \tag{B.4}$$

$$b_n = \frac{2}{T}\int_0^T f(\tau)\sin\left(\omega_n \tau\right) d\tau. \tag{B.5}$$

Define new functions $h_n(t)$ denoting the n'th individual harmonic com-

ponent of $f(t)$ as

$$h_n(t) = \begin{cases} \frac{1}{2}a_0 & \text{if } n = 0, \\ a_n \cos(\omega_n t) + b_n \sin(\omega_n t) & \text{if } n > 0. \end{cases} \tag{B.6}$$

Also define new functions $h_n^{90^\circ}(t)$ denoting $h_n(t)$ shifted by 90° to be

$$h_n^{90^\circ}(t) = \begin{cases} \frac{1}{2}a_0 & \text{if } n = 0, \\ a_n \cos\left(\omega_n t - \frac{\pi}{2}\right) + b_n \sin\left(\omega_n t - \frac{\pi}{2}\right) & \text{if } n > 0. \end{cases} \tag{B.7}$$

Timeshifting any of equations defined by B.6 by m thirds of a period give

$$h_n(t - m\frac{T}{3}) = \begin{cases} \frac{1}{2}a_0 & \text{if } n = 0, \\ (a_n C_{nm} - b_n S_{nm})\cos(\omega_n t) & \\ \quad + (a_n S_{nm} + b_n C_{nm})\sin(\omega_n t) & \text{if } n > 0, \end{cases} \tag{B.8}$$

where

$$C_{nm} = \cos(\frac{2\pi}{3}nm), \tag{B.9}$$

$$S_{nm} = \sin(\frac{2\pi}{3}nm). \tag{B.10}$$

This can be rewritten in matrix form as

$$\begin{aligned} h_n(t - m\frac{T}{3}) &= \begin{bmatrix}\cos(\omega_n t) & \sin(\omega_n t)\end{bmatrix} \left(\begin{bmatrix} -\frac{1}{2} & -\frac{\sqrt{3}}{2} \\ \frac{\sqrt{3}}{2} & -\frac{1}{2} \end{bmatrix} \right)^{nm} \begin{bmatrix} a_n \\ b_n \end{bmatrix} \\ &= \boldsymbol{\theta}_n^T(t)\boldsymbol{K}^{nm}\boldsymbol{c}_n. \end{aligned} \tag{B.11}$$

If k is an integer, the matrix $\boldsymbol{K}$ has the following basic properties

$$\boldsymbol{K}^{3k} = \boldsymbol{I}, \tag{B.12}$$

$$\boldsymbol{K}^{3k+1} = \boldsymbol{K}, \tag{B.13}$$

$$\boldsymbol{K}^{3k+2} = \boldsymbol{K}^2 = \boldsymbol{K}^T. \tag{B.14}$$

Furthermore, the following properties are useful here

$$\frac{2\boldsymbol{I} - \boldsymbol{K}^{3k+1} - \boldsymbol{K}^{2(3k+1)}}{3} = \frac{2\boldsymbol{I} - \boldsymbol{K}^{3k+2} - \boldsymbol{K}^{2(3k+2)}}{3} = \boldsymbol{I}, \tag{B.15}$$

$$\frac{\boldsymbol{K}^{3k+1} - \boldsymbol{K}^{2(3k+1)}}{\sqrt{3}} = -\frac{\boldsymbol{K}^{3k+2} - \boldsymbol{K}^{2(3k+2)}}{\sqrt{3}} = \begin{bmatrix} 0 & -1 \\ 1 & 0 \end{bmatrix}, \tag{B.16}$$

$$\frac{\boldsymbol{I} + \boldsymbol{K}^{3k+1} + \boldsymbol{K}^{2(3k+1)}}{3} = \frac{\boldsymbol{I} + \boldsymbol{K}^{3k+2} + \boldsymbol{K}^{2(3k+2)}}{3} = \boldsymbol{0}. \tag{B.17}$$

Define a vector of the n'th harmonic as

$$\boldsymbol{h}_n^{abc}(t) = \begin{bmatrix} h_n(t) \\ h_n(t-\frac{T}{3}) \\ h_n(t-\frac{2T}{3}) \end{bmatrix} = \begin{bmatrix} \boldsymbol{\theta}_n^T(t)\boldsymbol{c}_n \\ \boldsymbol{\theta}_n^T(t)\boldsymbol{K}^n\boldsymbol{c}_n \\ \boldsymbol{\theta}_n^T(t)\boldsymbol{K}^{2n}\boldsymbol{c}_n \end{bmatrix}. \tag{B.18}$$

This vector can be transformed using the $\alpha\beta 0$-transform

$$\begin{aligned} \boldsymbol{h}_n^{\alpha\beta 0}(t) &= \begin{bmatrix} h_{\alpha,n}(t) \\ h_{\beta,n}(t) \\ h_{0,n}(t) \end{bmatrix} = \mathbf{T}_{abc}^{\alpha\beta 0}\boldsymbol{h}_n^{abc}(t) \\ &= \frac{1}{3}\begin{bmatrix} 2 & -1 & -1 \\ 0 & \sqrt{3} & -\sqrt{3} \\ 1 & 1 & 1 \end{bmatrix} \begin{bmatrix} \boldsymbol{\theta}_n^T(t)\boldsymbol{c}_n \\ \boldsymbol{\theta}_n^T(t)\boldsymbol{K}^n\boldsymbol{c}_n \\ \boldsymbol{\theta}_n^T(t)\boldsymbol{K}^{2n}\boldsymbol{c}_n \end{bmatrix}. \end{aligned} \tag{B.19}$$

The α-component is

$$\begin{aligned} h_{\alpha,n}(t) &= \boldsymbol{\theta}_n^T(t)\frac{2\boldsymbol{I} - \boldsymbol{K}^n - \boldsymbol{K}^{2n}}{3}\boldsymbol{c}_n \\ &= \begin{cases} 0 & \text{if } n = 0,3,6,\ldots, \\ h_n(t) & \text{if } n = 1,2,4,5,7,8,\ldots. \end{cases} \end{aligned} \tag{B.20}$$

The β-component is

$$\begin{aligned} h_{\beta,n}(t) &= \boldsymbol{\theta}_n^T(t)\frac{\boldsymbol{K}^n - \boldsymbol{K}^{2n}}{\sqrt{3}}\boldsymbol{c}_n \\ &= \begin{cases} 0 & \text{if } n = 0,3,6,\ldots, \\ h_n^{90^\circ}(t) & \text{if } n = 1,4,7,\ldots, \\ -h_n^{90^\circ}(t) & \text{if } n = 2,5,8,\ldots. \end{cases} \end{aligned} \tag{B.21}$$

The null-component is

$$\begin{aligned} h_{0,n}(t) &= \boldsymbol{\theta}_n^T(t)\frac{\boldsymbol{I} + \boldsymbol{K}^n + \boldsymbol{K}^{2n}}{3}\boldsymbol{c}_n \\ &= \begin{cases} h_n(t) & \text{if } n = 0,3,6,\ldots, \\ 0 & \text{if } n = 1,2,4,5,7,8,\ldots. \end{cases} \end{aligned} \tag{B.22}$$

These results suggests splitting the original function $f(t)$ into three new

functions:

$$f_0(t) = \sum_{k=0}^{\infty} h_{3k}(t), \tag{B.23}$$

$$f_p(t) = \sum_{k=1}^{\infty} h_{3k+1}(t), \tag{B.24}$$

$$f_n(t) = \sum_{k=1}^{\infty} h_{3k+2}(t), \tag{B.25}$$

where

$$f(t) = f_0(t) + f_p(t) + f_n(t). \tag{B.26}$$

The $\alpha\beta 0$-transform of the original vector in equation B.1 is

$$\begin{aligned}
\boldsymbol{x}^{\alpha\beta 0}(t) =& \mathbf{T}_{abc}^{\alpha\beta 0} \begin{bmatrix} f_0(t) + f_p(t) + f_n(t) \\ f_0(t - \frac{T}{3}) + f_p(t - \frac{T}{3}) + f_n(t - \frac{T}{3}) \\ f_0(t - \frac{2T}{3}) + f_p(t - \frac{2T}{3}) + f_n(t - \frac{2T}{3}) \end{bmatrix} \\
=& \sum_{k=0}^{\infty} \mathbf{T}_{abc}^{\alpha\beta 0} \begin{bmatrix} h_{3k}(t) \\ h_{3k}(t - \frac{T}{3}) \\ h_{3k}(t - \frac{2T}{3}) \end{bmatrix} \\
&+ \sum_{k=1}^{\infty} \mathbf{T}_{abc}^{\alpha\beta 0} \begin{bmatrix} h_{3k+1}(t) \\ h_{3k+1}(t - \frac{T}{3}) \\ h_{3k+1}(t - \frac{2T}{3}) \end{bmatrix} \\
&+ \sum_{k=1}^{\infty} \mathbf{T}_{abc}^{\alpha\beta 0} \begin{bmatrix} h_{3k+2}(t) \\ h_{3k+2}(t - \frac{T}{3}) \\ h_{3k+2}(t - \frac{2T}{3}) \end{bmatrix} \\
=& \sum_{k=0}^{\infty} \begin{bmatrix} 0 \\ 0 \\ h_{3k}(t) \end{bmatrix} + \sum_{k=1}^{\infty} \begin{bmatrix} h_{3k+1}(t) \\ h_{3k+1}^{90^\circ}(t) \\ 0 \end{bmatrix} + \sum_{k=1}^{\infty} \begin{bmatrix} h_{3k+2}(t) \\ -h_{3k+2}^{90^\circ}(t) \\ 0 \end{bmatrix} \\
=& \begin{bmatrix} 0 \\ 0 \\ f_0(t) \end{bmatrix} + \begin{bmatrix} f_p(t) \\ f_p^{90^\circ}(t) \\ 0 \end{bmatrix} + \begin{bmatrix} f_n(t) \\ -f_n^{90^\circ}(t) \\ 0 \end{bmatrix},
\end{aligned} \tag{B.27}$$

and thus, finally:

$$\boldsymbol{x}^{\alpha\beta 0}(t) = \begin{bmatrix} f_p(t) + f_n(t) \\ f_p^{90^\circ}(t) - f_n^{90^\circ}(t) \\ f_0(t) \end{bmatrix}. \tag{B.28}$$